eman ta zabal zazu

Universidad
del País Vasco

Euskal Herriko
Unibertsitatea

Advanced Perovskite:Fullerene Blend Films for Perovskite Solar Cells with Innovative Configurations

PhD Thesis

Jorge Pascual Mielgo

Supervised by

Dr. Juan Luis Delgado Cruz

Dr. Ramón Tena Zaera

Donostia

2019

Contents

Abbreviations

AFM	Atomic force microscopy
BCP	Bathocuproine
BHJ	Bulk heterojunction
CB	Conduction band
Cl-Cy	Chlorocyclohexane
DFT	Density functionally theory
DMF	*N*,*N*-dimethylformamide
DMSO	Dimethylsulfoxide
EELS	Electron energy loss spectroscopy
ETL	Electron-transporting layer
EQE	External quantum efficiency
FA	Formamidinium
FE-SEM	Field emmision scanning electron microscopy
FF	Fill factor
FTO	Fluorine-doped tin oxide
HAADF	High-angle annular dark-field imaging
HIV	Human immunodeficiency virus
HTL	Hole-transporting layer
ICBA	Indene-C_{60} bisadduct
ITO	Indium tin oxide
LiTFSI	lithium bis(trifluoromethane) sulfonimidate
MA	Methylammonium
Me-Cy	Methylcyclohexane
o-DCB	*ortho*-Dichlorobenzene

Abbreviations

OFET	Organic field-effect transistor
OPV	Organic photovoltaics
P3HT	Poly(3-hexylthiophen-2,5-dyil)
PCBM	Phenyl-C_{61}-butyric acid methyl ester
PCE	Power conversion efficiency
PSC	Perovskite solar cell
PTAA	Poly[bis(4-phenyl)(2,4,6-trimethylphenyl)amine]
PV	Photovoltaic
SAM	Self-assembled monolayer
Spiro-OMeTAD	2,2',7,7'-tetrakis-(*N,N*-di-4-methoxyphenylamino)-9,9'-spirobifluorene
STEM	Scanning transmission electron microscopy
TRPL	Time-resolved photoluminiscence
VB	Valence band

Summary

Among the different energy sources currently available, photovoltaic technology represents one of the most promising ones considering the total energy that the Earth receives from the Sun every day. In particular, silicon solar cells have attracted the attention of the field since their discovery, until more recent organic and hybrid types of solar cells were found.

This is the case of perovskites, hybrid materials that experienced a tremendous improvement in efficiency since its first photovoltaic application in 2009. Perovskites hold many characteristics that makes their use particularly appealing, such as the low-cost, easy and versatile processing, allowing their application in devices of diverse configurations.

However, perovskites still have to overcome certain issues that hinder them from being applied in industrial scale. The main one is the stability of the devices, due to the several paths of degradation that perovskite solar cells present. The deterioration of these devices is related, first, to the characteristics of the particular materials used for the fabrication of the solar cells and, second, to the quality of the films and so the density of defects that these may contain. In this sense, there is a strong need to find optimized materials and layers for new configurations showing enhanced stability.

Considering these points, our attention was focused on molecules or components that would give perovskites the stability they lacked. In the search for new strategies that would provide a solution, this thesis looked at fullerenes, as they proved their potential to improve the performance of perovskite solar cells in few reported studies.

Fullerenes are a specific allotrope of carbon, in which the atoms are forming single and double bonds leading to a closed structure. The interest in fullerenes grew with new ways to functionalize them, since it was an easy way to obtain new molecules with specific properties. In particular, fullerenes reactivity is determined by its polyenic and electrophilic nature. In this regard, fullerenes can undergo several reactions, being the nucleophilic additions and cycloadditions the most common ones.

In fact, the electron-accepting nature of fullerenes has made them perfect candidates for their application as n-type semiconductors in perovskite solar cells, more in particular as electron-selective layers in perovskite solar cells. Their use in the photovoltaic field has been one of their most relevant recent achievements, gaining a lot of recognition in the development of polymer/fullerene bulk heretojunction organic solar cells, due to their fast-quenching ability of the excitons generated in this type of devices.

In the case of perovskite solar cells, the potential of fullerenes was going much further than their use as electron-transporting/hole-blocking layers. The density of defects of certain layers and configurations, which is one of the main issues in perovskite materials, was found to be reduced by the presence of fullerenes. Therefore, fullerenes showed additional application in these devices, producing beneficial effects when introduced inside the perovskite layer.

With this in mind, the present thesis aimed to introduce fullerenes in perovskite films in order to improve the performance and stability of devices. Once proved their beneficial character as additives in perovskite solar cells, new strategies for optimizing their use would be found. Considering the chemical versatility of fullerenes, the scope of this strategy would be proven to several fullerene derivatives. Last, the origin of the beneficial effects would have to be addressed.

Therefore, the present thesis aims to develop new strategies for the full exploitation of fullerenes in perovskite solar cells, being their potential to be use for perovskite:fullerene blend film processing and passivating defects among the main key features. The thesis is composed of nine chapters, which are briefly explained below.

The first chapter introduces the main two pillars of this thesis: perovskite and fullerenes. An introduction to the characteristics and development of these materials is provided, as well as the few works carried out on perovskite-fullerene systems before the beginning of this thesis. Additionally, the objectives of this work are presented.

The second chapter provides the reader with experimental details about the techniques used in the work of this thesis for the fabrication and characterization of perovskite films and solar cells. Some practical characteristics are also pointed out.

In the third chapter, perovksite:C_{70} blend films are presented as effective light-absorbing layer for the preparation of electron-transporting layer-free perovskite solar cells. The presence of C_{70} is proven to improve the morphology of the perovskite films, reducing largely the density of pinholes in them. In turn, devices fabricated from these blends show improved efficiency and photostability. These results present fullerenes preferent candidates for the fabrication of efficient and stable electron-transporting layer-free perovskite solar cells through their use as additives.

In the fourth chapter it is shown how perovskite:C_{70} blend films are highly affected by the nature of the perovskite solution, in terms of film and device properties. In particular, adding aromatic solvents in small relative volumes to perovskite precursor solution enhances the beneficial character of fullerenes, resulting in even more efficient electron-transporting layer-free perovskite solar cells. A combination of microscopic techniques suggests that the use of these cosolvents is influencing how fullerenes distribute in the perovskite layer. Aromatic cosolvents particularly reduce the pinhole density in the layers, compared to the aliphatic ones. The reason for this might be the ability of fullerenes to preferentially interact with aromatic cosolvents than with the perovskite-dissolving solvents, as proven by a set of spectroscopic techniques. In this way, aromatic cosolvents might be avoiding the aggregation of fullerenes, promoting them to distribute in a much more homogenous way.

In the fifth chapter, derivatized fullerenes are proven to work better enhancing the performance of the devices than non-functionalized ones. In particular, high and reproducible efficiency values (i.e. >14% in electron-transporting layer-free devices) are achieved by combining a novel isoxazoline-derivatized fullerene with the cosolvent approach from previous chapter. The fullerene derivatives, that were designed in order to hold specific electronic properties, present a correlation between their LUMO level and the V_{oc} value of the device, what suggests that fullerenes have an electronic role when used in blends with perovskite. In fact, this is been proven in another work under a collaboration by time-resolved photoluminescence measurements, showing that there is electron transfer from perovskite to fullerene in the picoseconds scale. However, the improvement in the photostability is observed to be comparable independently of the

structure and derivatization of fullerene, suggesting that the fullerene cage is the one involved in the processes that increase the stability of devices.

In the sixth chapter, the interactions between perovskite and fullerenes in the precursor solution have been identified with a set of spectroscopic techniques. First of all, the fullerene cage might preferentially bind PbI_2, which would affect the whole perovskite precursor complex in solution. Second, functionalizing the fullerene cage with a Lewis base allows fullerenes to form a stronger complex with perovskite, allowing them to bind at the same time the amines of the perovskite precursors. The different strength that fullerenes have shown to bind perovskite is also shown to have direct effects on morphological and device properties. In this sense, the most efficient perovskite solar cells are seen to be obtained from perovskite:fullerene solutions forming the strongest complexes. Additionally, the benefits of using this strategy are proven to be universal for different configurations of perovskite solar cells. In particular, for electron-transporting layer-free the photovoltaic parameters and their reproducibility is enhanced, as well as for p-i-n devices; however, for n-i-p devices, the fill factor was seen to be the most benefited one.

The conclusions of the work are summarized in chapter seven, placing them in the scientific context and giving them the corresponding relevance for the development of the field. An additional outlook covers the main benefits of fullerenes in perovskite solar cells, as well as their future challenges, pointing out the contribution of this thesis to solve them.

Chapter eight lists the contributions that the work included in this thesis has provided, considering publications in high impact journals and oral communications in congresses.

The thesis is closed with the chapter nine, containing annexes referenced in the main text.

Overall, this thesis represents a significant contribution to the development of efficient and stable electron-transporting layer perovskite solar cells, through the employment of perovskite:fullerene blend films in a one-step process, dissolving the fullerene in the perovskite precursor solution. This thesis does not limit itself to the application of these films, but provides a deeply studied "cosolvent approach" for the optimization of this

method. In addition, the scope of this strategy is investigated for different fullerene functionalizations, proving a structure-performance relationship, as well as new insights on the beneficial origin of fullerenes for the improvement of the device stability. Finally, the interactions between perovskite and fullerenes are studied, proving that the functional groups of fullerenes for their application in perovskite:fullerene blend films have an important effect in the final characteristics of the films and device performance. All in all, this thesis represents a guideline for the use of perovskite:fullerene blend films for the fabrication of efficient, stable and reproducible perovskite solar cells of any configuration, with special details on electron-transporting layer-free devices.

Laburpena

Gaur egun eskuragarri ditugun energi-iturrien artean, energia fotovoltaikoa etorkizun handiena daukatenetarikoa da, kontuan hartuz Lurrari egunero Eguzkitik iristen zaion energia kopuru totala. Zehazki, silizioko eguzki-zelulak izan dira gehien bat komunitate zientifikoaren arreta irabazi dutenak, beste eguzki-zelula mota organiko eta hibrido berriagoak aurkitu ziren arte.

Hau da perovskiten kasua, bere lehen aplikazio fotovoltaikotik 2009an izugarrizko igoera izan duten material hibridoak. Material hauek paregabeak egiten dituzten ezaugarri oso bereziak dituzte, haien kostu baxua eta prozesatzeko aukera anitzak bezala, bere erabilera konfigurazio desberdinetan ahalbidetuz.

Hala ere, perovskitek oraindik oztopo batzuk gainditu behar dituzte, haien fabrikazioa eskala industrialean posible izan dadin. Oztoporik nagusiena egonkortasuna da, izan ere perovskita eguzki-zelulek degradazio prozesu asko pairatzen dituzte. Gailu hauen hondatzea erlazionatuta dago, lehenik eta behin, haien fabrikaziorako erabili diren material espezifikoen ezaugarriekin eta, bigarren, geruzen kalitate eta ezaugarriekin eta, beraz, haien akatsen dentsitatearekin. Zentzu honetan, egonkortasuna luzatzen duten material optimizatuak eta konfigurazio berritarako geruzak aurkitzeko behar garrantzitsua dago.

Puntu hauek kontuan hartuta, perovskiten egonkortasuna hobetu dezaketen molekuletan edo osagaietan erreparatu genuen. Konponbidea ekar zezaketen estrategia berrien bilaketa zela eta, tesi honek fulerenoetan jarri zuen arreta, haien potentziala perovskita eguzki-zelulen etekina hobetzeko frogatu baitzuten, hainbat ikerketa berrien arabera.

Fulerenoak karbono alotropo bat dira, non atomoek lotura sinple eta bikoitzak eratzen duten pilota itxurako egitura itxian amaitzeko. Fulerenoak funtzionalizatzeko erak ugaritu ahala handitu zen haienganako interesa, modu erraza baitzen molekula berriak lortzeko ezaugarri zehatz batzuekin. Fulerenoen erreaktibotasuna haien izaera polieniko eta elektrofiloan dago oinarrituta gehien bat. Beraz, fulerenoak errakzio mota batzuetan parte har dezakete, bereziki adizio nukleofiletan eta zikloadizioetan.

Are gehiago, haien elektroi-hartzaile izaerak n-motako semieroale bikainetan bihurtu ditu, haien aplikazioa perovskite eguzki-zeluletan ahalbidetuz. Fulerenoen erabilera ikerketa fotovoltaikoan haien lorpen garratzitsu berrienetarikoen artean koka daiteke, bereziki polímero/fulereno heteroestrukturadun eguzki-zelula organikoen garapenean, haien ahalera mota honetako gailuetan sortutako exzitoiak azkar ezabatzeko dela eta.

Perovskite eguzki-zelulen kasuan, fulerenoen potentziala haien erabilera elektroi-garraiatzaile/huts-blokeatzaile geruza bezala baino haratago heldu zen. Ikusi zen nola hainbat geruza eta konfigurazioetako akatsen dentsitatea, gaur egun perovskitei begira betebehar garrantzitsuenetako bat, txikitu zen, perovskita geruzan fulerenoa zela eta. Hau dela eta, fulerenoek aplikazio berriak erakutsi zituzten mota hauetako gailuetan, eragin positiboak lortuz hauek perovskita geruzaren barnean sartzean.

Hau kontuan izanda, tesi honek fulerenoak perovskita geruzan sartzea bilatu zuen, hauen etekina eta egonkortasuna hobetzeko. Behin frogatuta haien izaera positiboa aditiboak bezala, estrategia hau optimizatzeko metodoak bilatu beharko ziren. Fulerenoen eta deribatuen aniztasun kimikoa dela eta, estrategia honen norainokoa frogatu beharko zen fulereno funtzionalizatuak erabilita. Azkenik, fulerenoen eragin positiboen arrazoiak eztabaidatu beharko ziren.

Hortaz, tesi honen helburu nagusia fulerenoen aplikazioa perovskita eguzki-zeluletan guztiz aztertzeko estrategia berrien garapena izango da, batez ere bere potentziala perosvskita:fulereno geruzak prozesatzeko eta haien ahalera akatsak pasibatzeko. Tesi hau hurrengo bederatzi ataletan dago banatuta.

Lehen kapituluak tesiaren bi material garrantzitsuenei ematen die sarbidea: perovskitak eta fulerenoak. Material hauen ezaugarri eta garapenari buruzko introdukzioa egiten da, tesia aurretik zeuden perovskita-fulereno sistemari buruzko lanak azalduz. Gainera, lan honen helburuak aurkezten dira.

Bigarren atalak ezaugarri esperimentalak aurkezten ditu eta perovskita gailuen fabrikazioan eta karakterizazioan erabilitako teknika nagusiei sarrera ematen die. Beste informazio praktikoa era ematen da.

Hirugarren atalean perovskita:C_{70} geruza konposatuak geruza elektroi-garraiatzaile gabeko perovskita eguzki-zelulen fabrikaziorako geruza aktibo eraginkorrak bezala aurkezten dira. Konprobatzen da nola C_{70}-ren adizioak perovskita filmaren morfologia positiboki eragiten duen, filmaren hutsune dentsitatea ederki murrizten. Ondorioz, geruza konposatu hauetan oinarritutako gailuak etekin eta fotoegonkortasun hobetua izaten dute. Emaitza hauek berresten dituzte fulerenoak lehentasunezko hautagaiak bezala haien erabilerarako aditibo gisa geruza elektroi-garraiatzaile gabeko perovskita eguzki-zelula efiziente eta egonkorren fabrikaziorako.

Laugarren kapituluan aurkezten da nola perovskita disoluzioaren ezaugarriek perovskita:C_{70} geruza konposatuak eragiten dituzten, film eta gailu ezaugarriei dagokionez. Zehazki, disolbatzaile aromatikoen adizioa volumen erlatibo txikietan perovskitaren disoluzioan fulerenoen eragin positiboa are gehiago handitzen du, etekin are eta handiagoko geruza elektroi-garraiatzaile gabeko perovskita eguzki-zelulak lortuz. Teknika mikroskopikoek proposatu zuten kodisolbatzaileen erabilera fulerenoen distribuzioan perovskita geruzan zehar eragina izaten zuela. Bereziki, disolbatzaile aromatikoek geruza hauetako hutsune dentsitatea murrizten dute, analogo alifatikoekin konparatuta. Azalpena fulerenoak eta disolbatzaile aromatikoak lehentasunez elkarri eragiteko gaitasunarekin erlazionatuta egon daiteke, teknika espektroskopiko batzuekin

frogatu zen moduan. Modu honetan, kodisolbatzaile aromatikoak fulerenoen agregazioa sahiesten dute, haien distribuzio homogeneoagoa perovskita geruzan bultzatuz.

Bosgarren kapituluan ikusten da nola fulerenoen deribatizazioa fulerenoen eragin positiboa handitzen duen, deribatizatuak izan ez diren fulerenoekin alderatura. Zehazki, erraz errepika daitezkeen etekin balio altuak lortu ziren (i.e. >14% geruza elektroi-garraiatzaile gabeko gailuak) isoxazolino taldearekin funtzionalizatutako fulerenoa eta azken kapituluko kodisolbatzailearen estrategia konbinatuz. Fulereno deribatuetarako, funtzionalizatzen direnak e.g. ezaugarri elektroniko zehatz batzuk izan ditzaten, haien LUMO eta gailuen V_{oc} balioen arteko erlazio bat aurkitu zen, beraz proposatuz fulerenoek rol elektroniko bat daukatela perovskita geruzetan sartzen direnenean. Izan ere, fenómeno hau geroago frogatua izan zen kolaborazio lan batean egin ziren denboran ebatzitako fotoluminiszentzia neurketen arabera, frogatuz transferentzia elektronikoa gertatzen dela perovskitatik fulerenora pikosegunduen mailan. Hala ere, aurkitu zen gailuen fotoegonkortasuna fulerenoaren estrukturarenganako independientea zela, proposatuz fulerenoaren kaxa zela gailuen fotoegonkortasunarekin erlazionantutako prosezuaren arduraduna.

Seigarren atalean perovskita eta fulerenoen arteko interakzioak disoluzio egoeran aztertu eta identifikatu dira teknika espektroskopiko batzuen konbinaziari esker. Hasteko, fulerenoaren nukleoa PbI_2-rekin konplexatzen da lehentasunez, disoluzioan konplexu guztian eragina duena. Bigarren, fulerenoa Lewisen base batekin funtzionalizatzeak ahalbidetzen die era berean perovskiten aminekin lotura intermolekularrak eratzea. Perovskita-fulereno konplexu hauen indarrak film eta gailuen ezaugarriengan eragina zuela ikusi zen. Zentzu honetan, perovskite eguzki-zelula efizienteenak perovskita-fulereno konplexurik indartsuenak eratzen zituzten disoluzioetatik lortu ziren. Gainera, estrategia honen eragin positiboak unibertsaltasuna frogatu zuten konfigurazio ezberdinetarako. Zehazki, geruza elektroi-garraiatzaile gabeko eta p-i-n gailuetarako parametro fotovoltaikoak handitu ziren, baita balio hauek erreproduzitzeko erraztasuna. Fill factorra izan zen n-i-p konfiguraziodun gailuetan ikusi zen hobekuntzarik handiena.

Lan hauen konlusioak zazpigarren kapituluan laburbiltzen dira, hauek kontestu zientifiko aproposan jarriz eta komunitate zientifikoan izan duen eragina eta lortu diren

aurrerapenak esleituz. Artikulu osagarri batek fulerenoek perovskita eguzki-zeluletan daukaten eragin positiboari buruz kritikoki eztabaidatzen du, haien hurrengo erronkak azalduz eta hauek ebazteko tesi honen lanak zer laguntza egin duen kontuan hartuz.

Zortzigarren kapituluak tesi honen lanatik ateratako kontribuzioak biltzen ditu, publikazioak inpaktu altuko aldizkarietan eta hitzaldiak kongresuetan, hots.

Tesia bederatzigarren kapituluarekin ixten da, testu nagusian erreferentziatutako anexoak bilduz.

Orokorrean, tesi honek perovskita eguzki-zelula eficiente eta egonkorrak lortzeko kontribuzio handiak ekarri ditu, pasu bakarrean proseza daitezkeen perovskita:fulereno geruza konposatuak erabiliz, fulerenoa perovskita disoluzioan disolbatuz. Tesi hau ez du soilik geruza hauek erabiltzen, baizik eta estrategia hau optimizatzeko kodisolbatzailearen metodoa proposatzen du. Halaber, estrategia honen erabilgarritasuna fulereno deribatu ezberdinekin aztertzen da, hainbat egitura-etekin erlazioak aurkituz, eta era berean gailuen egonkortasunean fulerenoen eragin positiboari buruzko mekanismoren gaineko ezagutza handitu. Azkenik, perovskita eta fulerenoen arteko interakzioak aztertu dira, perovskita eguzki-zeluletarako fulerenoen talde funtzionalek film eta gailu sistemetan garrantzi handia dutela frogatuz. Laburtzeko, tesi hau perovskita eguzki-zelulak fabrikatzeko perovskita:fulereno film konposatuak erabiltzeko gida moduko bat da komunitate zientifikorako, konfigurazio ezberdinetarako baina, batez ere, geruza elektroi garraiatzaileak ez dituzten haietarako.

Resumen

Entre las diferentes fuentes de energía actualmente disponibles, la tecnología fotovoltaica representa una de las más prometedoras, considerando la energía total que recibe la Tierra del Sol cada día. En concreto, las celdas solares de silicio han atraído la atención del campo desde su descubrimiento, hasta que se encontraron nuevos tipos de celdas solares orgánicas e híbridas más recientes.

Este es el caso de las perovskitas, materiales híbridos que han experimentado un crecimiento en eficiencia increíble desde su primera aplicación fotovoltaica en 2009. Estos materiales tienen unas propiedades únicas que los hacen particularmente atractivos, tales como su bajo coste y versátil procesamiento, permitiendo su uso en dispositivos de diversas configuraciones.

Sin embargo, las perovskitas todavía tienen que superar varios obstáculos que dificultan su aplicación a escala industrial. El principal es la estabilidad, debido a los numerosos mecanismos de degradación presentes en las celdas solares de perovskita. El deterioro de estos dispositivos está relacionado, primero, con las características de los materiales específicos utilizados para la fabricación de las celdas solares y, segundo, con la calidad y propiedades de las capas y, por tanto, también con la densidad de defectos que estas contengan. En este sentido, existe una necesidad imperante de encontrar materiales optimizados y capas para nuevas configuraciones que presenten estabilidades mejoradas.

Considerando estos puntos, nuestra atención se centró en moléculas o componentes que pudieran aportar a las perovskitas la estabilidad que les faltaba. En la búsqueda de nuevas estrategias que proporcionaran una solución, esta tesis se fijó en los fullerenos, pues probaron su potencial para mejorar el rendimiento de las celdas solares de perovskita, de acuerdo con algunos estudios recientes.

Los fullerenos son un tipo particular de alótropo de carbon, en el que los átomos forman enlaces simples y dobles para dar lugar a una estructura cerrada. El interés en los fullerenos creció con las nuevas formas de funcionalizarlos, ya que era una vía fácil para la obtención de moléculas con propiedades específicas. En concreto, la reactividad de los fullerenos está determinada por su naturaleza poliénica y electrófila. En este sentido, los fullerenos pueden participar en varios tipos de reacciones, siendo las adiciones nucleófilas y las cicloadiciones las más comunes.

De hecho, el carácter electrón-aceptor de los fullerenos los han hecho perfectos candidatos para su aplicación como semiconductores de tipo n en celdas solares de perovskita. Su uso en el campo fotovoltaico ha sido uno de sus más relevantes logros recientes, recibiendo un gran reconocimiento por el desarrollo de celdas solares

orgánicas de heteroestructura polímero/fullereno, debido a su habilidad para extinguir rápidamente los excitones generados en este tipo de dispositivos.

En el caso de las celdas solares de perovskita, el potencial de los fullerenos fue mucho más allá de su uso como capas transportadoras de electrones/bloqueadoras de huecos. Se observó que la densidad de defectos en diversas capas y configuraciones, uno de los principales asuntos pendientes dentro de los materiales de perovskita, se redujo debido a la presencia de fullerenos en el film de perovskita. Por lo tanto, los fullerenos mostraron aplicaciones adicionales en estos tipos de dispositivos, produciendo efectos positivos al introducirlos en la capa de perovskita.

Con esto en mente, esta tesis buscó introducir fullerenos en capas de perovskita para la mejora del rendimiento y la estabilidad de los dispositivos. Una vez probado su caracter beneficioso como aditivos, se deberían hallar métodos para optimizar esta estrategia. Considerando la versatilidad química de los fullerenos y sus derivados, el alcance de esta estrategia se probaría con el estudio de fullerenos funcionalizados. Por ultimo, se discutiría sobre el origen del carácter beneficioso de los fullerenos.

Por lo tanto, esta tesis tiene como objetivo principal el desarrollo de nuevas estrategias para explotar completamente el uso de fullerenos en celdas solares de perovskita, centrándonos en su potencial para el procesado de capas compuestas perovskita:fullereno y su habilidad para pasivar defectos. Esta tesis se compone de nueve capítulos, que se detallan brevemente a continuación.

El primer capítulo introduce los dos pilares sobre los que se basa esta tesis: las perovskitas y los fullerenos. Se hace una introducción a las características y el desarrollo de estos materiales, así como a los trabajos realizados hasta el incio de la tesis sobre sistemas perovskita-fullereno. Además, se presentan los objetivos de este trabajo.

El segundo capítulo aporta los detalles experimentales sobre las principales técnicas utilizadas en el trabajo de esta tesis para la fabricacion y caracterización de capas y dispositivos de perovskita. Otras características prácticas también son detalladas.

En el tercer capítulo, las capas compuestas de perovskita:C_{70} son presentadas como capas activas útiles para la fabricación de celdas solares de perovskita sin capa

transportadora de electrones eficientes. Se prueba que la presencia de C_{70} beneficia la morfología del film de perovskita, reduciendo ampliamente la densidad de agujeros en ella. Como consecuencia, los dispositivos fabricados a partir de estas capas compuestas muestran una eficiencia y fotoestabilidad mayores. Estos resultados confirman a los fullerenos como candidatos preferentes como aditivos para la fabricación de celdas solares de perovskita sin capa transportadora de electrones estables y eficientes.

En el cuarto capítulo de muestra cómo las capas compuestas perovskita:C_{70} se ven muy afectadas por las características de la disolución de perovskita, en términos de propiedades de film y dispositivo. En particular, la adición de disolventes aromáticos en pequeños volúmenes relativos a la disolución de perovskita aumenta aún más el efecto positivo de los fullerenos, dando lugar a celdas solares de perovskita sin capa transportadora de electrones aún más eficientes. La combinación de técnicas microscópicas sugirió que el uso de los codisolventes estaba condicionando cómo los fullerenos se distribuían en la capa de perovskita. Los disolventes aromáticos en particular reducían la densidad de agujeros en estas capas, en comparación con los análogos alifáticos. La explicación a esto podría ser la habilidad de los fullerenos de interactuar preferentemente con los disolventes aromáticos que con los disolventes típicos utilizados para disolver los precursores de perovskita, como fue probado por una serie de técnicas espectroscópicas. De esta manera, los codisolventes aromáticos estarían evitando la agregación de los fullerenos, promoviendo su distribución más homogénea en la capa de perovskita.

En el quinto capítulo, se comprueba que los fullerenos derivatizados generan un mayor incremento en la eficiencia de las celdas solares de perovskita, frente a los fullerenos no funcionalizados. En particular, valores altos y reproducibles de eficiencia fueron logrados (i.e. >14% para dispositivos sin capa transportadora de electrons) combinando un nuevo fullereno con un grupo funcional isoxazolínico con la estrategia del codisolvente del capítulo anterior. Los derivados de fullereno, que fueron diseñados con el fin de tener propiedades electrónicas específicas, demostraron la existencia de una correlación entre su valor de LUMO y el de V_{oc} de los dispositivos, lo cual sugiere que los fullerenos presentan un rol electrónico cuando son utilizados en capas compuestas de perovskita. De hecho, esto fue probado posteriormente en un trabajo en colaboración con

medidas de fotoluminiscencia resuelta en el tiempo, demostrando que existe una transferencia electrónica de la perovskita al fullereno en la escala de los picosegundos. Sin embargo, se comprueba que el aumento en la fotoestabilidad es independiente de la estructura del fullereno, sugiriendo que es el núcleo de la estructura del fullereno la responsable del proceso involucrado en el aumento de la estabilidad de los dispositivos.

En el sexton capítulo, las interaciones entre la perovskita y los fullerenos en la disolución de los precursores han sido identificadas a través de una serie de técnicas espectroscópicas. Primero, el núcleo del fullereno se complejaría preferentemente con PbI_2, lo que afectaría globalmente al complejo completo en disolución. Segundo, la funcionalización del núcleo de fullereno con una base de Lewis permitiría a los fullerenos formar complejos más fuertes con la perovskita al ser capaces de establecer al mismo tiempo enlaces no-covalentes con las aminas de los precursores de perovskita. La diferente fuerza con la que los fullerenos se complejan a la perovskita se vio que también afectaba directamente a las propiedades en capa y dispositivo. En este sentido, las celdas solares de perovskita más eficientes se obtuvieron a partir de las disoluciones en las que se formaban los complejos perovskita-fullereno más fuertes. Además, se observó que los beneficios de utilizar esta estrategia eran universales para diferentes configuraciones de celdas solares de perovskita. En particular, para dispositivos sin capa transportadora de electrones y p-i-n se observó un aumento de los parámetros fotovoltaicos y la reproducibilidad, mientras que para los dispositivos n-i-p el fill factor era el parámetro más beneficiado.

Las conclusiones de este trabajo se resumen en el capítulo siete, colocándolos en el contexto científico y dándoles la relevancia correspondiente de acuerdo con el impacto que han tenido en el desarrollo del campo. Un artículo adicional analiza con perspectiva los principales beneficios de los fullerenos en celdas solares de perovskita, así como sus futuros retos, poniendo sobre la mesa la contribución de esta tesis para avanzar en ellos.

El capítulo ocho reune las contribuciones del trabajo incluido en esta tesis, considerando publicaciones en revistas de alto impacto y comunicaciones verbales en congresos.

La tesis se cierra con el capítulo nueve, conteniendo los anexos referenciados en el texto principal.

En general, esta tesis representa una contribución significante al desarrollo de celdas solares de perovskita eficientes y estables, a través del empleo de capas compuestas perovskita:fullereno en procesos de un paso, disolviendo el fullereno en la disolución de los precursores de perovskita. Esta tesis no se limita a la aplicación de estas capas, sino que también contiene una estrategia de codisolvente ampliamente estudiada para la optimización de este método. Además, el alcance de esta estrategia se investiga para diferentes fullerenos funcionalizados, probando diferentes relaciones estructura-rendimiento, así como conocimiento añadido en el origen del efecto positivo de los fullerenos en la estabilidad de los dispositivos. Finalmente, se estudian las interacciones entre la perovskita y los fullerenos, probando que los grupos funcionales de los fullerenos para su uso en celdas solares de perovskita tienen un efecto importante en las propiedades en film y dispositivo. En resumen, esta tesis representa una guía para la comunidad científica para el uso de capas compuestas perovskita:fullereno para su uso en la fabricación de celdas solares de perovskita de cualquier configuración, haciendo estudiado en especial detalle aquellas sin capa transportadora de electrones.

# 1	Introduction

## 1.1	Introduction

One of the ways to look at the history of humanity is the obstinate search for new sources of energy, from the earliest uses of combustion for heating and cooking and the constructions of windmills for transforming wind energy into mechanical one, to the more sophisticated nuclear energy. However, there had not been invented yet the manner to harness the vast energy source that the Sun constituted for the Earth, until the so awaited landmark was achieved by Bell Laboratories in 1954, producing the first practical photovoltaic (PV) cell with efficiencies around 6%.[1] This discovery paved the way towards the application of solar cells in very diverse technological fields, also due to the high degree of development of the field, reaching high efficiency values of up to the current record of 46.0% for multijunction cells.

Solar cells benefit from the PV effect, which implies the generation of electrical current and voltage under the exposure to light. A material presenting this effect would then generate through excitation an electron-hole pair, which needs to be dissociated and extracted in the corresponding electrodes so as to produce electricity. The performance of a solar cell may be characterized by its current-voltage (*J-V*) characteristics under solar radiation. From the obtained *J-V* curve (Figure 1.1), the representative PV parameters can be defined. The current density of the device at *V* equal to zero, i.e. current density when the electrodes are short-circuited, named the short-circuit current density (J_{sc}) will depend on the absorption and photon-conversion properties of the solar cell. When the current flowing in the cell external circuit is zero, the highest *V* value that a solar cell can have is reached, named open-circuit voltage (V_{oc}). In a p-n junction, the V_{oc} would be the difference in the quasi-Fermi levels of electrons and holes. Finally, the fill factor (FF) is a parameter that determines the part under the curve that will be actual photoconverted energy. This parameter is directly related to voltage at maximum power point (V_{mpp}), which is the *V* value at which the FF will be the largest, and so the efficiency. This point will also have its current-density at maximum power point (J_{mmp}). The filling of the curve will depend on its shape, and therefore on the ability of the solar cell to generate high currents at high voltages, being ideal to have a current density equal

to J_{sc} at V higher than zero. This will depend on the different resistance terms that the device exerts on the charges transport and extraction, which are the series (R_s) and shunt resistances (R_{sh}). Finally, the power conversion efficiency (PCE) of the solar cell will be calculated with the Equation 1, combining the PV parameters J_{sc}, V_{oc} and FF, and the intensity of the irradiance.
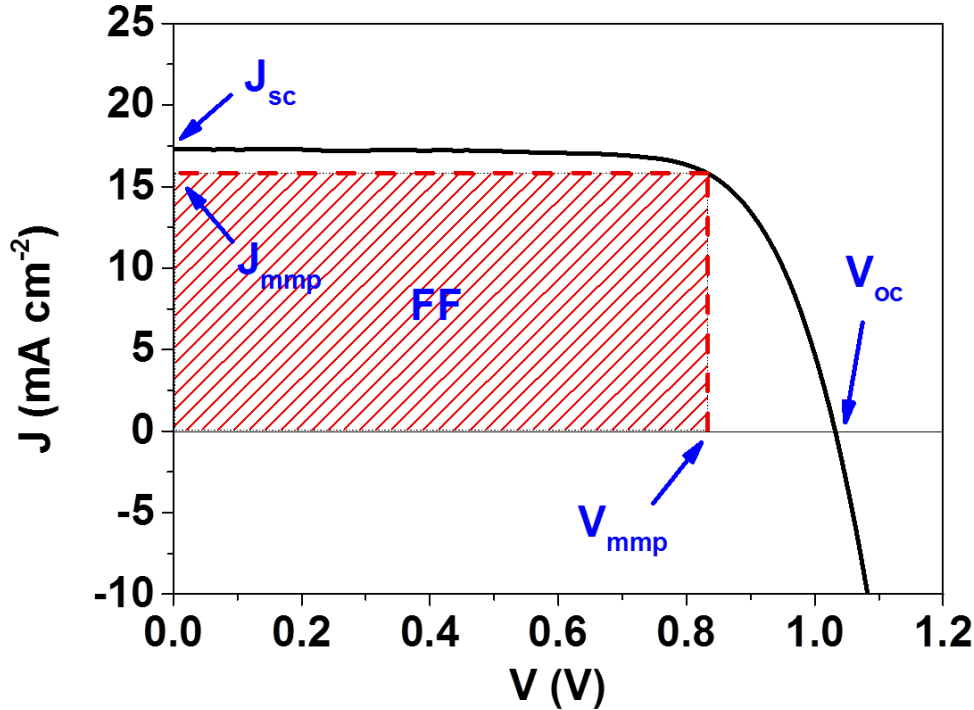
Figure 1.1. *J-V* characteristics of a solar cell and the main PV parameters.

$$PCE = \frac{J_{sc} \cdot V_{oc} \cdot FF}{Total\ irradiance}$$

Equation 1.1. Calculation of PCE from PV parameters.

In the last decades it has experienced the dawn of new types of PV devices containing organic parts.[2-5] These cells, named for their composition as organic photovoltaic (OPV) devices,[6] or hybrid-organic,[7] presented many differences in respect to the predominant silicon ones. The organic content brought several advantages, such as high absorption coefficient and easy processability, as the devices could be fabricated in such varied arrangements as vacuum-deposited, layered,[8-9] or in a bicontinuous mix of n- and p-phases known as bulk heterojunction (BHJ).[10] This allowed the coexistence of new

molecules and new fabrication methods like solution-processing, expanding the potential and possibilities of these technologies.

1.2   Perovskite solar cells: definition and properties

Since the first report in OPV in 1985,[11] the progress for this type of devices has been considerable.[6] These solar cells characterize for a high exciton binding energy, meaning that the absorption of light produces neutral electron-hole pairs. A diffusion of the exciton to an interface is required for dissociating it into free charges.[12] However, the recently discovered new type of hybrid materials for PV application, named lead halide perovskites, work elseways. Perovskite solar cells (PSCs), which have shaken in the last years the whole PV panorama, generate excitons with a low binding energy, therefore producing free charges (electrons and holes) in the perovskite layer, in contrast to OPV.[13] This and the rest of unique optoelectronic properties that this PV material holds are a result of the special characteristics of the hybrid perovskite material.

Perovskite compounds characterize for holding a certain crystalline structure, i.e. the same one as $CaTiO_3$, which was named after its discovery by the Russian scientist Lev Perovski. But not every perovskite material can be used to produce and separate charges through light absorption. In this regard, lead halide perovskites are the ones attracting the highest attention in the PV field. In this case, considering that perovskite structure has the formula ABX_3, for light-harvesting original perovskite materials A stands for an organic cation like methylammonium (MA), B for a metallic cation such as Pb^{2+} and X^- for a halide anion, originally iodide. The crystalline structure is based on layers of metallic halides with intercalated organic cation ones. Since the first reported study of PSCs by Kojima et al. in 2009,[14] the most used perovskite has been the methylammonium lead iodide ($MAPbI_3$), but it was followed by several studies on the modification of its structure. MA was successfully substituted by other organic cations of different size, like formamidinium (FA),[15] for which was found that the bandgap of the perovskite could be easily manipulated for broader absorption, or even metals, such as Cs.[16] It was also found that by modifying the anionic part of the structure, and in this sense bromide has been widely employed for substituting iodide, the bandgap can also

be tailored.[17] Finally, due to the toxicity and bioavailability of Pb, several efforts trying to remove it from PSCs have been carried out. Mainly, Sn has been used, but it faces stability issues due to the oxidation of Sn^{2+} to Sn^{4+}, additionally to some toxicity-related ones too.[18-20] The secret behind perovskite materials is their high light absorption in the visible range and high extinction coefficient, which allows achieving high photocurrent values with thin-film devices. In fact, the unique properties of perovskite allowed a fast development of this technology, quickly improving the initial 3.8% efficiency to values as high as 24.2% (i.e. significantly higher than the ones for OPV).[1]

Nevertheless, the research in PSCs is not only restricted to perovskite film study, but also to the parts that allow the device to separate charges. In fact, interfacial engineering is one of the most relevant aspects when building PSCs. These devices are composed of different layers that all together are able to generate, separate and extract the electric charges. In this case, generation of charges is done in the photoactive layer, which is the perovskite, while the charges are extracted in the electron- and hole-transporting layers (ETL and HTL, respectively, acting as selective contacts for electrons and holes) and directed towards the electrodes. The devices can even be structured in two different architectures, depending on the arrangement of the electronic levels of the different layers. In particular, PSCs can be built in n-i-p or p-i-n (Figure 1.2) configurations, in which the electrons are extracted towards the back contact and the top contact, respectively, being the opposite for the holes. These electrons and holes are separated and extracted thanks to the proper electronic alignment of the different layers, promoting the extraction of the charges by the existence of a favorable energy difference (Figure 1.3). In other words, HTL should have HOMO energy slightly higher than the valence band (VB) from perovskite so that the extraction of the holes is favorable and feasible, while LUMO energy should be much higher compared to the conduction band (CB) of perovskite so that the path of electrons is effectively blocked. In an opposite way, the ETL should have a slightly lower LUMO energy than the CB of perovskite and much lower HOMO than the VB of perovskite, as it is the responsible for extracting electrons and blocking holes. Finding the best charge transporting materials is therefore not trivial and really makes a difference. In fact, one of the key breakthroughs for the success of PSCs was the synthesis and application of 2,2',7,7'-tetrakis-(*N*,*N*-di-4-

methoxyphenylamino)-9,9'-spirobifluorene (spiro-OMeTAD), a hole-transporting material (HTM) that helped improving n-i-p configuration devices.[21,22] Not only HTLs, but ETLs of different nature were also developed, from planar ones like compact ZnO[23] or SnO$_2$,[24] to mesoporous scaffolds of TiO$_2$ or Al$_2$O$_3$.[21]
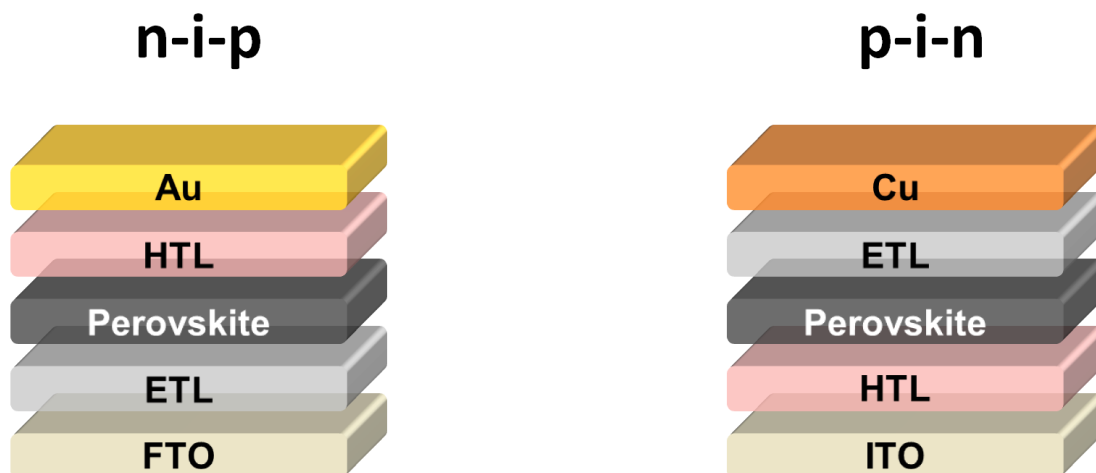

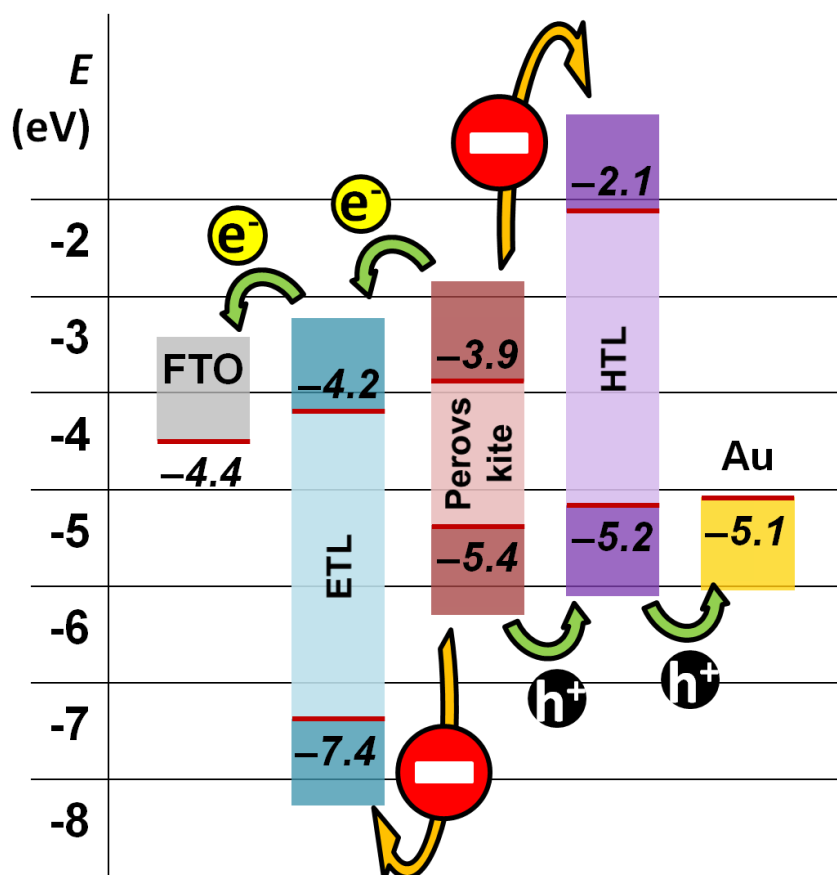**Figure 1.2.** n-i-p and p-i-n PSC architectures.

Figure 1.3. Energy level diagram of the different layers for a PSC of n-i-p configuration. The energy levels shown for perovskite, ETL and HTL belong to MAPbI$_3$, TiO$_2$ and spiro-OMeTAD, respectively.

So, considering all the advancements in the PSC field in so few years and all its advantages, current challenges should also be addressed. Perovskite improvements towards applicability in industry still need to overcome certain issues. The main challenges PSCs still face are related to the device performance, since, even if high efficiency cells keep improving with further research, the solar cells present strong hysteresis[25] and instability evidences.[26] The first one is related to the different *J-V* curve obtained for the device when the voltage is forward or reverser scanned. This directly affects the final efficiency of the device, and it has been claimed to have some relationship with the ion migration phenomenon characteristic from lead halide perovskites.[27] On the other hand, perovskite solar cells suffer from several stability issues. Perovskite materials for PV applications undergo various degradation processes that hinder the solar cell performance in the long-term. These have different origins, like thermal-, moisture- or oxygen-related decomposition but can also be caused as a side effect of the working mechanism of the devices.[28] In fact, the ion migration generated under operation of the cell has been linked to the origination of hysteresis, and the accumulation of defects in the interfaces affect negatively the cell performance.[28,29] Moreover, as it has been addressed in the literature, defects at perovskite grain boundaries are very active recombination sites.[30] Related to this, recombination processes are one of the main sources of loss of efficiency in the devices. Therefore, further knowledge on the perovskite defects, their passivation and processing conditions that allowed achieving better perovskite films by removing or limiting these defects would pave the way towards highly efficient and stable PSCs.

1.3   Fullerenes in perovskite solar cells

To understand how fullerenes could work this way in PSCs, knowing about their structure and physicochemical properties is a compulsory task. Fullerenes are a specific allotrope of carbon, made out of single and double bonds leading to a closed structure. The most famous fullerene, C_{60} (Figure 1.4a) has a sphere-shape structure containing 20 hexagons and 12 pentagons. X-ray diffraction (XRD) analysis confirmed, in contrast to what was thought, that the insaturated nature of fullerenes does not lead to a completely

aromatic molecule, but to a polyenic one.[31] Additionally, this family of molecules are known for their electron-accepting character. Also, their LUMO is triple-degenerated, being able to show the reduction peaks of up to 6 electrons, as first demonstrated experimentally for C_{60} by Echegoyen and co-workers by cyclic voltammetry characterization.[32]

As electron deficient molecules, fullerenes provide several ways for functionalization, and therefore the possibility to tailor their physicochemical properties for specific targeted purposes.[33,34] In this sense, the derivatization of fullerenes have led to completely unrelated applicabilities like, for instance, human immunodeficiency virus (HIV) inhibition with thiol-containing fullerenes,[35] or the well-known phenyl-C_{61}-butyric acid methyl ester (PCBM) shown in Figure 1.4b,[36] as n-type semiconductor for organic field-effect transistors (OFETs)[37] or PV devices.[38] In this sense, fullerenes can undergo several reactions, being the nucleophilic additions (e.g. Bingel reaction)[39] and cycloadditions (e.g. Prato reaction)[33] the most common ones. Nevertheless, these are just few examples of the high variety of synthetic opportunities that fullerenes offer. The chemical knowledge of these molecules kept increasing, and so did the available molecules for materials science applications. As an example of a purpose for the chemical functionalization of fullerenes, several studies have carried out in order to midify their hydrophobicity, whether for promoting some interactions or for facilitating its processing, as well as on tailoring its optoelectronic properties for different device applications.[33,34]
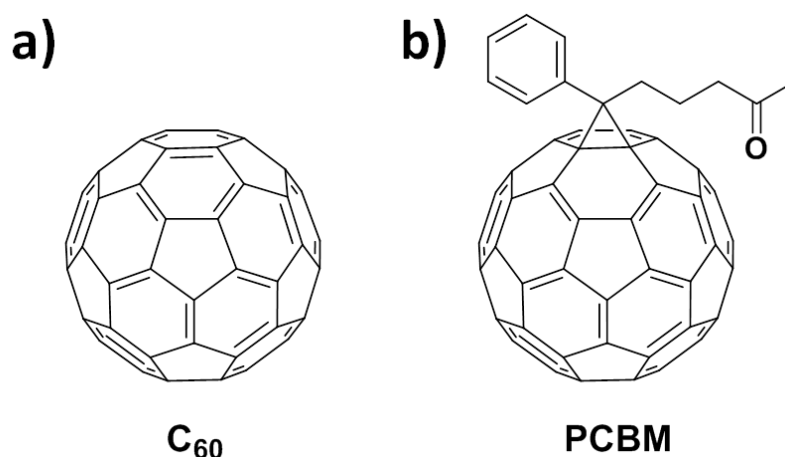

Figure 1.4. Molecular structures of a) C_{60} and b) PCBM.

In fact, their n-type semiconducting character is the main reason behind all their applications in different electronic devices. Translated to the case of PSCs field, fullerenes hold unique properties for their use as ETL. From the early years of PSC field development, fullerenes have been used mainly for ETL purposes for p-i-n devices.[40-49] Devices of p-i-n architecture imply that the ETL must be processable in compatible conditions with the layers below, particularly at a temperature that does not damage the perovskite layer. This means that traditional inorganic ETLs used in n-i-p devices cannot be used here. And fullerenes were the best candidate to solve this. PCBM was by far the most used fullerene,[40-45] due to the much higher solubility compared to pristine C_{60} and therefore much easier to solution-process. Nevertheless, other fullerene derivatives such as indene-C_{60} bisadduct (ICBA),[40,46,47] the isomeric mixture of the C_{70} analogue of PCBM, $PC_{71}BM$,[48] or an amine-derivatized DMAPA-C_{60}[49] were also successfully proposed, in this case as interlayers, achieving higher efficiency values than those obtained with PCBM. In the work by Liang and co-workers,[46] PBCM and ICBA were compared with C_{60}, pointing out that increased electron mobility of the fullerene led to higher solar cell performance. But in general, the FF increased when suitable fullerene derivatives were used.[47-49] The authors of the respective studies attribute these outcomes to the ability of the fullerenes they used to passivate trap states in the perovskite interface. Other findings by these groups suggest that $PC_{71}BM$ can also enhance V_{oc}, apart from FF, due to the decrease of the series resistance,[48] or that fullerenes with better surface coverage such as DMAPA-C_{60} can improve the physical and chemical stabilities of the PSC.[49]

However, fullerenes were also used in n-i-p devices for interface modification. Even if they could not compete with TiO_2 or SnO_2 ETLs, their ability as defect passivating agents made them very appealing molecules for modifying the ETL surface. In this sense, the multiply branched fullerene PCBB-2CN-2C8 was used to cover the TiO_2 ETL surface in the work by the group of Li.[50] The fullerene passivated the trap states on the TiO_2 layer surface, improving the V_{oc} and FF of the cells in 0.07 V and 7%, respectively. This increase was also seen for the study of fullerene self-assembled monolayer (SAM) for TiO_2 layer coverage by Abrusci and colleagues.[51] Using this TiO_2/C_{60}-SAM configuration, Wojciechowski and co-workers also found great improvement in the

stability of the devices compared to perovskites deposited on bare TiO_2, suggesting that the presence of fullerene greatly enhanced the electron extraction from the perovskite layer.[52] In another work carried out by the same group, a fullerene was derivatized with a benzoic acid moiety, which would be able to anchor on the TiO_2 surface forming a SAM.[53] The authors found that the presence of this fullerene was highly reducing the hysteresis of the cells, which in the TiO_2 as ETL-containing cells tended to be problematic.

Additionally, due to their low-temperature processing, their use as ETL in n-i-p devices was also interesting towards flexible devices fabrication. It has to be taken into account that TiO_2, the traditional and most used ETL in this configuration, is processed at very high temperatures that flexible substrates do not bear. An interesting study on rigid substrates employing fullerenes was reported by Collavini and colleagues.[54] The authors deposited layers of C_{60} and C_{70} on fluorine-doped tin oxide (FTO) as ETL for n-i-p devices. The efficiency was further improved when the perovskite layer was saturated with the corresponding fullerene, in order to avoid the degradation of the fullerene layer during the perovskite deposition process. These results suggest that fullerenes could be perfect candidates for the development of n-i-p flexible substrates.

Therefore, we know the important role that fullerenes played in the early scenario of PSCs development as ETLs, especially in p-i-n configurations. They hold great n-type semiconducting nature, and have additionally a passivating character that allows reducing the hysteresis of the devices and improving their performance and stability. Looking at the great benefits of these molecules, there is still to discover if all their potential has been properly exploited. Their working mechanism is not figured out yet, while their electron extraction and passivating abilities make us question if they as ETLs can give all they have.

In fact, during the accomplishment of the thesis, the field kept investigating fullerene in PSCs with p-i-n configuration, finding new insights on the origin of the beneficial character of fullerenes.[55,56] The interest of the community on fullerenes as ETL promoted the incorporation of many new derivatives,[56-58] allowing the improvement of PV parameters.[59-62] In this regard, a study by Shao and colleagues did find out how the

V_{oc} of the solar cell was correlated with the quasi-Fermi level of the fullerene deposited on top of perovskite.[63] Other relevant works for fullerenes at the charge transporting layer included ZnO nanoparticles anchoring,[64] electropolymerized layers of fullerenes,[65] n-doping of fullerene layers,[66] or the synthesis of a fullerene derivative with oligotriarylamine moieties for working as HTL.[67]

1.4   Perovskite:fullerene blend films

Fullerenes and derivatives have proven their great potential for interfacial modification of PSCs as ETLs or interlayers. However, the results obtained in the work by Shao and colleagues opened a new way for their application.[68] By depositing a [6,6]-phenyl C_{61}-butyric acid methyl ester (PCBM) interlayer between $MAPbI_3$ and C_{60} (Figure 1.5) they eliminated the photocurrent hysteresis that the cells suffered. The authors found a different passivation degree depending on the temperature of the annealing treatment that they applied to the PCBM layer, as supported by trap density of states (tDOS) and Hall effect characterization. It was suggested that fullerenes were percolating into the perovskite layer with the thermal treatment. Overall, this work presented fullerenes as an effective solution for removing hysteresis from perovskite devices.

These results inevitably bring up the next question: does the fullerene need to be incorporated in the perovskite layer so that the cell really gets all the benefits from it? In this line, Xu and co-workers introduced the PCBM as a blend together with the perovskite in the precursor solution.[69] The authors fabricated devices depositing these perovskite solutions on FTO/TiO_2 planar substrates, using spiro-OMeTAD as HTM. The reference devices suffered from strong hysteresis between forward and reverse *J-V* curve measuring directions. Moreover, the FF values were lower than 70%. The use of perovskite:PCBM blend solutions led to devices with no hysteresis, in agreement with the results obtained by Shao and colleagues, with a prominent increase in FF with values of up to 75%. Related with this, DFT calculations and spectroscopy measurements suggested that the fullerene might be involved in some interaction with iodide anions, and therefore passivating PbI_3^- defects. This would in turn limit the recombination processes in the perovskite layer, explaining the improvement in the PV parameters. This

work also included the key point behind the proper application of fullerene. As the studies of fullerenes in PSCs point out, the key role of these molecules may be their defect-passivating character. Nevertheless, they will not work out the same way when introduced somewhere with few defects in perovskites than in the most defect-dense areas, in the same way that it is not the same to use the fullerene as ETL or inside the perovskite layer. In a specific experiment Xu et al. used high concentrations of PCBM to promote their aggregation, so as to see where the fullerenes were distributing.[69] It was seen that the fullerene was accumulating at the grain boundaries, which have high density of defects. It is therefore concluded that the use of fullerenes inside the perovskite layer promotes an efficient passivation of defects throughout the film. Based on the same strategy, Wang and co-workers introduced a 10 times-carboxylic acid-substituted fullerene inside the perovskite layer, which led also to an improvement in the FF.[70] This finding suggests that the functional groups might be playing too a role in the annihilation of defects in the layer, indicating the high possibilities for derivatizing fullerenes for specific applications in perovskite:fullerene blend films. In the same way, such an undiscovered field brings to mind everything still to be found out. The study of these composites would shed light on their working mechanism and pave the way towards their efficient application in PSCs standard protocols.
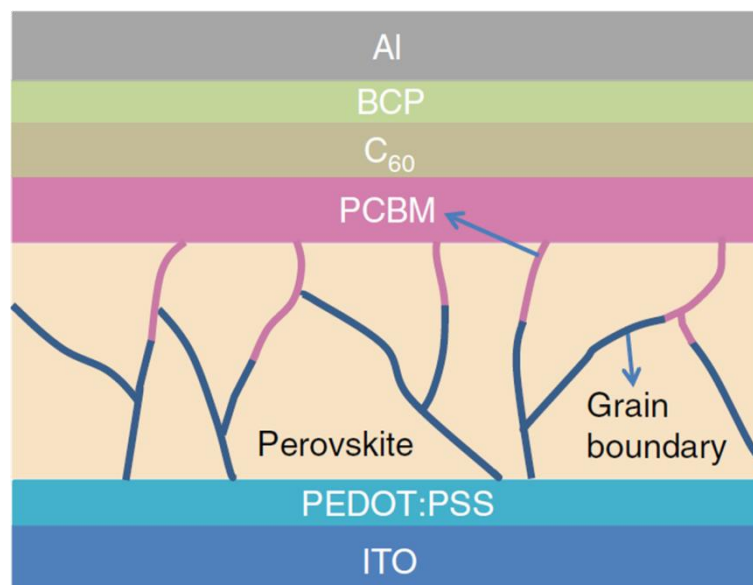

Figure 1.5. Device architecture by Shao et al. with percolating PCBM as ETL on top of perovskite.[68]

All in all, the studies on solar cells based on perovskite:fullerene blend films were quite limited at the beginning of this PhD thesis. Nevertheless, these few reports suggested the

great potential of fullerenes as passivating agents of perovskite defects, finding large improvements in hysteresis reduction and PV parameters. At the same time, several questions about the fullerene role in this kind of devices were opened, and the need for more knowledge on perovskite:fullerene blends was more and more evident. A better understanding on these layers would allow establishing advanced processing protocols in order to enhance the control of the fullerene integration into the perovskite:fullerene blend films. In the same line, it opens the way towards simplified configurations where the ETL and the absorbing layer are processed in a single step. In a more advanced scenario, the functionalization of fullerenes would be tailored in order to achieve optimized interactions with perovskite for the passivation of defects.

1.5   Objetives and outline of the thesis

The scenario of the PSC field at the beginning of this thesis was very promising. Great advances were being achieved in terms of efficiency in a very short period of time. Additionally, the hybrid perovskites present such versatility that they could be easily applied to different substrates and device architectures, and the possibilities for developing new types of charge-transporting materials were still huge. Yet, this technology was far from being applied in the industry. It had big deficiencies, such as hysteretic behavior and device stability issues. Some reports in literature on the use of fullerenes in PSCs as ETL pointed out the potential of these molecules to deal with these problems. In addition, few recent works suggested that the incorporation of fullerene derivatives inside the perovskite layer induced a reduction of the hysteresis.[68-70] In fact, the authors successfully achieved an improvement in the device performance, addressing them to the ability of these carbon allotropes to passivate defects in the perovskite film. These defects are known source for performance and stability loss, thus limiting them would provide strategies for tackling current perovskite field issues.

With this context, the present thesis aims to develop new strategies for the full exploitation of fullerenes in PSC, being their potential to be included during the perovskite film processing and passivate defects among the main key features. The objectives of the thesis are the following ones:

1. Development of strategies for the successful application of perovskite:fullerene blends in PSC based on films with potential high density of defects.

2. Development of strategies for controlling the distribution of fullerenes in the perovskite layer, with particular interest on passivating defects at the perovskite grain boundaries.

3. Study of the relationship of physicochemical properties of a set of structurally different fullerenes with their performance in solar cells, using perovskite:fullerene blends.

4. Study of the perovskite-fullerene interactions and their implications in the morphology and solar cell performance of perovskite:fullerene blends. Design and application of a novel fullerene for optimized perovskite-fullerene interactions.

In order to accomplish these objectives, the starting point will consider the simplest materials and solar cell architectures, so that the least factors are affecting the results. In this sense, MAPbI$_3$ perovskite will always be used. In the same way, non-derivatized fullerenes will be applied. Taking into account the low solubility of C$_{60}$, C$_{70}$ will be chosen as starting material. The device configuration that will be used in the first stages will be the ETL-free one, taking into account the poor quality morphology of perovskite films deposited on bare FTO and the potential high density of defects in them. The obtainment of satisfactory results in these systems would be followed by the implementation of the strategy on other types of PSC architectures.

The work is presented in accordance to the following outline (Figure 1.6):

In chapter 2, a presentation of the techniques and methods used in the next chapters for PSC fabrication and characterization is given.

Chapter 3 contains the development of perovskite:C$_{70}$ blend films for ETL-free devices, explaining the beneficial character of this fullerene towards improving the performance of this kind of devices.

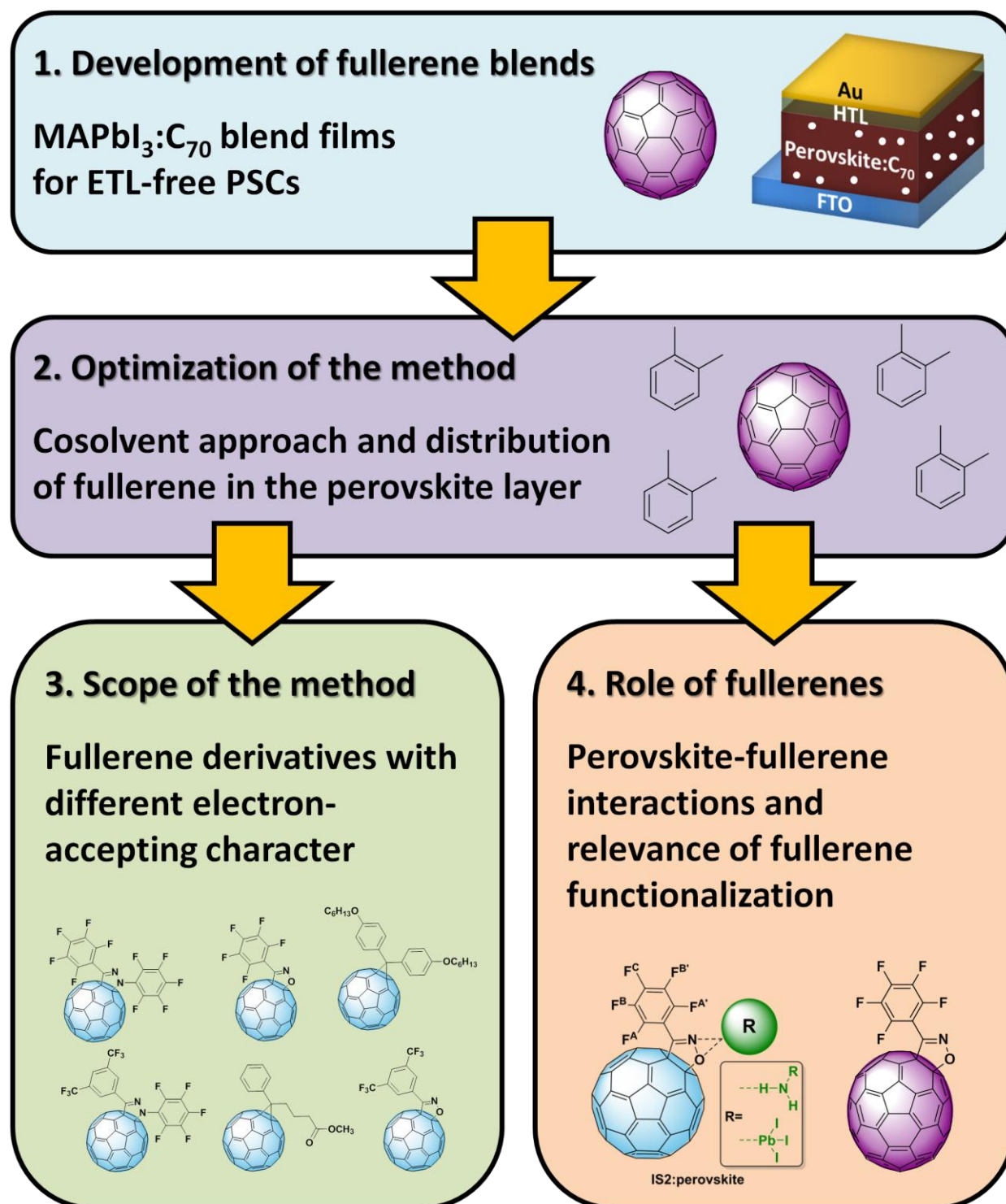**Figure 1.6.** Scheme of the research plan followed in the present thesis.

In chapter 4, the use of *o*-xylene as cosolvent in the perovskite:fullerene film processing for the enhancement of the efficiency is proposed. Additionally, the effect of the nature of the cosolvent used for perovskite:C_{70} blend films processing is explained. Implications of the cosolvent type on morphological and device characteristics are

provided, suggesting the application of mixtures with aromatic cosolvents for perovskite:C_{70} film processing.

Once the FTO/MAPbI$_3$:C_{70} architecture was optimized and its insights unraveled, chapters 5 and 6 go beyond and display the search for an optimized fullerene structure for the application in all kind of PSCs. In chapter 5, the use of fullerenes with isoxazoline, pyrazoline and methano functionalizations for tailored electrochemical properties is presented. An isoxazoline derivative led to the best-performing ETL-free PSC at that time. Similarly, in chapter 6 the interactions governing the perovskite-fullerene systems are investigated and discussed, linking them to perovskite morphology and device performance. The findings allowed the design of a structurally-optimized fullerene and its application for the enhancement of the performance of cells with different architectures.

Finally, the relevance of this work for the development of the field is commented in Chapter 7, not only summarizing the most relevant findings, but also providing with a critical view on the future of perovskite:fullerene blend films.

1.6   References

[1]   NRELBest Research-Cell Efficiencies: https://www.nrel.gov/pv/assets/pdfs/best-reserch-cell-efficiencies.pdf, accessed: June, 2019.

[2]   H. Spanggaard, F. C. Krebs. A Brief Story of the Development of Organic and Polymeric Photovoltaics. *Sol. Energy Mater. Sol. Cells.* **2004**, *83*, 125.

[3]   H. Hoppe, N. S. Sariciftci. Organic Solar Cells: An Overview. *J. Mater. Res.* **2004**, *19*, 1924.

[4]   D. Wohrle, D. Meissner. Organic Solar Cells. *Adv. Mater.* **1991**, *3*, 121.

[5]   S. Günes, H. Neugebauer, N. S. Sariciftci. Conjugated Polymer-Based Organic Solar Cells. *Chem. Rev.* **2007,** *107*, 1324.

[6]   A. Mishra, P. Bäuerle. Small Molecule Organic Semiconductors on the Move: Promises for Future Solar Energy Technology. *Angew. Chem. Int. Ed.* **2012**, *51*, 2020.

[7]   S. D. Stranks, H. J. Snaith. Metal-Halide Perovskites for Photovoltaic and Light-Emitting Devices. *Nat. Nanotechnol.* **2015**, *10*, 391.

[8] M. Liu, M. B. Johnston, H. J. Snaith. Efficient Planar Heterojunction Perovskite Solar Cells by Vapour Deposition. *Nature* **2013**, *501*, 395.

[9] M. Granström, K. Petritsch, A. C. Arias, A. Lux, M. R. Andersson, R. H. Friend. Laminated Fabrication Of Polymeric Photovoltaic Diodes. *Nature* **1998**, *395*, 257.

[10] J. J. M. Halls, C. A. Walsh, N. C. Greenham, E. A. Marseglia, R. H. Friend, S. C. Moratti, A. B. Holmest. Efficient Photodiodes from Interpenetrating Polymer Networks. *Nature* **1995**, *376*, 49.

[11] C. W. Tang. Two-Layer Organic Photovoltaic Cell. *Appl. Phys. Lett.* **1986**, *48*, 183.

[12] B. A. Gregg. Excitonic Solar Cells. *J. Phys. Chem. B* **2003,** *107,* 4688.

[13] V. D'Innocenzo, G. Grancini, M. J. P. Alcocer, A. R. S. Kandada, S. D. Stranks, M. M. Lee, G. Lanzani, H. J. Snaith, A. Petrozza. Excitons versus Free Charges in Organo-Lead Tri-Halide Perovskites. *Nat. Commun.* **2014**, *5*, 3586.

[14] A. Kojima, K. Teshima, Y. Shirai, T. Miyasaka. Organometal Halide Perovskites as Visible-Light Sensitizers for Photovoltaic Cells. *J. Am. Chem. Soc.* **2009**, *131*, 6050.

[15] G. E. Eperon, S. D. Stranks, C. Menelaou, M. B. Johnston, L. M. Herz, H. J. Snaith. Formamidinium Lead Trihalide: A Broadly Tunable Perovskite for Efficient Planar Heterojunction Solar Cells. *Energy Environ. Sci.* **2014**, *7*, 982.

[16] M. Saliba, T. Matsui, J.-Y. Seo, K. Domanski, J.-P. Correa-Baena, M. K. Nazeeruddin, S. M. Zakeeruddin, W. Tress, A. Abate, A. Hagfeldt, M. Grätzel. Cesium-Containing Triple Cation Perovskite Solar Cells: Improved Stability, Reproducibility and High Efficiency. *Energy Environ. Sci.* **2016**, *9*, 1989.

[17] J. H. Noh, S. H. Im, J. H. Heo, T. N. Mandal, S. I. Seok. Chemical Management for Colorful, Efficient, and Stable Inorganic-Organic Hybrid Nanostructured Solar Cells. *Nano Lett.* **2013**, *13*, 1764.

[18] F. Hao, C. C. Stoumpos, D. H. Cao, R. P. H. Chang, M. G. Kanatzidis. Lead-Free Solid-State Organic-Inorganic Halide Perovskite Solar Cells. *Nat. Photonics* **2014**, *8*, 489.

[19] N. K. Noel, S. D. Stranks, A. Abate, C. Wehrenfennig, S. Guarnera, A.-A. Haghighirad, A Sadhanala, G. E. Eperon, S. K. Pathak, M. B. Johnston, A. Petrozza, L. M. Herz, H. J. Snaith. Lead-Free Organic-Inorganic Tin Halide Perovskites for Photovoltaic Applications. *Energy Environ. Sci.* **2014**, *7*, 3061.

[20] A. Babayigit, D. D. Thanh, A. Ethirajan, J. Manca, M. Muller, H.-G. Boyen, B. Conings. Assessing the Toxicity of Pb-and Sn-Based Perovskite Solar Cells in Model Organism *Danio rerio. Sci. Rep.* **2016**, *6*, 18721.

[21] M. M. Lee, J. Teuscher, T. Miyasaka, T. N. Murakami, H. J. Snaith. Efficient Hybrid Solar Cells Based on Meso-Superstructured Organometal Halide Perovskites. *Science* **2012**, *338*, 643.

[22] H.-S. Kim, C.-R. Lee, J.-H. Im, K.-B. Lee, T. Moehl, A. Marchioro, S.-J. Moon, R. Humphry-Baker, J.-H. Yum, J. E. Moser, M. Grätzel, N.-G. Park. Lead Iodide Perovskite Sensitized All-Solid-State Submicron Thin Film Mesoscopic Solar Cell with Efficiency Exceeding 9%. *Sci. Rep.* **2012**, *2*, 591.

[23] D. Liu, T. L. Kelly. Perovskite Solar Cells with a Planar Heterojunction Structure Prepared Using Room-Temperature Solution Processing Techniques. *Nat. Photonics* **2014**, *8*, 133.

[24] W. Ke, G. Fang, Q. Liu, L. Xiong, P. Qin, H. Tao, J. Wang, H. Lei, B. Li, J. Wan, G. Yang, Y. Yan. Low-Temperature Solution-Processed Tin Oxide as an Alternative Electron Transporting Layer for Efficient Perovskite Solar Cells. *J. Am. Chem. Soc.* **2015**, *137*, 6730.

[25] H. J. Snaith, A. Abate, J. M. Ball, G. E. Eperon, T. Leijtens, N. K. Noel, S. D. Stranks, J. T.-W. Wang, K. Wojciechowski, W. Zhang. Anomalous Hysteresis in Perovskite Solar Cells. *J. Phys. Chem. Lett.* **2014**, *5*, 1511.

[26] T. Leijtens, G. E. Eperon, N. K. Noel, S. N. Habisreutinger, A. Petrozza, H. J. Snaith. Stability of Metal Halide Perovskite Solar Cells. *Adv. Energy Mater.* **2015**, *5*, 1500963.

[27] B. Chen, M. Yang, S. Priya, K. Zhu. Origin of *J-V* Hysteresis in Perovskite Solar Cells. *J. Phys. Chem. Lett.* **2016**, *7*, 905.

[28] Y. Yuan, J. Huang. Ion Migration in Organometal Trihalide Perovskite and its Impact on Photovoltaic Efficiency and Stability. *Acc. Chem. Res.* **2016**, *49*, 286.

[29] J. M. Azpiroz, E. Mosconi, J. Bisquert, F. De Angelis. Defect Migration in Methylammonium Lead Iodide and its Role in Perovskite Solar Cell Operation. *Energy Environ. Sci.* **2015**, *8*, 2118.

[30] R. Long, J. Liu, O. V. Prezhdo. Unravelling the Effects of Grain Boundary and Chemical Doping on Electron-Hole Recombination in $CH_3NH_3PbI_3$ Perovskite by Time-Domain Atomistic Simulation. *J. Am. Chem. Soc.* **2016**, *138*, 3884.

[31] J. M. Hawkins, A. Meyer, T. A. Lewis, S. Loren, F. J. Hollander. Crystal Structure of Osmylated C_{60}: Confirmation of the Soccer Ball Framework. *Science* **2003**, *252*, 312.

[32] Q. Xie, E. Perez-Cordero, L. Echegoyen. Electrochemical Detection of C_{60}^{6-} and C_{70}^{6-}: Enhanced Stability of Fullerides in Solution. *J. Am. Chem. Soc.* **1992**, *114*, 3978.

[33] M. Maggini, G. Scorrano, M. Prato. Addition of Azomethine Ylides to CM: Synthesis, Characterization, and Functionalization of Fullerene Pyrrolidines. *J. Am. Chem. Soc.* **1993**, *115*, 9798.

[34] R. C. Haddon, A. S. Perel, R. C. Morris, T. T. M. Palstra, A. F. Hebard, R. M. Fleming. C_{60} Thin Film Transistors. *Appl. Phys. Lett.* **1995**, *67*, 121.

[35] E. A. Khakina, A. A. Yurkova, A. S. Peregudov, S. I. Troyanov, V. V. Trush, A. I. Vovk, A. V. Mumyatov, V. M. Martynenko, J. Balzarini, P. A. Troshin. Highly Selective Reactions Of $C_{60}Cl_6$ with Thiols for the Synthesis of Functionalized [60]Fullerene Derivatives. *Chem. Commun.* **2012**, *48*, 7158.

[36] J. C. Hummelen, B. W. Knight, F. LePeq, F. Wudl. Preparation and Characterization of Fulleroid and Methanofullerene Derivatives. *J. Org. Chem.* **1995**, *60*, 532.

[37] C. Yang, S. Cho, A. J. Heeger, F. Wudl. Heteroanalogues of PCBM: N-Bridged Imino-PCBMs for Organic Field-Effect Transistors. *Angew. Chem. Int. Ed.* **2009**, *48*, 1592.

[38] J. Y. Kim, K. Lee, N. E. Coates, D. Moses, T.-Q. Nguyen, M. Dante, A. J. Heeger. Efficient Tandem Polymer Solar Cells Fabricated by All-Solution Processing. *Science* **2007**, *317*, 222.

[39] C. Bingel. Cyclopropanierung von Fullerenen. *Chem. Ber.* **1993**, *126*, 1957.

[40] J.-Y. Jeng, Y.-F. Chiang, M.-H. Lee, S.-R. Peng, T.-F. Guo, P. Chen, T.-C. Wen. $CH_3NH_3PbI_3$ Perovskite/Fullerene Planar-Heterojunction Hybrid Solar Cells. *Adv. Mater.* **2013**, *25*, 3727.

[41] S. Sun, T. Salim, N. Mathews, M. Duchamp, C. Boothroyd, G. Xing, T. C. Sum, Y. M. Lam. The Origin of High Efficiency in Low-Temperature Solution-Processable Bilayer Organometal Halide Hybrid Solar Cells. *Energy Environ. Sci.* **2014**, *7*, 399.

[42] P. Docampo, J. M. Ball, M. Darwich, G. E. Eperon, H. J. Snaith. Efficient Organometal Trihalide Perovskite Planar-Heterojunction Solar Cells on Flexible Polymer Substrates. *Nat. Commun.* **2013**, *4*, 2761.

[43] J. Y. Jeng, K. C. Chen, T. Y. Chiang, P. Y. Lin, T. D. Tsai, Y. C. Chang, T. F. Guo, P. Chen, T. C. Wen, Y. J. Hsu. Nickel Oxide Electrode Interlayer in $CH_3NH_3PbI_3$ Perovskite/PCBM Planar-Heterojunction Hybrid Solar Cells. *Adv. Mater.* **2014**, *26*, 4107.

[44] O. Malinkiewicz, A. Yella, Y. H. Lee, G. M. Espallargas, M. Grätzel, M. K. Nazeeruddin, H. J. Bolink. Perovskite Solar Cells Employing Organic Charge-Transport Layers. *Nat. Photonics* **2014**, *8*, 128.

[45] Y. Bai, H. Yu, Z. Zhu, K. Jiang, T. Zhang, N. Zhao, S. Yang, H. Yan. High Performance Inverted Structure Perovskite Solar Cells Based on a PCBM:Polystyrene Blend Electron Transport Layer. *J. Mater. Chem. A* **2015**, *3*, 9098.

[46] P.-W. Liang, C.-C. Chueh, S. T. Williams, A. K.-Y. Jen. Roles of Fullerene-Based Interlayers in Enhancing the Performance of Organometal Perovskite Thin-Film Solar Cells. *Adv. Energy Mater.* **2015**, 1402321.

[47] Q. Wang, Y. Shao, Q. Dong, Z. Xiao, Y. Yuan, J. Huang. Large Fill-Factor Bilayer Iodine Perovskite Solar Cells Fabricated by a Low-Temperature Solution-Process. *Energy Environ. Sci.* **2014**, *7*, 2359.

[48] C.-H. Chiang, Z.-L. Tseng, C.-G. Wu. Planar Heterojunction Perovskite/PC$_{71}$BM Solar Cells with Enhanced Open-Circuit Voltage via a (2/1)-Step Spin-Coating Process. *J. Mater. Chem. A* **2014**, *2*, 15897.

[49] H. Azimi, T. Ameri, H. Zhang, Y. Hou, C. O. R. Quiroz, J. Min, M. Hu, Z.-G. Zhang, T. Przybilla, G. J. Matt, E. Spiecker, Y. Li, C. J. Brabec. A Universal Interface Layer Based on an Amine-Functionalized Fullerene Derivative with Dual Functionality for Efficient Solution Processed Organic and Perovskite Solar Cells. *Adv. Energy Mater.* **2015**, *5*, 1401692.

[50] Y. Li, Y. Zhao, Q. Chen, Y. M. Yang, Y. Liu, Z. Hong, Z. Liu, Y.-T. Hsieh, L. Meng, Y. Li, Y. Yang. A Multifunctional Fullerene Derivative for Interface Engineering in Perovskite Solar Cells. *J. Am. Chem. Soc.* **2015**, *137*, 15540.

[51] A. Abrusci, S. D. Stranks, P. Docampo, H.-L. Yip, A. K.-Y. Jen, H. J. Snaith. High-Performance Perovskite-Polymer Hybrid Solar Cells via Electronic Coupling with Fullerene Monolayers. *Nano Lett.* **2013**, *13*, 3124.

[52] K. Wojciechowski, T. Leijtens, S. Siprova, C. Schlueter, M. T. Hörantner, J. T.-W. Wang, C.-Z. Li, A. K.-Y. Jen, T.-L. Lee, H. J. Snaith. C$_{60}$ as an Efficient n-Type Compact Layer in Perovskite Solar Cells. *J. Phys. Chem. Lett.* **2015**, *6*, 2399.

[53] K. Wojciechowski, S. D. Stranks, A. Abate, G. Sadoughi, A. Sadhanala, N. Kopidakis, G. Rumbles, C.-Z. Li, R. H. Friend, A. K.-Y. Jen, H. J. Snaith. Heterojunction Modification for Highly Efficient Organic-Inorganic Perovskite Solar Cells. *ACS Nano* **2014**, *8*, 12701.

[54] S. Collavini, I. Kosta, S. F. Völker, G. Cabanero, H. J. Grande, R. Tena-Zaera, J. L. Delgado. Efficient Regular Perovskite Solar Cells Based on Pristine [70]Fullerene as Electron-Selective Contact. *ChemSusChem* **2016**, *9*, 1263.

[55] Y. Fang, C. Bi, D. Wang, J. Huang. The Functions of Fullerenes in Hybrid Perovskite Solar Cells. *ACS Energy Lett.* **2017**, *2*, 782.

[56] T. Gatti, E. Menna, M. Meneghetti, M. Maggini, A. Petrozza, F. Lamberti. The Renaissance of Fullerenes with Perovskite Solar Cells. *Nano Energy* **2017**, *41*, 84.

[57] C. Cui, Y. Li, Y. Li. Fullerene Derivatives for the Applications as Acceptor and Cathode Buffer Layer Materials for Organic and Perovskite Solar Cells. *Adv. Energy Mater.* **2017**, *7*, 1601251.

[58] L.-L. Deng, S.-Y. Xie, F. Gao. Fullerene-Based Materials for Photovoltaic Applications: Toward Efficient, Hysteresis-Free, and Stable Perovskite Solar Cells. *Adv. Electron. Mater.* **2018**, *4*, 1700435.

[59] C. Tian, E. Castro, T. Wang, G. Betancourt-Solis, G. Rodriguez, L. Echegoyen. Improved Performance and Stability of Inverted Planar Perovskite Solar Cells Using Fulleropyrrolidine Layers. *ACS Appl. Mater. Interfaces* **2016**, *8*, 31426.

[60] E. Castro, A. Artigas, A. Pla-Quintana, A. Roglans, F. Liu, F. Perez, A. Lledó, X.-Y. Zhu, L. Echegoyen. Enhanced Open-Circuit Voltage in Perovskite Solar Cells with Open-Cage [60]Fullerene Derivatives as Electron-Transporting Materials. *Materials* **2019**, *12*, 1314.

[61] Q. Xue, Y. Bai, M. Liu, R. Xia, Z. Hu, Z. Chen, X.-F. Jiang, F. Huang, S. Yang, Y. Matsuo, H.-L. Yip, Y. Cao. Dual Interfacial Modifications Enable High Performance Semitransparent Perovskite Solar Cells with Large Open Circuit Voltage and Fill Factor. *Adv. Energy Mater.* **2017**, *7*, 1602333.

[62] D. B. Khadka, Y. Shirai, M. Yanagida, T. Noda, K. Miyano. Tailoring the Open-Circuit Voltage Deficit of Wide-Band-Gap Perovskite Solar Cells Using Alkyl Chain-Substituted Fullerene Derivatives. *ACS Appl. Mater. Interfaces* **2018**, *10*, 22074.

[63] Y. Shao, Y. Yuan, J. Huang. Correlation of Energy Disorder and Open-Circuit Voltage in Hybrid Perovskite Solar Cells. *Nat. Energy* **2016**, *1*, 1.

[64] K. Yao, S. Leng, Z. Liu, L. Fei, Y. Chen, S. Li, N. Zhou, J. Zhang, Y.-X. Xu, L. Zhou, H. Huang, A. K.-Y. Jen. Fullerene-Anchored Core-Shell ZnO Nanoparticles for Efficient and Stable Dual-Sensitized Perovskite Solar Cells. *Joule* **2019**, *3*, 1.

[65] M. B. Suárez, C. Aranda, L. Macor, J. Durantini, D. A. Heredia, E. N. Durantini, L. Otero, A. Guerrero, M. Gervaldo. Perovskite Solar Cells with Versatile Electropolymerized Fullerene as Electron Extraction Layer. *Electrochim. Acta* **2018**, *292*, 697.

[66] C.-Y. Chang, W.-K. Huang, Y.-C. Chang, K.-T. Lee, C.-T. Chen. A Solution-Processed n-Doped Fullerene Cathode Interfacial Layer for Efficient and Stable Large-Area Perovskite Solar Cells. *J. Mater. Chem. A* **2016**, *4*, 640.

[67] S. F. Völker, M. Vallés-Pelarda, J. Pascual, S. Collavini, F. Ruipérez, E. Zuccatti, L. E. Hueso, R. Tena-Zaera, I. Mora-Seró, J. L. Delgado. Fullerene-Based Materials as Hole-Transporting/Electron-Blocking Layers: Applications in Perovskite Solar Cells. *Chem. Eur. J.* **2018**, *24*, 8524.

[68] Y. Shao, Z. Xiao, C. Bi, Y. Yuan, J. Huang. Origin and Elimination of Photocurrent Hysteresis by Fullerene Passivation in $CH_3NH_3PbI_3$ Planar Heterojunction Solar Cells. *Nat. Commun.* **2014**, *5*, 5784.

[69] J. Xu, A. Buin, A. H. Ip, W. Li, O. Voznyy, R. Comin, M. Yuan, S. Jeon, Z. Ning, J. J. McDowell, P. Kanjanaboos, J.-P. Sun, X. Lan, L. N. Quan, D. H. Kim, I. G. Hill, P. Maksymovych, E. H. Sargent. Perovskite-Fullerene Hybrid Materials Suppress Hysteresis in Planar Diodes. *Nat. Commun.* **2015**, *6*, 7081.

[70] K. Wang, C. Liu, P. Du, J. Zheng, X. Gong. Bulk Heterojunction Perovskite Hybrid Solar Cells with Large Fill Factor. *Energy Environ. Sci.* **2015**, *8*, 1245.

2 Concepts and experimental procedures

2.1 Introduction

The present thesis involves the use of light-harvesting-lead halide perovskites and fullerene materials. These materials possess some properties that will influence the way they are handled, being crucial the processing conditions.

The objective of this chapter is to introduce the characteristics of the main materials that are going to be used in the next chapter and their impact in the device processing conditions. Additionally, the specific considerations in device fabrication and characterization used in this thesis will be addressed. General procedures used throughout the thesis will be explained, although specific variations might be included in each chapter.

2.2 Core materials

The most important materials used in the following chapters can be divided in two main groups: hybrid lead-halide materials and fullerenes. The first one is the main light-harvester and, as a quite unique material, will have to be treated according to certain special considerations. Fullerenes are a much more robust and known materials that will not require so many special conditions when using them, although understanding their physicochemical characteristics is vital for their proper application.

2.2.1 Hybrid lead-halide perovskites

Hybrid lead-halide perovskites are the most widely used perovskite materials for the PV field, although the research on other types of perovskites, such as inorganic[1] or lead-free ones,[2] is gaining more interest lately. Nonetheless, hybrid lead-halide ones remain as the most efficient and studied ones. Additionally, as the name says, they are hybrid materials so part of their composition is organic.

They have very particular physicochemical properties, being especially relevant the ones affecting such important factors as the stability. In fact, these perovskites are highly hygroscopic and undergo several degradation processes;[3] therefore their study will have to be under strictly controlled conditions. In particular, glove boxes are the most used equipments (Figure 2.1), since they allow working with several equipments under very controlled atmospheres. In this thesis glove boxes filled and with constant flow of N_2 or Ar were used, with negligible levels of H_2O and O_2 (i.e. <1 ppm).

Figure 2.1. Photograph of a glove box used in this thesis for the processing of perovskite materials.

2.2.2 Fullerenes and derivatives

Fullerenes are carbon allotropes arranged in form of balls. The structure is composed of unsaturated rings of 5 and 6 members leading to a final molecule of polyenic character. The investigations on these molecules found out their great electronegativity, being able to get up to 6 electrons.[4] Although the most famous ones are C_{60} and C_{70},[5] they can be functionalized in many different ways due to the relief in strain that that implies.[6]

Functionalizing fullerenes increases their solubility in organic solvents, which is a critical point for their integration in thin film technologies. As they are unsaturated molecules, they will have higher solubility in aromatic solvents, which will be taken into account. This thesis involves the introduction of fullerenes in the perovskite precursor solutions, which are prepared generally in *N*,*N*-dimethylformamide (DMF) and dimethyl sulfoxide (DMSO). The concentration ranges that will be studied will be inexorably affected by the solubility of fullerenes in these solvents.

Considering all these points, this thesis aims to understand the role that the simplest fullerenes can have in PSCs, as well as how a structural modification can affect this. Therefore, the fullerenes that will be used in this work go from the original C_{60} and C_{70}, to fullerenes with different functionalizations. In this regard, as the synthesis of these fullerene derivatives are not part of this thesis, details in the synthesis and characterization of these compounds will be referenced to their corresponding existing reports.

2.3 Perovskite-based films

The objective of this section is to summarize the key points of the processing and characterization of perovskite-based films, from its chemical composition and fabrication conditions to all the techniques employed to characterize the film morphological and physicochemical properties.

2.3.1 Processing of perovskite-based films

Considering the particularities of lead halide perovskite materials, the fabrication of solar cells was carried out inside glove boxes with controlled N_2 or Ar atmosphere. The thin-film PSCs were processed with the spin-coating technique, which allows obtaining layers with controlled thickness. Figure 2.2 shows an example of a spin-coater, which allows processing the PSC layers by this technique. The spin coater spins at rates of thousands of revolutions, creating flat layers in the nanometric scale. The spin-coating conditions can be tuned in terms of rpm, time, slope and number of steps, allowing the

user to optimize the thickness and crystallization of the layer. This means that fluids and solutions can be used, and therefore the perovskite films can be prepared by wet chemistry approach.
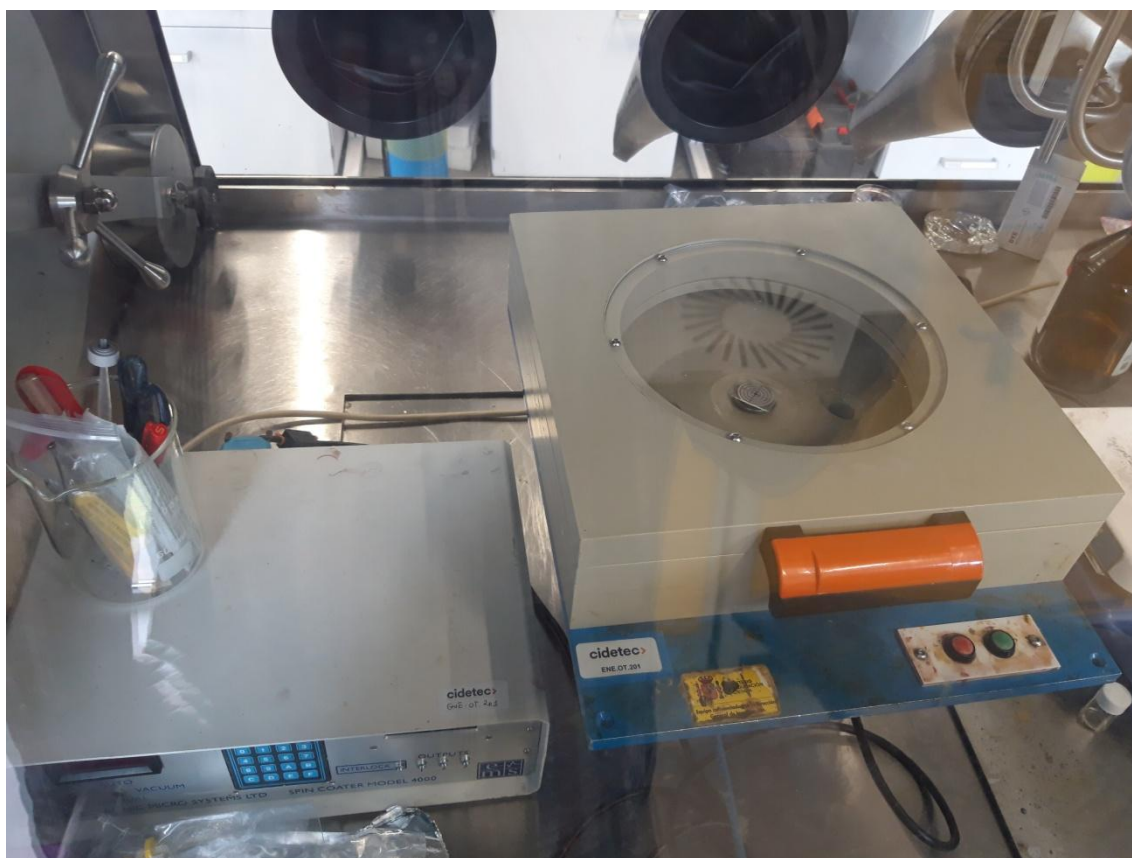

Figure 2.2. Photograph of a spin-coater used this thesis for the processing of the different layers of PSCs.

Although perovskite can also be processed by vacuum-deposition,[2.7] the most traditional method is indeed the spin-coating. The solutions are prepared by mixing the different precursors in DMF and DMSO generally. Depending on the perovskite type, the precursors would be most commonly lead halides (e.g. PbI_2, $PbBr_2$, $PbCl_2$) and organic amine salts (e.g. MAI, MABr, FAI, FABr), although other compositions are used for the previously mentioned inorganic or lead-free perovskites. Nevertheless, the deposited precursor solution needs annealing at certain temperature, generally around 100°C, in order to evaporate the remaining solvent and give the system the required energy for transforming into the perovskite structure with high absorption coefficient.

In the case of this particular thesis, different fullerenes were inserted as a blend together with perovskite. The procedure involved dissolving the fullerenes in the perovskite

precursor solution and filtering it, in order to avoid having sediments on the substrates of non-dissolved fullerene, or dissolving the fullerene in the pure solvent and filtering, previous to perovskite precursor solution preparation.

However, the perovskite layer is not the only one that can be processed by spin-coating. The charge transporting layers to be used in the devices fabricated in this thesis were also deposited by this technique. In this sense, ETLs like TiO_2 and HTLs like poly[bis(4-phenyl)(2,4,6-trimethylphenyl)amine (PTAA) and spiro-OMeTAD were also deposited in this way.

Unless specified, spiro-OMeTAD hole-selective contact was deposited on top of the perovskite layer from a solution that contained spiro-OMeTAD (108.4 mg) in chlorobenzene (953.43 μL), LiTFSI solution in acetonitrile (17.17 μL, 520 mg mL^{-1}), and *tert*-butylpyridine (29.4 μL). The HTL was deposited by spin-coating the solution at 3000 rpm for 30 s. The samples were left in a desiccator overnight. Finally, an array of round Au back contacts (ca. 0.07 cm^2) was deposited by thermal evaporation at more than 5 x 10^{-6} torr with a NANO38 (Kurt J. Lesker) apparatus with a shadow mask.

A critical point to always consider for a proper deposition of every layer is the cleaning of the substrates. Whether the perovskite is deposited on ETLs or on bare FTO, the substrates require of cleaning in specific conditions. This step usually combines the use of different solvents (e.g. water, acetone, 2-propanol) with ultrasound bath treatment for 15 min each. Additionally, the wettability and therefore the final quality of the films deposited in this thesis by spin-coating may also highly depend on the surface-treatment of the substrates. In this regard, UV and/or O_3 treatment will also be employed as pretreatment for different deposition steps in this thesis.

2.3.2   Characterization of perovskite-based films

The morphology of the films has been characterized by field-emission scanning electron microscopy (FE-SEM). Furthermore, this technique was also used to determine the film thickness by analysing the cross section of the samples. It is worth noting that further morphological characterization by atomic force microscopy (AFM) was also carried out

by our co-worker Dr. Elisa Palacios (Universidad de Murcia). As a complementary surface characterization, hydrophobic character of perovskite films was also analyzed by contact angle measurements. Furthermore, transmission electron microscope-electron energy loss spectroscopy (TEM-EELS) was used for the chemical characterization of perovskite film cross-sections. In particular, carbon maps were obtained for analyzing the distribution of fullerene in the perovskite film. These measurements were carried out by our colleague Dr. Andrey Chuvilin (CIC nanoGUNE). UV-vis spectroscopy was used for the optical (i.e. in particular, transmittance) characterization of perovskite films.

2.4   Perovskite solar cells configurations

The composition of the solar cell will completely depend on the type of configuration; i.e. different charge-transporting materials will be used if it is n-i-p or p-i-n, or the special case of ETL-free devices studied in this thesis:

- n-i-p devices: FTO was used as back contact, on which compact and mesoporous TiO_2 were deposited as ETL scaffold. Then, $MAPbI_3$ perovskite was deposited, and spiro-OMeTAD spin-coated on top as HTL. Top contact Au was deposited using a thermal evaporator (Figure 2.3).
- p-i-n devices: indium tin oxide (ITO) was used as back contact, on which PTAA was deposited as HTL. After the deposition of $MAPbI_3$ perovskite, C_{60} as ETL, BCP as buffer layer and Cu top contact were deposited by thermal evaporation.
- ETL-free devices: perovskite $MAPbI_3$ was directly deposited on FTO back contact. As for n-i-p devices, spiro-OMeTAD was used as HTL and Au as top contact.

Figure 2.3. Photograph of a thermal evaporator used in this thesis for the evaporation of the top contacts of PSCs.

2.5   Characterization of perovskite solar cells

In order to analyze the performance of a solar cell, it has to be exposed to a controlled light irradiation. A sun simulator (Figure 2.4) can establish the same conditions as, for instance, 1 sun of light, so that the solar cell is exposed to simulated solar irradiance. The

sun simulator is calibrated with a reference silicon solar cell, so that the precise intensity can be known. The distance of the cell to the light source is also relevant since the intensity would increase with a shorter distance; this will also be calibrated with the reference Si solar cell.

Figure 2.4. Photograph of a sun simulator and EQE setup used in this thesis for the PV characterization of PSCs.

The measuring system is composed of the following parts:

- Lamp simulator: light source.
- Spectral filter: incorporated in the lamp simulator in order to have a certain spectrum of the light.
- Multimeter: measures the *J-V* characteristics of the solar cell.
- Software: analyzes acquired data.

In this thesis, the *J-V* characteristics of the solar cells were measured under a xenon arc lamp simulator equipped with an AM1.5G spectral filter (Sun 2000, ABET

Technologies). The intensity was adjusted to provide 1 sun illumination (100 mW cm^{-2}) by using a calibrated silicon solar cell. Unless otherwise mentioned, the *J-V* characteristics were recorded by scanning the potential from higher than the V_{oc} to zero (i.e. "reverse mode") at approximately 300 mV s^{-1}. Before the measurement, a voltage of approximately 1.2 V was applied to the devices for 1 min.

Another possibility of the sun simulator setup is recording the maximum power point tracking (mppt) of the cell. This means, measuring the electrical response of the solar cell working at the point of maximum power, which is given by the *J-V* characteristics (i.e. J_{sc}, V_{oc} and FF), with time. This feature is particularly useful, considering that the *J-V* characteristics of a solar cell depend on temperature and irradiance, therefore V_{mpp} and J_{mpp} will change, and so the power of the solar cell.[8]

The measurement of the *J-V* characteristics depends on the area of the contact under measurement. If the area is not exactly known, there might be some mismatch between the measured *J* and real *J*. In order to check this, an instrument for measuring the external quantum efficiency (EQE) of the cell is required. The resulting spectrum can be integrated to calculate the real J_{sc} of the cell, which can be then compared to the measured one in the sun simulator.

The EQE system is composed of the following parts:

- Lamp: light source.
- Monochromator: selects a certain wavelength for the incident light.
- Mechanical chopper: modulates the incident light
- Lock-in amplifier: amplifies and measures the voltage (i.e. from the solar cell coupled to an ohmic resistance).
- Calibrated Si photodiode: references the incident light.
- Software: manages acquired data.

In particular, in this Thesis, EQE was measured as a function of wavelength from 300 to 850 nm with a step of 10 nm using a home-built small-spot EQE system. A Stanford Research SR830 Lock-In amplifier is used to measure the response of the device under test.

2.6 References

[1] G. E. Eperon, G. M. Paterno, R. J. Sutton, A Zampetti, A. A. Haghighirad, F. Cacialli H. J. Snaith. Inorganic Caesium Lead Iodide Perovskite Solar Cells. *J. Mater. Chem. A* **2015**, *3*, 19688.

[2] F. Hao, C. C. Stoumpos, D. H. Cao, R. P. H. Chang, M. G. Kanatzidis. Lead-Free Solid-State Organic-Inorganic Halide Perovskite Solar Cells. *Nat. Photonics* **2014**, *8*, 489.

[3] T. Leijtens, G. E. Eperon, N. K. Noel, S. N. Habisreutinger, A. Petrozza, H. J. Snaith. Stability of Metal Halide Perovskite Solar Cells. *Adv. Energy Mater.* **2015**, *5*, 1500963.

[4] Q. Xie, E. Perez-Cordero, L. Echegoyen. Electrochemical Detection of C_{60}^{6-} and C_{70}^{6-}: Enhanced Stability of Fullerides in Solution. *J. Am. Chem. Soc.* **1992**, *114*, 3978.

[5] H. W. Kroto, J. R. Heath, S. C. O'Brien, R. F. Curl, R. E. Smalley. C_{60}: Buckminsterfullerene. *Nature* **1985**, *318*, 162.

[6] R. C. Haddon. Chemistry of the Fullerenes: The Manifestation of Strain in a Class of Continuous Aromatic Molecules. *Science* **1993**, *261*, 1545.

[7] M. Liu, M. B. Johnston, H. J. Snaith. Efficient Planar Heterojunction Perovskite Solar Cells by Vapour Deposition. *Nature* **2013**, *501*, 395.

[8] A. Smets, K. Jäger, O. Isabella, R. van Swaaij, M. Zeman. Solar Energy: The Physics and Engineering of Photovoltaic Conversion, Technologies and Systems. UIT Cambridge Ltd, Cambridge, England, 2016.

3 Perovskite:C$_{70}$ blend films for ETL-free perovskite solar cells

3.1 Introduction

As presented in Chapter 1, PSCs still need to overcome different obstacles that prevent them from being applicable for industrial production. To solve this, further progress on the perovskite layer and the charge-selective contacts is required.[1,2] Currently, in regular architecture PSCs with the general n-i-p structure glass/ETL/absorber/HTL/back contact, the deposition of the usual TiO$_2$ ETL results in significant limitations for the substrate choice. Furthermore, the use of TiO$_2$ enhances the UV-degradation of perovskite, and requires very high sintering temperatures (i.e. generally >400°C), although there have already been some investigations for avoiding it.[3,4] Some alternative ETLs (e.g., ZnO,[5,6] SnO$_2$,[7] and fullerene films[8-10]) have been recently demonstrated, showing promising results. However, their deposition requires an additional step, including additional solvents,[5,6,8,9] and/or techniques,[5-7,10] in the device fabrication.

Therefore, removing the ETL would be the ideal scenario, while the perovskite layer still being able by itself to separate the electrons from the holes and extract them at the electrode. This would avoid the problems derived from the current ETLs and additional processing steps. In this regard, there are few reports on ETL-free PSCs, although they still present some drawbacks for this architecture.[11-14] Liu and co-workers tried this configuration obtaining good results of efficiencies of up to 13.5% with poly(3-hexylthiophen-2,5-dyil) (P3HT) and spiro-OMeTAD as HTL, but still far from the reference devices of that time.[11] In the work by Hu and colleagues the ETL-free solar cells, in which the perovskite layer was deposited on bare ITO, the efficiency values were 4.3%, which is much lower than their devices with TiO$_2$ as ETL (14.2%).[12] However, they managed to largely improve the efficiency up to 15.1%, but the processing required of surface-modification with the basic salt Cs$_2$CO$_3$. Another interesting study was carried out by Ke et al., where they found the relevance of using chloride in the perovskite mixture for fabricating efficient ETL-free devices.[13] The

authors address the obtained high V_{oc} values of up to 1.06 V to the ability of chloride to diffuse and passivate the FTO/perovskite interface. Nevertheless, they also point out that there are unsolved hysteresis issues when the perovskite is deposited directly on the FTO substrate. In this sense, there is still a long way for improvement in ETL-free devices, considering the deficiencies of FTO/perovskite interfaces and its effects in defect density and device performance.

Therefore, ETL-free configuration requires of a passivating agent that allows achieving efficient devices while overcoming the disadvantages of FTO/perovskite interfaces. In this case, there would be particular interest in fullerenes, since some reports addressed the ability to passivate defects in the perovskite. Indeed, perovskite:PCBM blend films have been recently shown as a straightforward approach to improve the FF and suppress hysteresis in PSCs.[15,16] Furthermore, photostability improvement was also seen for devices based on perovskite:PCBM films.[17] In te same way, the recently reported fullerene saturation approach proposed by Collavini and co-workers, which was initially proposed to avoid damage of fullerene ETL during perovskite processing, opens wide possibilities to process perovskite:fullerene blend films.[9] Nevertheless, to the best of our knowledge, the work reported in this chapter was the first one using perovskite:fullerene blend films in semiconducting ETL-free solar cells. Therefore, the potential benefits that their insertion in this configuration would bring were still to be discovered at that moment.

In this chapter, the deposition of pinhole-free $MAPbI_3$:C_{70} fullerene blend films on FTO-coated glass substrates is presented, showing the use of the $MAPbI_3$:C_{70} in efficient and reproducible ETL-free PSCs with commonly used spiro-OMeTAD as the HTL. In addition, a comparative analysis of the resulting devices (glass/FTO/$MAPbI_3$:C_{70}/spiro-OMeTAD/Au) compared with analogous devices containing a simple perovskite film (glass/FTO/$MAPbI_3$/spiro-OMeTAD/Au) and a compact TiO_2 (c-TiO_2) as ETL (glass/FTO/c-TiO_2/$MAPbI_3$/spiro-OMeTAD/Au) is also provided. Finally, the photostability of unencapsulated solar cells with the three different architectures is discussed.

3.2   Experimental Section

3.2.1   Materials

The materials used in this study were obtained from commercial suppliers in high purity and used without further purification: glass/FTO (TEC15, Hartford Glass), C_{70} (99%, SES Research), MAI (DYESOL), $PbCl_2$ (98%, Sigma-Aldrich), spiro-OMeTAD (99%, Feiming Chemicals Limited), lithium bis(trifluoromethane) sulfonimidate (LiTFSI, 99.9%, Solvionic), *tert*-butylpyridine (96%, Sigma-Aldrich), *N,N*-dimethylformamide (DMF, extra pure, Scharlab), 2-propanol (synthetic grade, Scharlab), acetone (technical grade, Scharlab), chlorobenzene (99.8%, Sigma-Aldrich), toluene (99.8%, Sigma-Aldrich), *o*-xylene (98%, Sigma-Aldrich) and acetonitrile (UV HPLC grade, Scharlab).

3.2.2   Device fabrication

The perovskite solution was prepared by dissolving 7.71 mmol of MAI and 2.57 mmol of $PbCl_2$ (molar ratio 3:1) in 3 mL of DMF and stirring overnight. Prior to deposition, the C_{70} was added to the perovskite solution. Different $C_{70}/PbCl_2$ molar ratios in the range from 1:14400 to 1:1270 were studied. The resulting solution was spin coated on the substrates following a two-step protocol, which consisted of a first step of 500 rpm for 5 s followed by a second step of 2000 rpm for 45 s. Subsequently, the samples were annealed at 100°C for 2 h to ensure complete perovskite formation. Spiro-OMeTAD and Au layers were deposited on top of perovskite layer as described in Chapter 2.

3.2.3   Thin films and device characterization

The morphological properties of the films were analyzed with an ULTRA plus ZEISS field-emission scanning electron microscopy (FE-SEM).

The chemical composition of the films was investigated by scanning transmission electron microscopy (STEM) characterization, which was carried out by Andrey Chuvillin at CIC nanoGUNE.

The *J-V* chracteristics of the solar cells were measured under simulated solar light by using the setup decribed in chapter 2. The EQE spectra of the devices were also obtained from the home-made specific setup and methodology described in chapter 2.

3.3   Results and Discussion

3.3.1   Perovskite:fullerene blend films

$PbCl_2$, MAI, and C_{70}-containing DMF-based formulations were used to deposit films on glass/FTO substrates. Figure 3.1a shows representative top-view FE-SEM micrographs of the obtained samples. The morphology of the films processed from C_{70}-free solutions on FTO and FTO/c-TiO_2 substrates are also shown (Figures 3.1b and 3.1c, respectively) for comparison. The mean thickness was in the 400-500 nm range for all films. Interestingly, in contrast to the samples processed from the C_{70}-free solutions that showed significant concentration of pinholes when deposited on the glass/FTO (i.e. bright regions in Figure 3.1b), no pinholes were detected in the films processed from C_{70}-containing solutions (Figure 3.1a). The latter films showed indeed competitive homogeneity and grain size to the films deposited on the most frequently used glass/c-TiO_2 substrates (Figure 3.1c). Therefore, using C_{70}-containing processing solutions appears to be a straightforward approach to improve the pinhole issue in perovskite films directly processed on FTO surfaces, which has been identified as the main limitation of the semiconducting ETL-free PSCs.[18] The simplicity of C_{70}-containing formulation based film processing compared with previously proposed approaches, such as FTO UV-O_3 treatment, is a major advantage.[14]
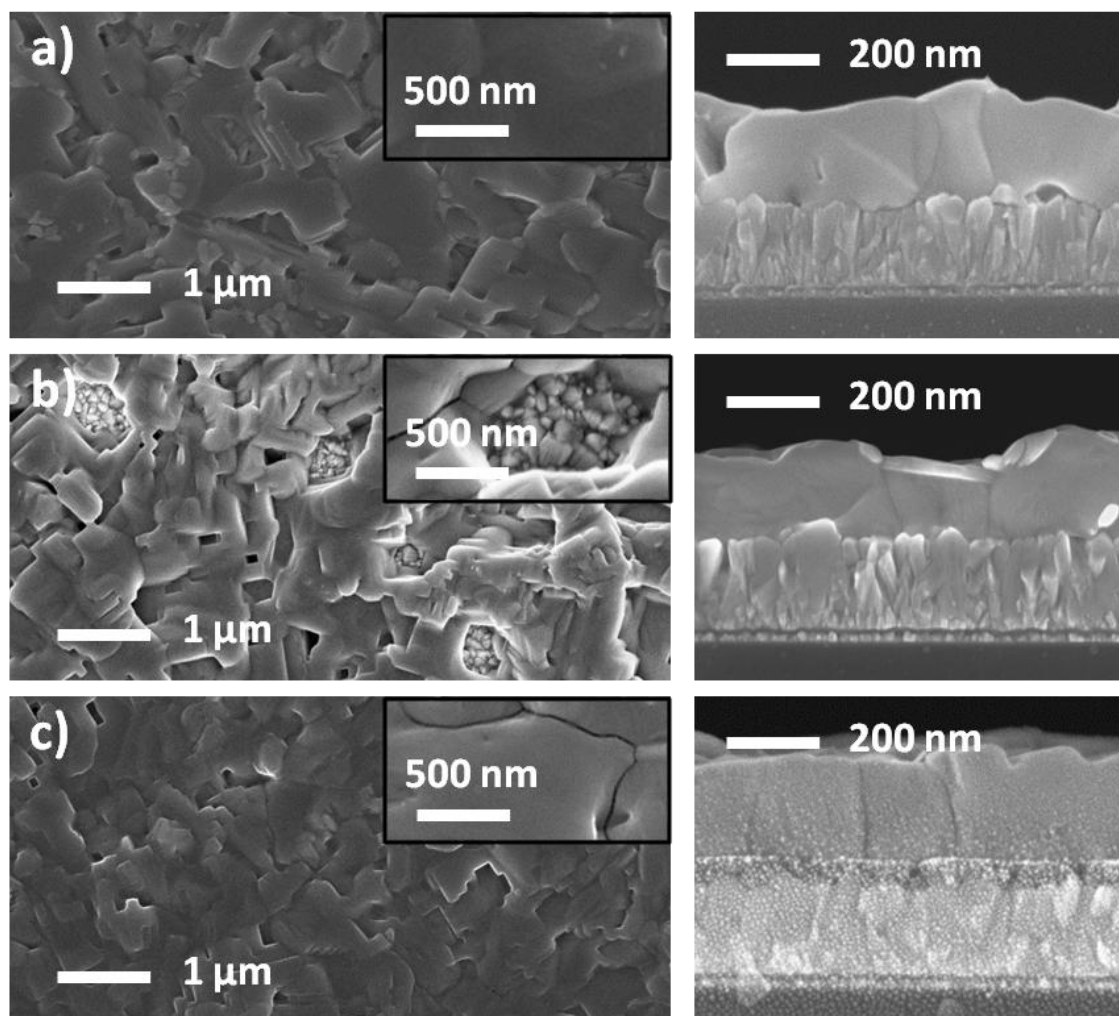
Figure 3.1. Top-view and cross-section FE-SEM micrographs of a) MAPbI$_3$:C$_{70}$ and b) MAPbI$_3$ films deposited on glass/FTO substrates, and c) micrographs of MAPbI$_3$ films deposited on glass/FTO/c-TiO$_2$. The insets show higher magnification views of a pinhole (b) and grains (a, c).

The chemical composition of the films processed from C$_{70}$-containing solutions was investigated by STEM. Figure 3.2 displays the high angle annular dark-field (HAADF) STEM micrographs and chemical maps obtained by EELS of carbon K and iodine M edges. At a scale of tens of nm, the carbon distribution (Figure 3.2b), determined mainly by the distribution of C$_{70}$ in the film, does not follow the distribution of iodine (Figure 3.2c). As is evident from the carbon map, the excess concentration of carbon is observed in linear and circular shapes, which leads to the assumption that C$_{70}$ and/or its derivatives are distributed along the interfaces of the MAPbI$_3$ crystals. Therefore, the inclusion of C$_{70}$ and/or derivatives into the perovskite film was successful. It is noted that the perovskite matrix is referred as MAPbI$_3$ for simplicity. However, deviations from this

stoichiometry owing to the preparation of the film from the PbCl$_2$ and MAI precursors cannot be fully ruled out.
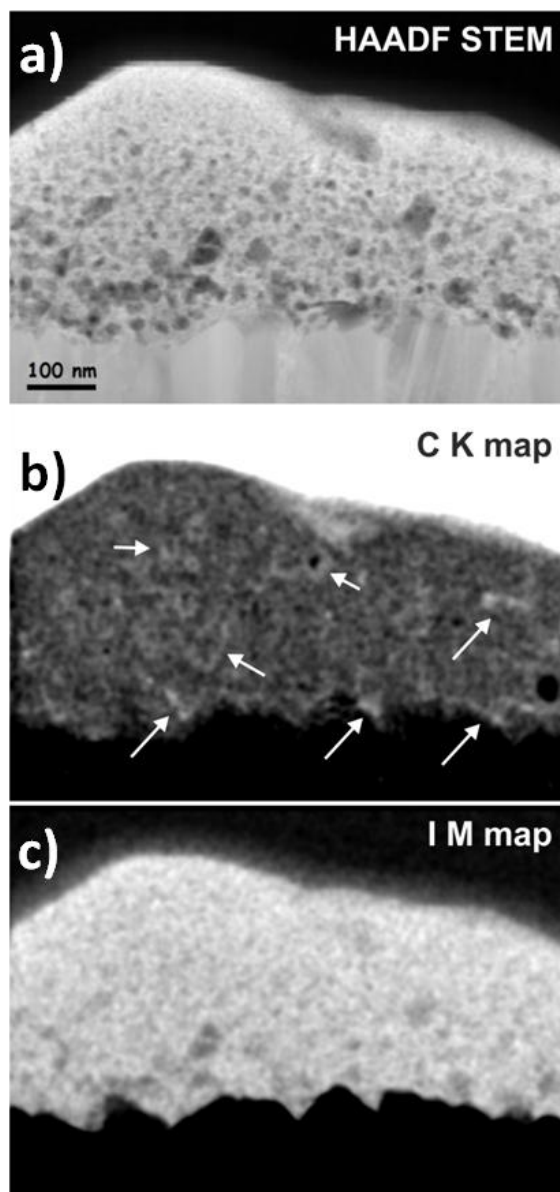

Figure 3.2. a) HAADF STEM micrograph of the cross section of a glass/FTO/MAPbI$_3$:C$_{70}$ sample and EELS chemical maps of b) carbon K edge and c) iodine M edge. Arrows point to the regions enriched by carbon.

3.3.2 Solar cells

The three different types of samples (i.e. glass/FTO/MAPbI$_3$:C$_{70}$, glass/FTO/MAPbI$_3$ and glass/FTO/c-TiO$_2$/MAPbI$_3$) were used to prepare solar cells with spiro-OMeTAD and Au as hole-selective and back contact, respectively. As a result, a preliminary series

of hybrid halide PSCs with three different architectures (I, II, and III in Scheme 3.1) was investigated. Table 3.1 summarizes the PV parameters extracted from the *J-V* curves of the best devices (Figure 3.3). The statistics of all the devices can be seen in Figure 3.4.
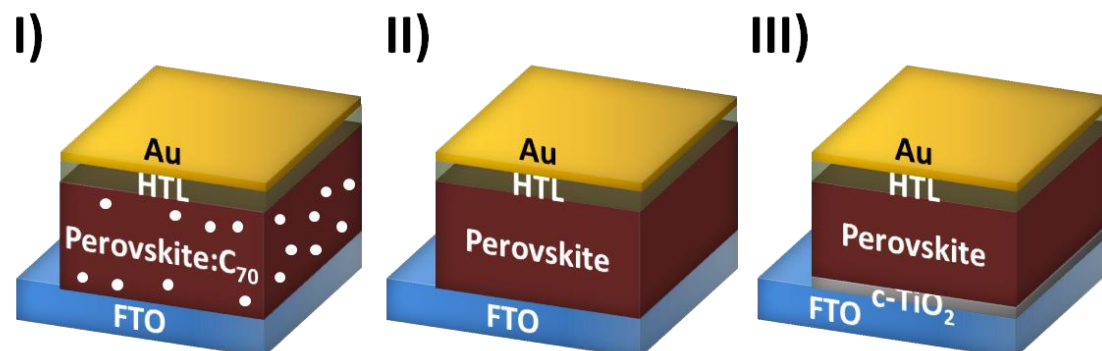
Scheme 3.1. Three different architectures for PSCs: devices based on ETL-free perovskite (I) and perovskite:C_{70} blend (II) films, and containing a c-TiO_2 ETL (III). The white dots in Scheme I represent C_{70} fullerene.
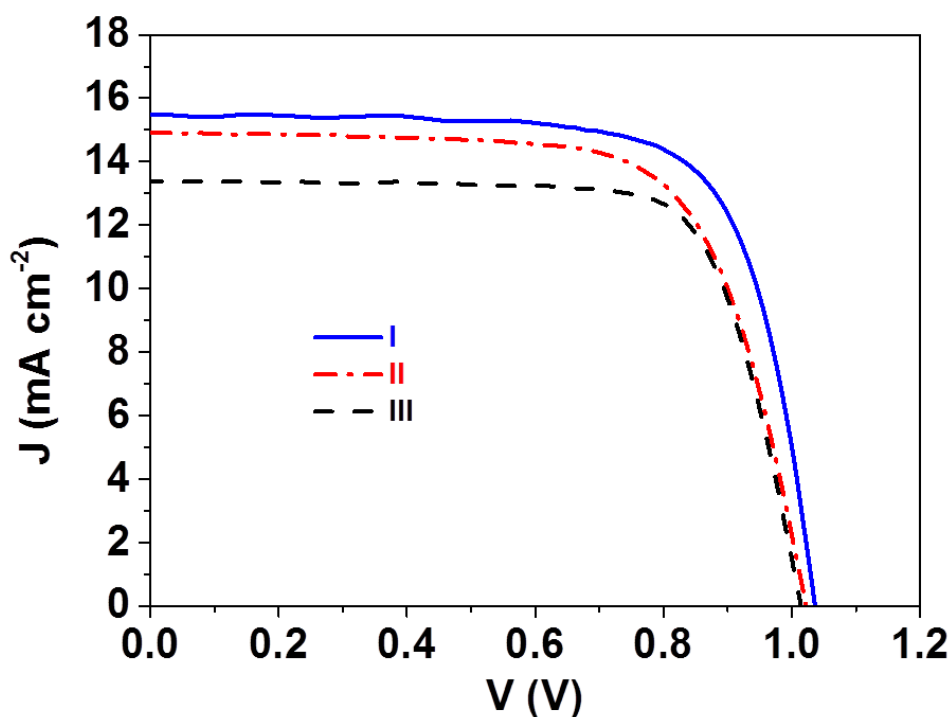

Figure 3.3. *J-V* characteristics, under AM1.5 simulated sunlight, of the best devices from the preliminary series with the different architectures (i.e. I, II and III). The corresponding PV parameters are summarized in Table 3.1.

Table 3.1. PV parameters of the best devices from the preliminary series of solar cells with the different architectures (i.e. I, II, and III) under AM1.5G simulated sunlight.[a]

Device	ETL	J_{sc} (mA cm^{-2})	V_{oc} (V)	FF (%)	PCE (%)
I	ETL-free	15.4	1.04	73	11.7
II	ETL-free	14.9	1.02	70	10.6
III	c-TiO$_2$	13.4	1.01	75	10.2
III	C$_{70}$[b]	10.9	0.97	58	6.1
III	C$_{70}$ discont[b]	15.1	1.00	69	10.4

[a] The statistical analysis of the PV parameters, including devices prepared in further series, can be found in Figure 3.4. [b] Data from solar cells with architecture type III based on the C$_{70}$ ETL (instead of c-TiO$_2$) are also shown.[9]
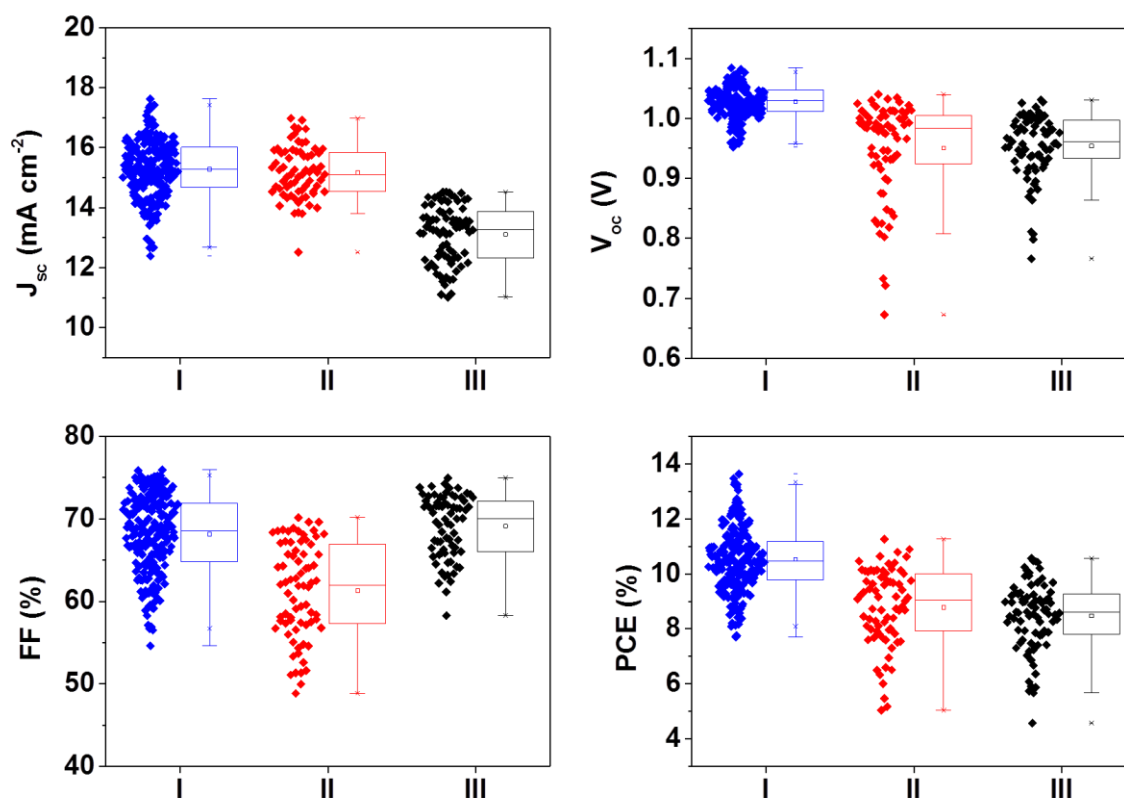
Figure 3.4. PV parameters for PSCs with architectures I, II and III.

Interestingly, a significant increase of the short-circuit current density (J_{sc}) was detected in ETL-free devices (I and II). However, the ETL-based device (III) showed the highest FF value (i.e. 75%), which decreased for devices without ETL. This decrease in FF, though, was only moderate for the case of the cells based on the MAPbI$_3$:C$_{70}$ blend,

reaching values close to those based on type III c-TiO$_2$ (i.e. 73.0%). All in all, an overall improvement in the PV performance, reaching PCE of 11.7%, was detected for the MAPbI$_3$:C$_{70}$ blend-based solar cells. Regarding this improvement, the impedance spectroscopy analysis, carried out in collaboration with Iván Mora-Seró group (Universitat Jaume I), pointed out that ETL-free solar cells based on MAPbI$_3$:C$_{70}$ exhibit larger recombination resistance (i.e. slower recombination rate) than those based on single MAPbI$_3$ films (Figure 3.5a).[19] This finding, together with lower transport resistance in comparison to the compact TiO$_2$ ETL-based devices (Figure 3.5b), could be making the glass/FTO/MAPbI$_3$:C$_{70}$/spiro-OMeTAD/Au a competitive heterostructure for perovskite solar cells. Therefore, C$_{70}$ seems to act as passivating agent for some perovskite defects, decreasing the recombination loss pathways. Furthermore, type I devices provided significantly larger J_{sc} and FF than solar cells with a C$_{70}$ as the dedicated ETL (i.e. type III with C$_{70}$ ETL instead c-TiO$_2$), as reported previously.[9] It is worth noting that the latter only reached PCE values larger than 10% when based on discontinuous C$_{70}$ films. Therefore, different PV behavior of the type I devices versus the solar cells with C$_{70}$ ETL may be concluded. This finding was supported by the STEM characterization (Figure 3.2), which suggests that there is no C$_{70}$/perovskite planar heterojunction in the cross section of the glass/FTO/MAPbI$_3$:C$_{70}$ samples.
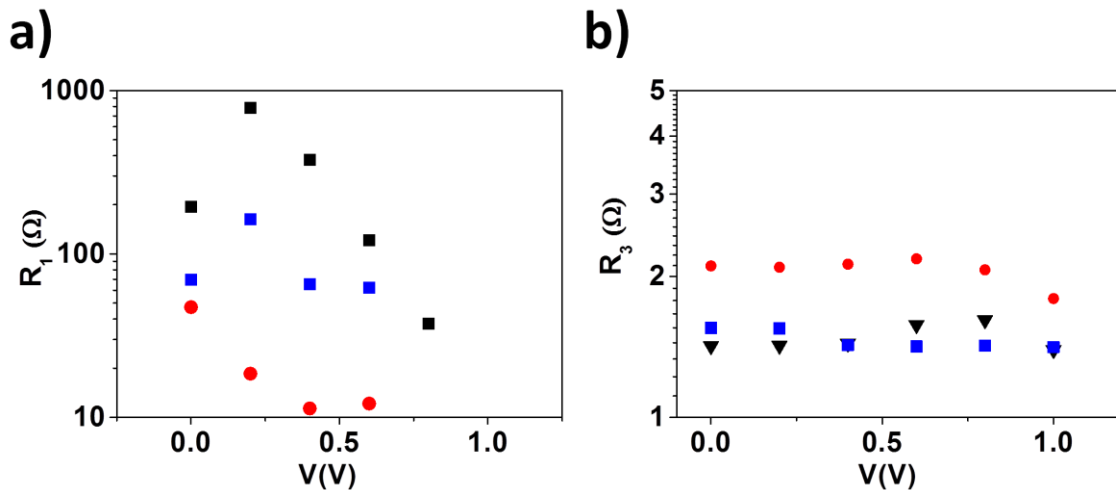

Figure 3.5. Resistances obtained from the impedance spectra fit a) R$_1$, related to the recombination resistance and b) R$_3$, related to the transport and injection at selective contacts. Further experimental details can be found in the reference [19].

To gain a further insight into the C_{70} effect in the solar cell performance, type I devices were prepared from $MAPbI_3$:C_{70} blend films processed from solutions with different C_{70} concentrations. Figure 3.6 shows the statistics of the different PV parameters as a function of the C_{70} to $PbCl_2$ ratio in the precursor solution. In general, an increasing trend as a function of C_{70} content was detected, especially for the V_{oc} and FF. The improvement may be correlated to the pinhole evolution of the perovskite films. In Figure 3.7 a clear decrease of the pinhole density with increasing the C_{70} concentration can be noted. Furthermore, taking into account the carbon accumulation detected in the Carbon K-edge EELS map (Figure 3.2b), C_{70} may also play other roles, such as defect passivation at the perovskite grain boundaries as previously suggested for other carbon nanostructures (e.g. PCBM[15-16]).
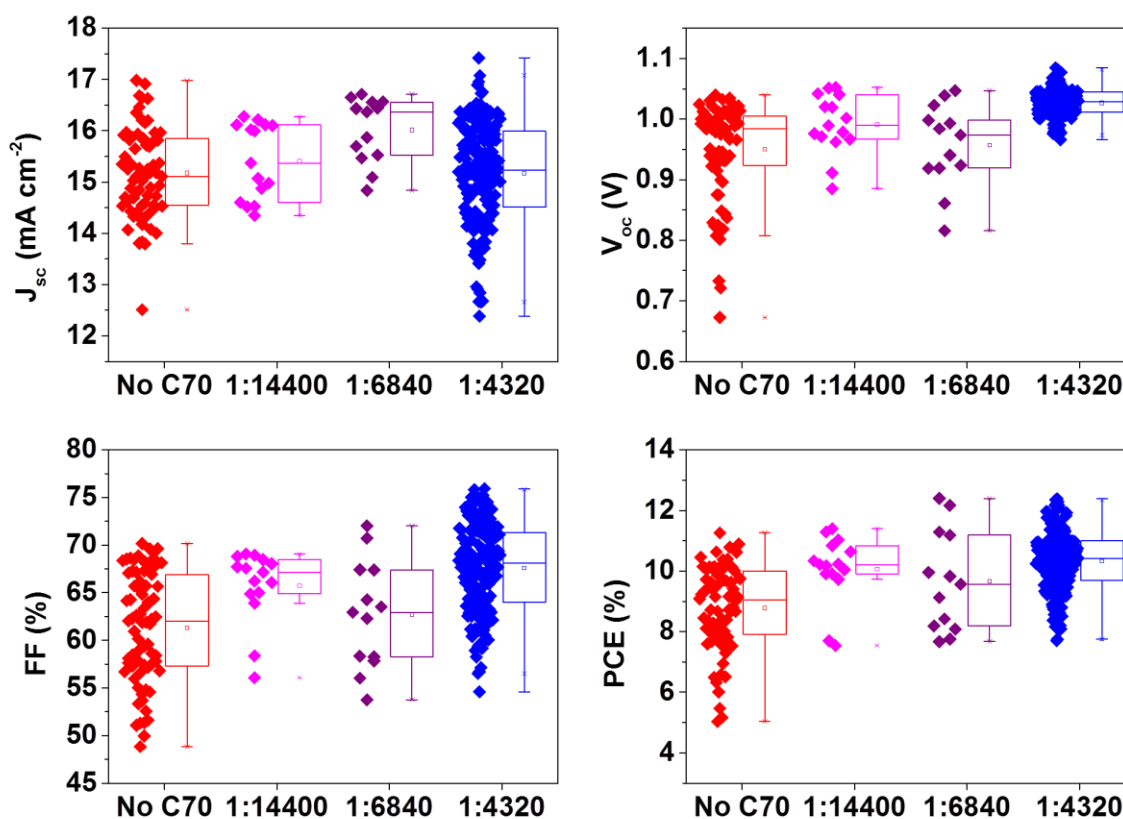

Figure 3.6. PV parameters for PSCs based on $MAPbI_3$:C_{70} blend films processed from formulations with different C_{70}/$PbCl_2$ ratios.

As a result, the best PCE was obtained for the devices prepared through C_{70}-saturated perovskite solutions (1:4320 C_{70}/$PbCl_2$ ratio), pointing out that higher concentration values of C_{70} lead to more efficient solar cells.
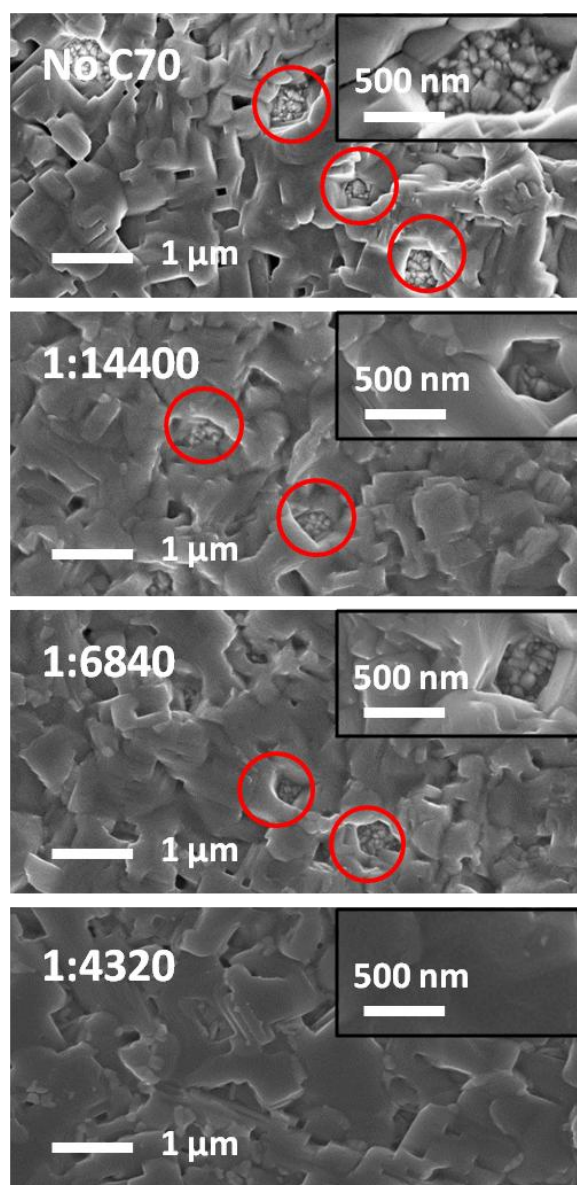
Figure 3.7. Top-view FESEM micrographs of films deposited from formulations with different $C_{70}:PbCl_2$ ratios (i.e. 0, 1:14400, 1:6840 and 1:4320) on glass/FTO substrates.

3.3.3 Photostability of devices

The durability may be one of the main issues for the development of hybrid halide perovskite-based PV. The effect of the $MAPbI_3:C_{70}$ blend films on the photostability of unencapsulated PSCs was investigated. In Figure 3.8a the *J-V* characteristics measured just before the photostability test are provided. Figure 3.8b shows the evolution of the PV parameters versus time under continuous AM1.5G simulated sunlight for devices with architectures I, II, and III (Scheme 3.1).
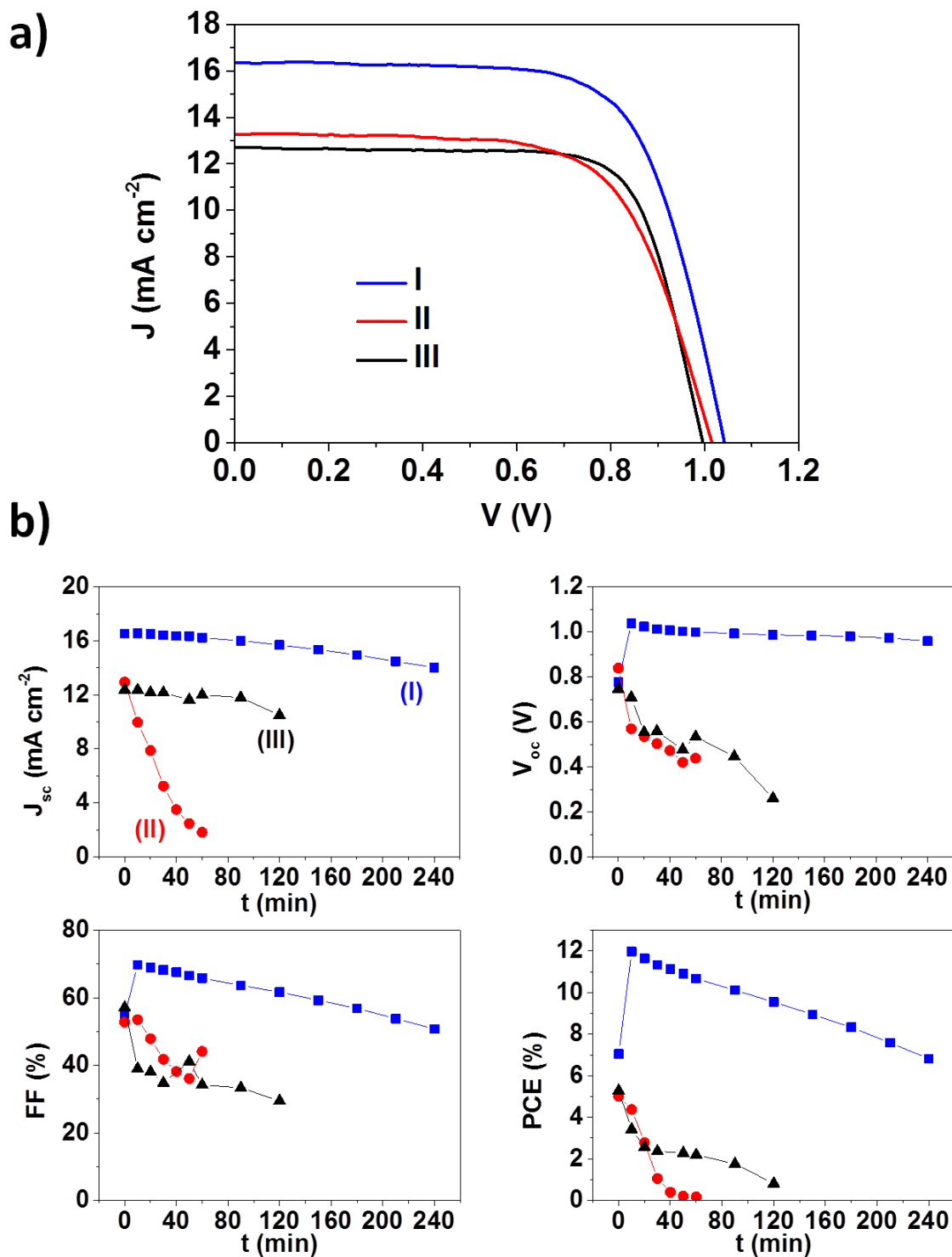
Figure 3.8. a) *J-V* curves for I, II and III architecture devices before being used for the photostability measurements. It is noted that the *J-V* characteristics were recorded, after applying a voltage of approximately 1.2 V during 1 min, by scanning the potential in the "reverse mode" at approximately 300 mV s^{-1}. b) Evolution of the PV parameters with time under continuous AM1.5G simulated sunlight for unencapsulated solar cells with different architectures (I: blue squares, II: red circles, and III: black triangles).

Table 3.2. PV parameters extracted from the *J-V* characteristics displayed in Figure 3.8b.

Device	J_{sc} (mA cm^{-2})	V_{oc} (V)	FF (%)	PCE (%)
I	16.4	1.04	68.9	11.8
II	13.3	1.02	66.4	8.9
III	12.7	0.97	74.0	9.4

It is worth to note that the solar cells based on MAPbI$_3$:C$_{70}$ blend films (type I) exhibited the best V_{oc} and FF values after 10 min under illumination, reaching the same PCE that was estimated from the *J-V* characteristic measured under PCE maximization conditions (i.e. after applying a constant potential of 1.2 V, Figure 3.8b and Table 3.2). In contrast, the devices based on MAPbI$_3$ single films (type II and III) provided significantly lower V_{oc} and FF than those extracted from the *J-V* characteristics measured after applying constant potential. Furthermore, the solar cells based on MAPbI$_3$:C$_{70}$ blend films (type I) showed enhanced photostability in comparison with architectures II and III. The J_{sc} and V_{oc} of type I devices suffered only about 10% reduction after 3 h under continuous illumination. Nevertheless, the FF decreased by approximately 25% of the initial value, which was the main cause of the 40% loss in the PCE. However, a PCE larger than 7% still remains after 3 h under 1 sun AM1.5G simulated sunlight, and no temperature control. Significant photostability improvement in comparison to the conventional regular architecture (i.e. III) can be highlighted. Although further investigations are needed to gain insights into origin of the photostability improvement, the significant enhancement detected in solar cells with regular architecture (i.e. including c-TiO$_2$ ETL) based on MAPbI$_3$:C$_{70}$ blend films (Figure 3.9) provided a further support to claim the beneficial effect of the C$_{70}$ addition.

The work that was carried out by Gharibzadeh et al. in collaboration with us may shed some light on the possible role of fullerene in the stability of PSCs based on perovskite:fullerene blend films.[20] By analyzing MAPbI$_3$:C$_{70}$ films by time-resolved femtosecond-to-nanosecond optical spectroscopy, the authors found out that electrons were being transferred from perovskite to C$_{70}$ with a time constant of 20 ps. However, the high FF and improved V_{oc} for these ETL-free cells suggested that these electrons

were not trapped in C_{70} but could go back into perovskite. These findings point out the ability of electron-accepting molecules to reduce the trap density of the perovskite film when blended with it, which could enhance the photostability of the devices. These conclusions seem indeed to support the results obtained in Figure 3.8b.

These findings, together with the recently reported photostability improvements reported for other carbon-based nanostructure additives, such as PCBM 1D nanorods,[17] seem to point towards some universality for carbon-based nano-additives and may open wide avenues for the development of stable PSCs.
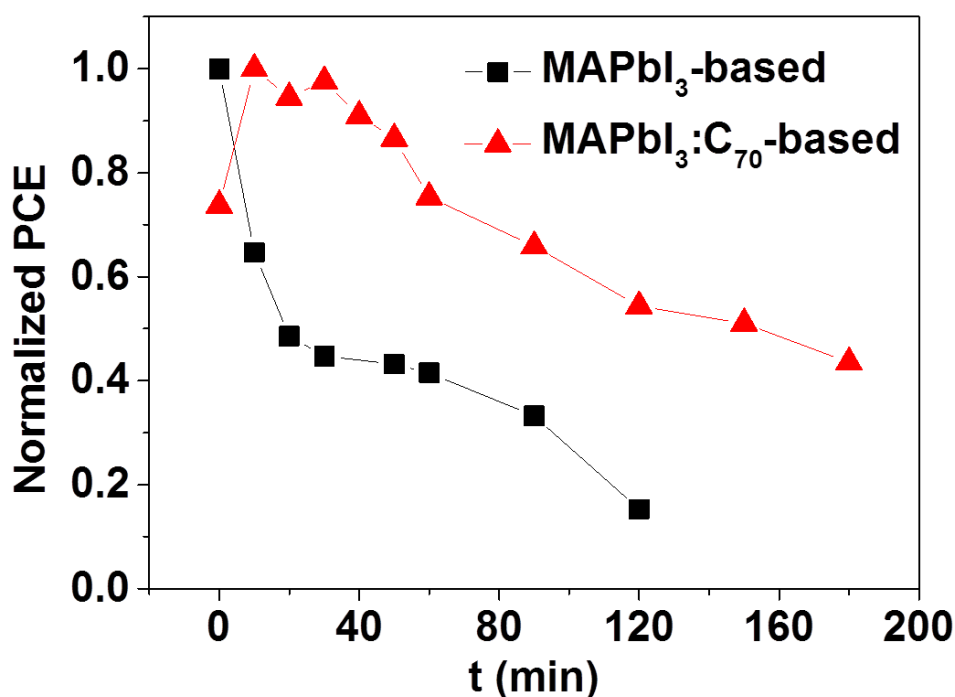
Figure 3.9. Evolution versus time of the normalized power conversion efficiency (PCE) under continuous AM1.5 simulated sunlight for glass/FTO/c-TiO$_2$/light harvester/spiro-OMeTAD/Au solar cells with different light harvesting films: MAPbI$_3$ (black squares) and MAPbI$_3$:C$_{70}$ (red triangles).

3.4   Conclusions

A robust solution-processing protocol for the deposition of pinhole-free methylammonium lead triiodide MAPbI$_3$:C$_{70}$ blend films on FTO-coated glass substrates and their integration into efficient (13.6% under AM1.5G simulated sunlight) ETL-free

PSCs is demonstrated in this chapter. This finding, together with lower transport resistance in comparison to the compact TiO_2 ETL-based devices,[19] makes the glass/FTO/MAPbI$_3$:C$_{70}$/spiro-OMeTAD/Au a competitive heterostructure for PSCs. Furthermore, enhanced photostability of the unencapsulated MAPbI$_3$:C$_{70}$-based ETL-free solar cells is also demonstrated. The comparison of the PV performance versus the regular architecture PSCs based on C$_{70}$ ETL[9] revealed significant differences, suggesting that other working principles than in planar junction solar cells are possible. Therefore, one of the main issues concerning PSCs in this configuration, which is stability, is improved, while achieving good, reproducible efficiencies. All in all, the present results open wide avenues for the deposition of perovskite:fullerene and derivatives blend films and their use in solar cells with simplified architecture, improved manufacturing process, and enhanced stability.

3.5   References

[1]   G. Yang, H. Tao, P. Qin, W. Ke, G. Fang. Recent Progress in Electron Transport Layers for Efficient Perovskite Solar Cells. *J. Mater. Chem. A* **2016**, *4*, 3970.

[2]   L. Calió, S. Kazim, M. Grätzel, S. Ahmad. Hole-Transport Materials for Perovskite Solar Cells. *Angew. Chem. Int. Ed.* **2016**, *55*, 14522.

[3]   T. Leijtens, G. E. Eperon, S. Pathak, A. Abate, M. M. Lee, H. J. Snaith. Overcoming Ultraviolet Light Instability of Sensitized TiO_2 with Meso-Superstructured Organometal Tri-Halide Perovskite Solar Cells. *Nat. Commun.* **2013**, *4*, 2885.

[4]   K. Wojciechowski, M. Saliba, T. Leijtens, A. Abate, H. J. Snaith. Sub-150°C Processed Meso-Superstructured Perovskite Solar Cells with Enhanced Efficiency. *Energy Environ. Sci.* **2014**, *7*, 1142.

[5]   D. Liu, T. L. Kelly. Perovskite Solar Cells with a Planar Heterojunction Structure Prepared Using Room-Temperature Solution Processing Techniques. *Nat. Photonics* **2014**, *8*, 133.

[6]   J. You, L. Meng, T.-B. Song, T.-F. Guo, Y. Yang, W.-H. Chang, Z. Hong, H. Chen, H. Zhou, Q. Chen, Y. Liu, N. De Marco, Y. Yang. Improved Air Stability of Perovskite Solar Cells via Solution-Processed Metal Oxide Transport Layers. *Nat. Nanotechnol.* **2016**, *11*, 75.

[7] J. Song, E. Zheng, J. Bian, X.-F. Wang, W. Tian, Y. Sanehira, T. Miyasaka. Low-Temperature SnO_2-Based Electron Selective Contact for Efficient and Stable Perovskite Solar Cells. *J. Mater. Chem. A* **2015**, *3*, 10837.

[8] K. Wojciechowski, T. Leijtens, S. Siprova, C. Schlueter, M. T. Hörantner, J. T.-W. Wang, C.-Z. Li, A. K.-Y. Jen, T.-L. Lee, H. J. Snaith. C_{60} as an Efficient n-Type Compact Layer in Perovskite Solar Cells. *J. Phys. Chem. Lett.* **2015**, *6*, 2399.

[9] S. Collavini, I. Kosta, S. F. Völker, G. Cabanero, H. J. Grande, R. Tena-Zaera, J. L. Delgado. Efficient Regular Perovskite Solar Cells Based on Pristine [70]Fullerene as Electron-Selective Contact. *ChemSusChem* **2016**, *9*, 1263.

[10] W. Ke, D. Zhao, C. R. Grice, A. J. Cimaroli, J. Ge, H. Tao, H. Lei, G. Fang, Y. Yan. Efficient Planar Perovskite Solar Cells Using Room Temperature Vacuum-Processed C_{60} Electron Selective Layers. *J. Mater. Chem. A* **2015**, *3*, 17971.

[11] D. Liu, J. Yang, T. L. Kelly. Compact Layer Free Perovskite Solar Cells with 13.5% Efficiency. *J. Am. Chem. Soc.* **2014**, *136*, 17116.

[12] Q. Hu, J. Wu, C. Jiang, T. Liu, X. Que, R. Zhu, Q. Gong. Engineering of Electron-Selective Contact for Perovskite Solar Cells with Efficiency Exceeding 15%. *ACS Nano* **2014**, *8*, 10161.

[13] W. Ke, G. Fang, J. Wan, H. Tao, Q. Liu, L. Xiong, P. Qin, J. Wang, H. Lei, G. Yang, M. Qin, X. Zhao, Y. Yan. Efficient Hole-Blocking Layer-Free Planar Halide Perovskite Thin-Film Solar Cells. *Nat. Commun.* **2015**, *6*, 6700.

[14] L. Huang, Z. Hu, J. Xu, X. Sun, Y. Du, J. Ni, H. Cai, J. Li, J. Zhang. Efficient Planar Perovskite Solar Cells without a High Temperature Processed Titanium Dioxide Electron Transport Layer. *Energy Mater. Sol. Cells* **2016**, *149*, 1.

[15] Y. Shao, Z. Xiao, C. Bi, Y. Yuan, J. Huang. Origin and Elimination of Photocurrent Hysteresis by Fullerene Passivation in $CH_3NH_3PbI_3$ Planar Heterojunction Solar Cells. *Nat. Commun.* **2014**, *5*, 5784.

[16] J. Xu, A. Buin, A. H. Ip, W. Li, O. Voznyy, R. Comin, M. Yuan, S. Jeon, Z. Ning, J. J. McDowell, P. Kanjanaboos, J.-P. Sun, X. Lan, L. N. Quan, D. H. Kim, I. G. Hill, P. Maksymovych, E. H. Sargent. Perovskite-Fullerene Hybrid Materials Suppress Hysteresis in Planar Diodes. *Nat. Commun.* **2015**, *6*, 7081.

[17] C. Ran, Y. Chen, W. Gao, M. Wang, L. Dai. One-Dimensional (1D) [6,6]-Phenyl-C_{61}-Butyric Acid Methyl Ester (PCBM) Nanorods as Efficient Additive for Improving the Efficiency and Stability of Perovskite Solar Cells. *J. Mater. Chem. A* **2016**, *4*, 8566.

[18] L. Huang, J. Xu, X. Sun, Y. Y. Du, H. Cai, J. Ni, J. Li, Z. Hu, J. Zhang. Towards Revealing the Critical Role of Perovskite Coverage in Highly Efficient Electron-Transport Layer-Free Perovskite Solar Cells: an Energy Band and Equivalent Circuit Model Perspective. *ACS Appl. Mater. Interfaces* **2016**, *8*, 9811.

[19] J. Pascual, I. Kosta, N. Tuyen, A. Chuvilin, G. Cabanero, H. J. Grande, E. M. Barea, I. Mora-Seró, J. L. Delgado, R. Tena-Zaera. Electron Transport Layer-Free Solar Cells Based on Perovskite-Fullerene Blend Films with Enhanced Performance and Stability. *ChemSusChem* **2016**, *9*, 2679.

[20] S. Gharibzadeh, F. V. d. A. Camargo, C. Roldán-Carmona, G. C. Gschwend, J. Pascual, R. Tena-Zaera, G. Cerullo, G. Grancini, Md. K. Nazeeruddin. Picosecond Capture of Photoexcited Electrons Improves Photovoltaic Conversion in MAPbI$_3$:C$_{70}$-Doped Planar and Mesoporous Solar Cells. *Adv. Mater.* **2018**, 1801496.

4   Cosolvent approach for perovskite:C$_{70}$ blends processing

4.1   Introduction

The results of Chapter 3 present MAPbI$_3$:C$_{70}$ blend films as improved light-absorbing layers for their use in ETL-free PSCs in comparison to traditional MAPbI$_3$ ones. The reduction in pinhole-density in the perovskite layer and the enhancement of the solar cell efficiency and stability proved C$_{70}$ as a preferential additive in this kind of devices. However, the application of fullerenes blended in the perovskite layer is far from optimized, and a strategy in order to obtain more efficient and reproducible ETL-free devices is still to be achieved.

In this sense, it has to be taken into account that there may be room for improvement in the processing of MAPbI$_3$:C$_{70}$ blend layers reported in the previous chapter.[1] It has to be considered the low affinity of fullerenes to a solvent such as DMF (i.e. solubility 0.5 mg mL^{-1}), which might have an impact in the final characteristics of the blend layer, such as perovskite crystallization or fullerene distribution. As it has been presented in literature, how fullerenes are introduced in polymer:fullerene OPVs completely affect the final outcome.[2-4] The ability of these p-n heterojunction solar cells to separate charges was highly influenced by how fullerene and polymer were intermixed. Although the same criteria might not be applicable in the present scenario of PSCs, the importance of how fullerene is being introduced in blend films may be very significant. In fact, works in literature suggest that perovskite grain boundaries are domains with higher density of defects.[5] Considering this and that the works so far on perovskite:fullerene blend films point out the ability of fullerenes to passivate defects,[6-8] a strategy to distribute fullerenes throughout the grain boundaries of perovskite could enhance the performance and stability of the devices. In this regard, further research tuning the way in which fullerene aggregates, distributes and interacts within the perovskite layer is required in order to fully understand these systems and being able to develop standard protocols for their use in PSCs.

Going back to the low affinity of fullerenes towards the main solvents used in perovskite layer processing, the search for solvents that could vary how perovskite:fullerene blend

films crystallize could shed light on this issue and open new opportunities. DMF, DMSO, *N*-methyl-2-pyrrolidone, and γ-butyrolactone are the most common examples for perovskite processing. These solvents and many others have been combined for the improvement of perovskite solution-processing, leading to more efficient devices through the formation of more uniform and dense perovskite films.[9-12] However, the typical solvents used for fullerene chemistry are quite different, varying from CS_2 to aromatic ones like toluene or chlorobenzene. The effective combination of solvents with different affinities towards fullerene and perovskite in blend films processing may be complicated, but critical so as to achieve improved devices.

In this chapter the use of *o*-xylene in 1:4 ratio vs DMF for the processing of improved $MAPbI_3$:C70 blend films-based ETL-free PSCs is presented. Additionally, a variety of cosolvents with certain structural and physicochemical properties are employed for this type of devices and the results are analyzed, in order to unravel the origin of the positive effect of this cosolvent approach. PV results and the discussion of the parameters obtained for each cosolvent are combined with further spectroscopic and microstructural characterization. Some practical guidelines for the choice of an appropriate cosolvent for the fabrication of fullerene-containing PSCs are also discussed.

4.2   Experimental Section

4.2.1   Materials

The materials used in this study were obtained from commercial suppliers in high purity and used without further purification: glass/FTO (TEC15, Hartford Glass), C70 (99%, SES Research), MAI (DYESOL), $PbCl_2$ (98%, Sigma-Aldrich), spiro-OMeTAD (99%, Feiming Chemicals Limited), LiTFSI (99.9%, Solvionic), *tert*-butylpyridine (96%, Sigma-Aldrich), DMF (extra pure, Scharlab), 2-propanol (synthetic grade, Scharlab), acetone (technical grade, Scharlab), chlorobenzene (99.8%, Sigma-Aldrich), *o*-xylene (98%, Sigma-Aldrich), *o*-dichlorobenzene (*o*-DCB, 99%, Sigma-Aldrich), methylcyclohexane (Me-Cy, 99%, Sigma-Aldrich), chlorocyclohexane (Cl-Cy, 99%, Sigma-Aldrich), and acetonitrile (UV HPLC grade, Scharlab).

4.2.2 Device Fabrication

The perovskite solution was prepared by dissolving 7.71 mmol of MAI and 2.57 mmol of PbCl$_2$ (molar ratio 3:1) in 3 mL of DMF and stirring the solution overnight. Prior to deposition, the C$_{70}$ was added to the perovskite solution in a 1:4320 molar ratio to PbCl$_2$, which corresponds to the C$_{70}$ saturation value in DMF (0.5 mg mL^{-1}).[1] Different cosolvents (i.e. *o*-xylene, *o*-DCB, Me-Cy, Cl-Cy) were added to perovskite solution in a 1:4 ratio vs DMF. For the initial experiment with *o*-xylene it was added to perovskite solution in the ratios 1:8, 1:4 and 1:2 (cosolvent:DMF). The resulting solution was spin coated on the substrates following a two-step protocol, which consisted of a first step of 500 rpm for 5 s followed by a second step of 2000 rpm for 45 s. Subsequently, the samples were annealed at 100°C for 2 h to ensure complete perovskite formation. Spiro-OMeTAD and Au layers were deposited on top of perovskite layer as described in Chapter 2.

4.2.3 Thin Film and Device Characterization

The morphological properties of the films were characterized by field emission scanning electron microscopy using an ULTRA plus ZEISS FE-SEM.

The *J-V* chracteristics of the solar cells were measured under simulated solar light by using the setup decribed in chapter 2. The EQE spectra of the devices were also obtained from the home-made specific setup and methodology described in chapter 2.

4.3 Results and Discussion

4.3.1 Cosolvent approach

Taking into account the increasing PCE trend with C$_{70}$ content in Chapter 3, it was thought that higher concentrations of C$_{70}$ in the perovskite layer would enhance this effect even more in ETL-free devices. Regarding this, the chosen solvents in this thesis

with the ability to play with the concentration of C_{70} were considered as cosolvents. In particular, *o*-xylene was chosen as starting point for this study, not only because of its superior C_{70}-solubilising ability (ca. 4 mg mL^{-1}), although significantly lower than previously reported,[13] but also due to its inert character in respect to perovskite precursors. Several series of MAPbI$_3$:C$_{70}$ blend films were deposited from *o*-xylene/DMF (1:4 v/v) solutions with different C_{70}/PbCl$_2$ ratios (i.e. from 1:10000 to saturation at 1:2170) on bare FTO (i.e. type I architecture from Chapter 3). Interestingly, the best PCE conversion was reached for the 1:4320 C_{70}/PbCl$_2$ ratio, which is the saturation value for the perovskite solution in DMF. However, adding *o*-xylene resulted in a significant increase of the PCE, reaching 13.6% for the best devices (Table 4.1). *J-V* curves of champion devices and full statistics are available in Figures 4.1 and 4.2, respectively.
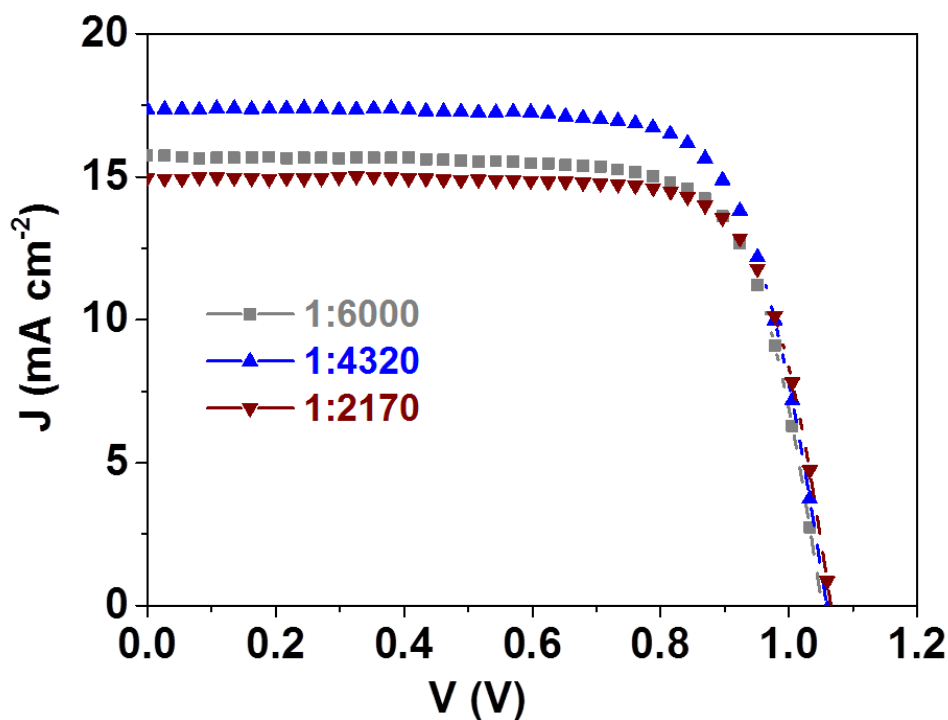

Figure 4.1. *J-V* curves of the best ETL-free solar cells based on MAPbI$_3$:C$_{70}$ blend films processed from different C_{70}/PbCl$_2$ ratios in DMF:*o*-xylene (4:1) solutions.

Figure 4.2. PV parameters for ETL-free solar cells based on MAPbI$_3$:C$_{70}$ blend films processed from different C$_{70}$/PbCl$_2$ ratios in DMF:*o*-xylene (4:1) solutions.

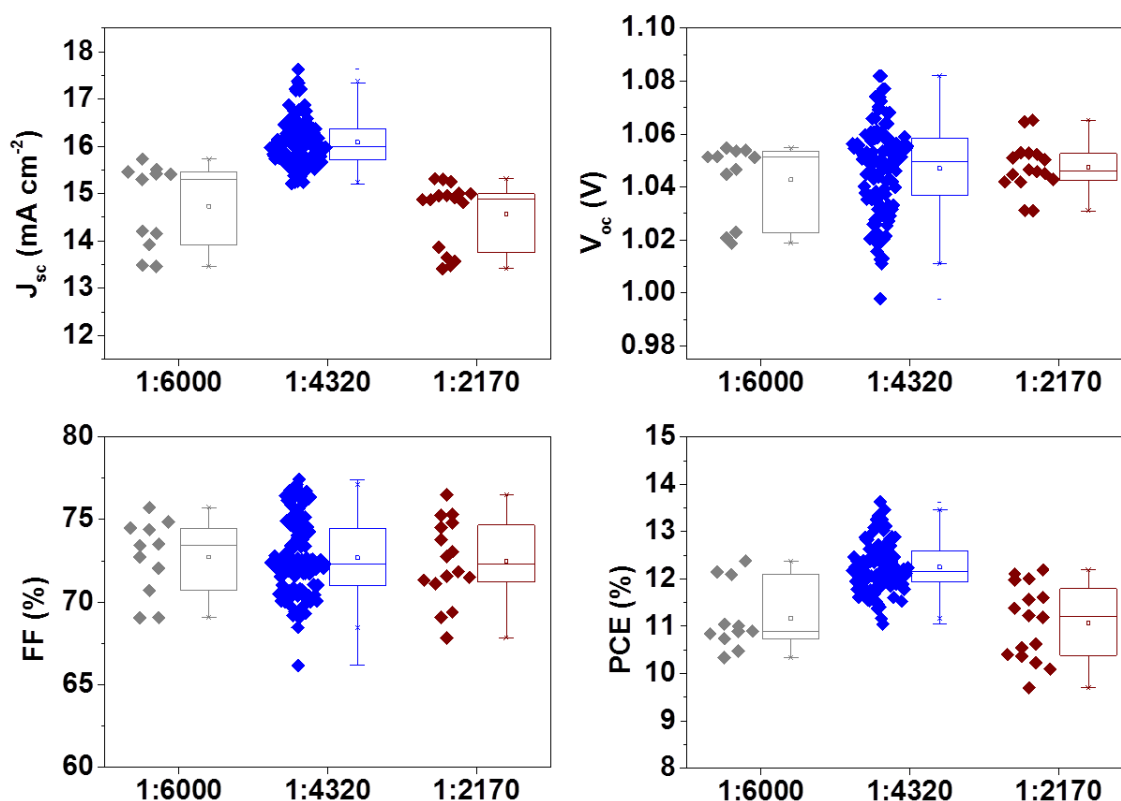**Table 4.1.** PV parameters of the best performing ETL-free solar cells based on MAPbI$_3$:C$_{70}$ blend films processed from DMF:*o*-xylene (4:1) solutions with different C$_{70}$/PbCl$_2$ ratios.

C$_{70}$/PbCl$_2$	J_{sc} (mA cm^{-2})	V_{oc} (V)	FF (%)	PCE (%)
1:6000	15.7	1.05	74.9	12.4
1:4320[a]	15.6	1.05	75.2	12.4
1:4320	17.4	1.06	74.1	13.6
1:2170	15.0	1.07	76.5	12.2

[a] Solar cells processed from cosolvent-free solutions.

Indeed, the use of *o*-xylene resulted not only in a higher PCE, but also in considerably higher reproducibility (i.e. narrower dispersion) of the PCE values of solar cells based on MAPbI$_3$:C$_{70}$ blend films at the same 1:4320 C$_{70}$/PbCl$_2$ ratio (Figure 4.3). This finding points out the enhanced robustness of the *o*-xylene cosolvent-based device preparation protocol.
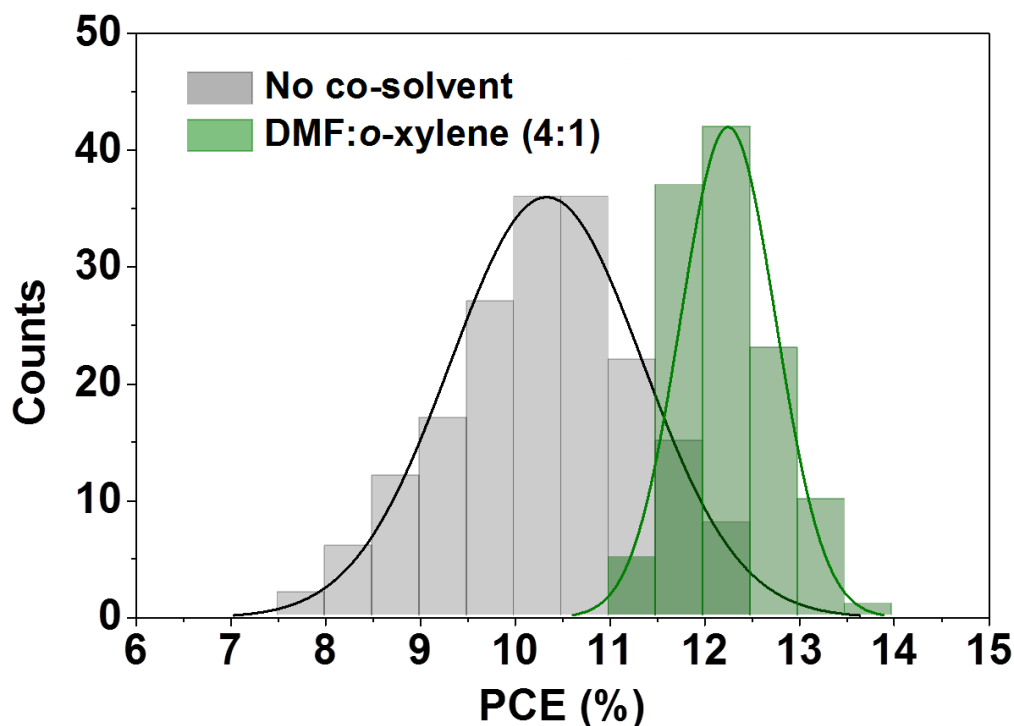
Figure 4.3. Distribution of PCE values of ETL-free solar cells based on MAPbI$_3$:C$_{70}$ blend films processed with and without ¼ volume fraction of *o*-xylene, in green and grey respectively.

4.3.2   Cosolvent comparison in devices

As seen in the previous section, *o*-xylene works very well for MAPbI$_3$:C$_{70}$ blend films processing with the cosolvent approach. Nevertheless, there was no evidence on what its role could be, as well as the possible effect of using other solvents of different nature. Therefore, various solvents that were found inert to perovskite were selected in next study in order to ravel out these issues. Due to the improved performance obtained in the previous studies with *o*-xylene, it was set as a reference for cosolvent comparison. Me-Cy was chosen as the aliphatic equivalent so as to check the relevance of this characteristic and, for further comparison with differently substituted rings, *o*-DCB and Cl-Cy were chosen as a second aromatic-aliphatic pair (Figure 4.4). Table 4.2 summarizes some physicochemical properties of relevance for the processing of MAPbI$_3$:C$_{70}$ for the four cosolvents. The effect of these cosolvents was studied for the ETL-free architecture glass/FTO/MAPbI$_3$:C$_{70}$ (DMF 4:1 cosolvent) and with spiro-

OMeTAD and Au as hole-selective and back contact, respectively. Several devices were prepared with each cosolvent for statistical comparison.
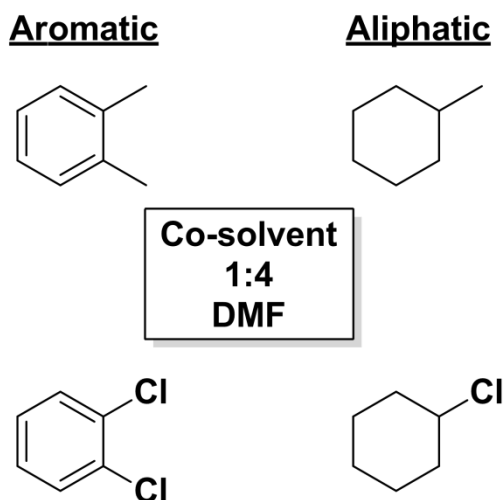

Figure 4.4. Molecular structure of studied cosolvents for the processing of PSCs.

Table 4.2. Density (d), boiling point (bp), dipole moment (μ), and vapor pressure (P_V) values for selected solvents.

Solvent	d (mg mL^{-1})	bp (°C)	μ	P_V (mbar, 25°C)
o-xylene	0.88	111	0.62	6.9, 264.0[a]
o-DCB	1.30	181	2.27	1.6, 84.0[a]
Me-Cy	0.77	101	-	110.7
Cl-Cy	1.00	142	-	10.7

[a] At a temperature value of 100°C.

It has to be noted that all four cosolvents do show different effects on solar cells, pointing out their relevance in the perovskite:fullerene film processing conditions. According to the mean values reported in Table 4.3 for each processing conditions, the highest PV parameters were obtained for aromatic cosolvents (i.e. o-xylene and o-DCB). The *J-V* curve of the best device for each cosolvent and PV parameter data and dispersion are shown in Figure 4.5. Excluding the lower short-circuit current density (J_{sc}) obtained for o-DCB, open-circuit voltage (V_{oc}) and fill factor (FF) were positively affected by the use of any of these two cosolvents, which meant an improvement in comparison to results for cosolvent-free processed perovskite. However, aliphatic cosolvents did not show any significant difference to cosolvent-free strategy. Me-Cy

provided similar mean values, although with a smaller deviation than no-cosolvent formulations. In the case of Cl-Cy worse results were obtained though. Still better than fullerene-free devices, a negative effect was found for the application of Cl-Cy as cosolvent in C_{70}-containing devices (Figure 4.6).

Table 4.3. Average PV parameters values for ETL-free solar cells processed with the different selected cosolvents in 1:4 ratio vs DMF.

Processing conditions	J_{sc} (mA cm^{-2})	V_{oc} (V)	FF (%)	PCE (%)[a]
o-xylene:C_{70}	16.1	1.04	71.9	12.2 (13.6)
o-DCB:C_{70}	14.4	1.05	74.4	11.2 (12.0)
Me-Cy:C_{70}	15.4	1.03	68.6	10.9 (11.4)
Cl-Cy:C_{70}	15.1	1.01	64.8	9.8 (10.8)
C_{70}	15.3	1.02	68.1	10.4 (12.0)
Fullerene-free	15.2	0.95	61.2	9.0 (10.5)

[a] Maximum PCE value for each condition provided in parentheses.
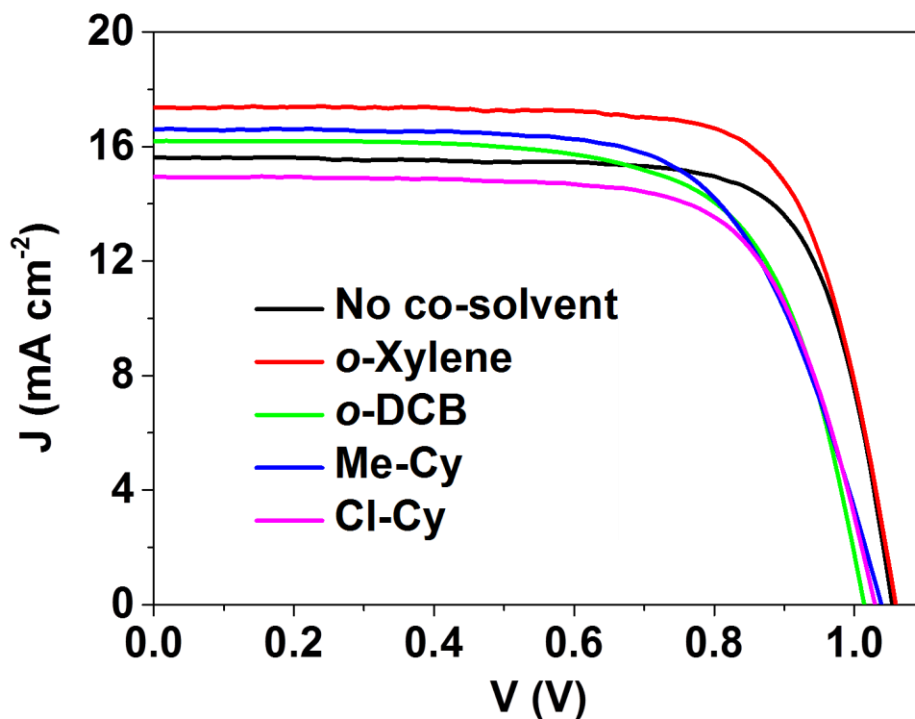

Figure 4.5. *J-V* curves of the best PSCs based on MAPbI$_3$:C_{70} blend films processed with different cosolvents.
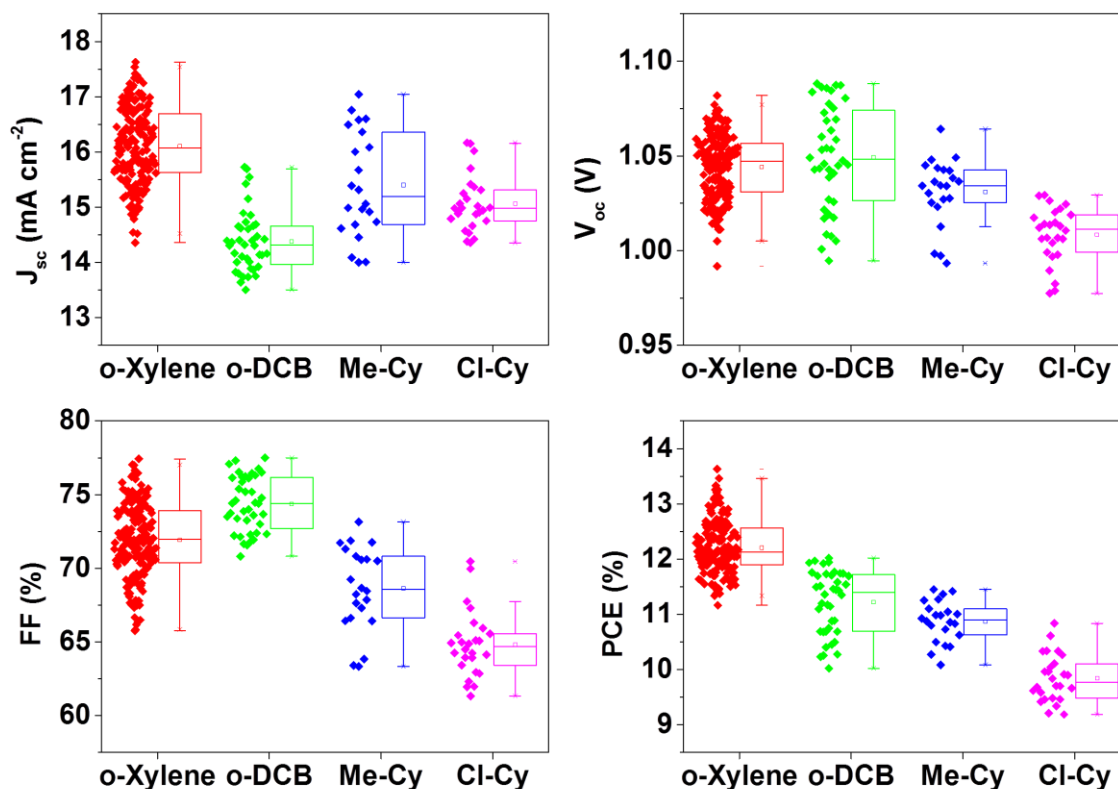
Figure 4.6. PV parameters for PSCs based on MAPbI$_3$:C$_{70}$ blend films processed with different cosolvents.

All in all, higher PCE were reached for aromatic cosolvents (Figure 4.6). If each pair was studied separately, aromatics led to more efficient devices in contrast to their corresponding aliphatic analogue. Not only that, although exhibiting physicochemical properties such as boiling point, density, and dipole moment in the opposite extremes among the selected solvents (Table 4.2), both *o*-xylene and *o*-DCB provided the most efficient cells. Furthermore, the pair with alkyl substituents provided higher efficiencies overall, in comparison to the halogenated pair (i.e. *o*-xylene vs *o*-DCB and Me-Cy vs Cl-Cy), suggesting that this feature is more beneficial for cosolvent strategy. It is noted that no difference in PCE or other PV parameter was found among the four cosolvents when fullerene was not introduced (Figure 7).
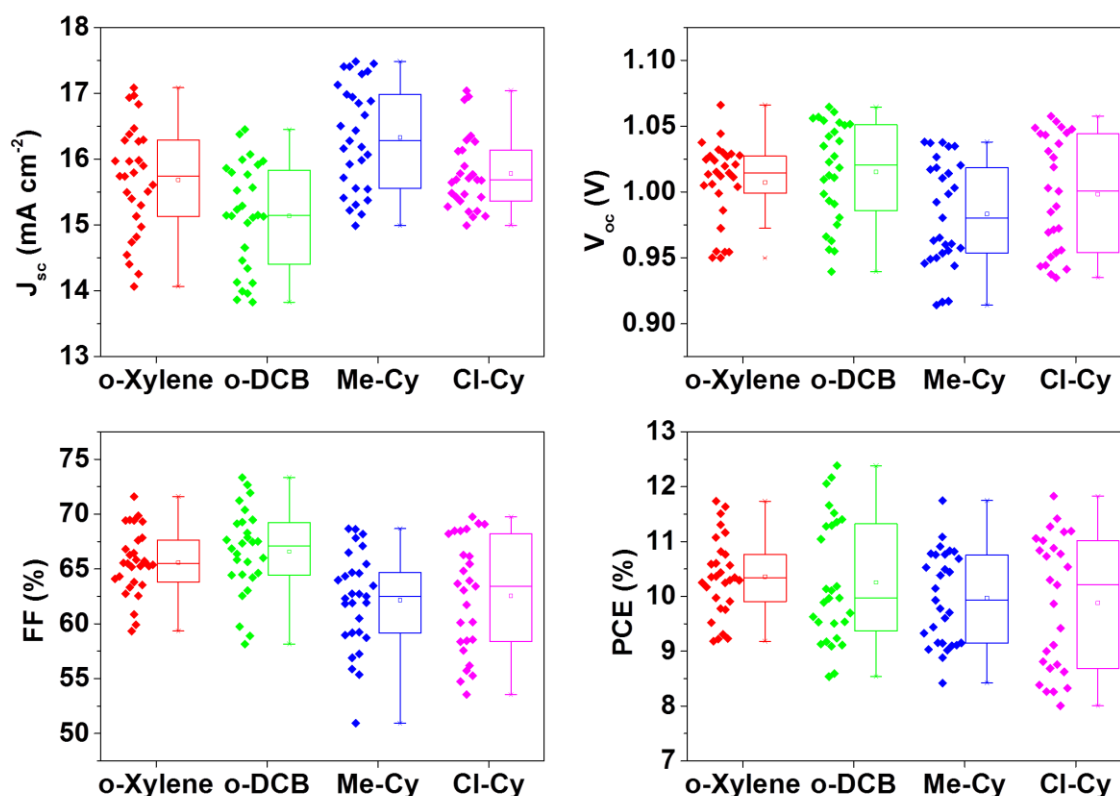
Figure 4.7. PV parameters for PSCs based on MAPbI$_3$ films processed with different cosolvents.

In the results in Table 4.3 and Figure 4.6, the most interesting observation can be made on the increase of FF for aromatic cosolvents. In fact, quite high mean values were obtained for them (i.e. >70%), in contrast to aliphatic cosolvents, which provided no improvement over cosolvent-free-processed devices. As shown in Figure 4.8, it is the presence of C$_{70}$ that provided an improvement of FF value; aromatic cosolvents by themselves did not result in any FF difference to cosolvent free devices when C$_{70}$ was not present. Thus, only the combination of the aromatic cosolvents with C$_{70}$ in perovskite blends led to highly improved FF values (narrower dispersion is also noted). Indeed, a highest value of 77.5% was recorded for *o*-DCB, very high considering the values achieved in literature for ETL-free PSCs.
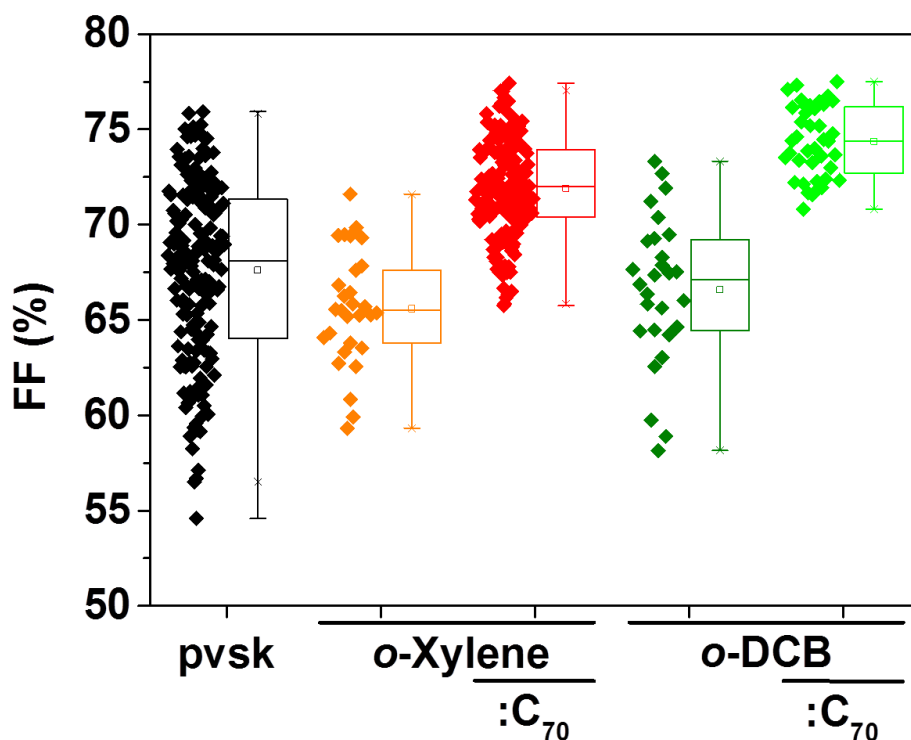
Figure 4.8. Change in FF when C_{70} also used in cosolvent-processed ETL-free PSCs.

In collaboration with our co-workers Giulia Grancini and Mohammad Khaja Nazeeruddin the photoluminescence (PL) spectra of some these layers were also investigated.[14] Interestingly, MAPbI$_3$:C$_{70}$ blend films processed by using *o*-xylene exhibited significantly faster decay than those obtained from Me-Cy (i.e. faster component <1 ns vs 2.7 ns, Figure 4.9). Therefore, the use of aromatic cosolvents seems to play a beneficial impact on the charge-transfer dynamics. This may be due to the differences in the energy diagram (i.e. pointed out by the absorption spectra) and consequent additional pathways for the electron transfer from the MAPbI$_3$ conduction band to the C$_{70}$. However, this does not reflect in huge differences in the PL emission of glass/MAPbI$_3$:C$_{70}$ samples processed using the different cosolvents.
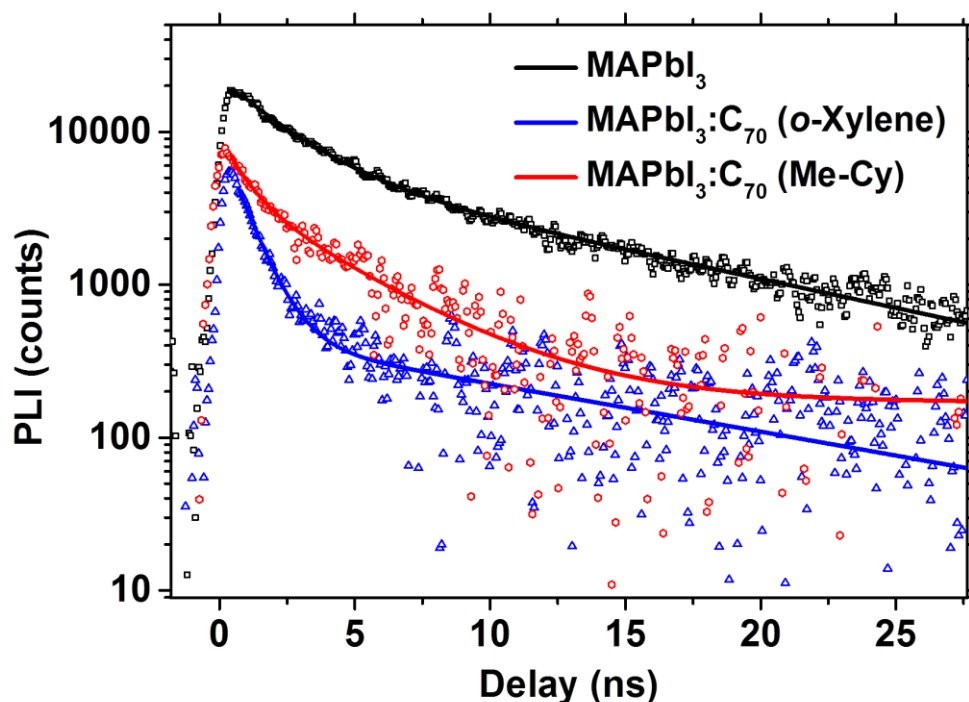
Figure 4.9. PL decays of glass/MAPbI$_3$ and glass/MAPbI$_3$:C$_{70}$ samples, excitation at 460 nm, fluence 50 nJ cm^{-2}. The biexponential fits are also shown. The cosolvent used in the preparation of the MAPbI$_3$:C$_{70}$ films is included in parentheses. Further information is available in reference [14].

4.3.3   Cosolvent-fullerene interactions

Thus, the differences presented in Figures 4.6-8 suggest the presence of some interaction between the cosolvents and C$_{70}$. In this regard, UV-vis absorption (Abs) spectra of C$_{70}$ dissolved in the four studied cosolvents (0.008 mg mL^{-1}) were carried out, showing clear differences between aromatic and aliphatic ones (Figure 4.10). The main band at a wavelength position of 300 nm is shifted to higher energy values for aliphatic cosolvents, while the bands in the 300-500 nm range show very low intensity for aliphatics in comparison to aromatics.

Figure 4.10. UV-vis absorption spectra for C_{70} dissolved in each studied cosolvent in 0.008 mg mL^{-1} concentration.

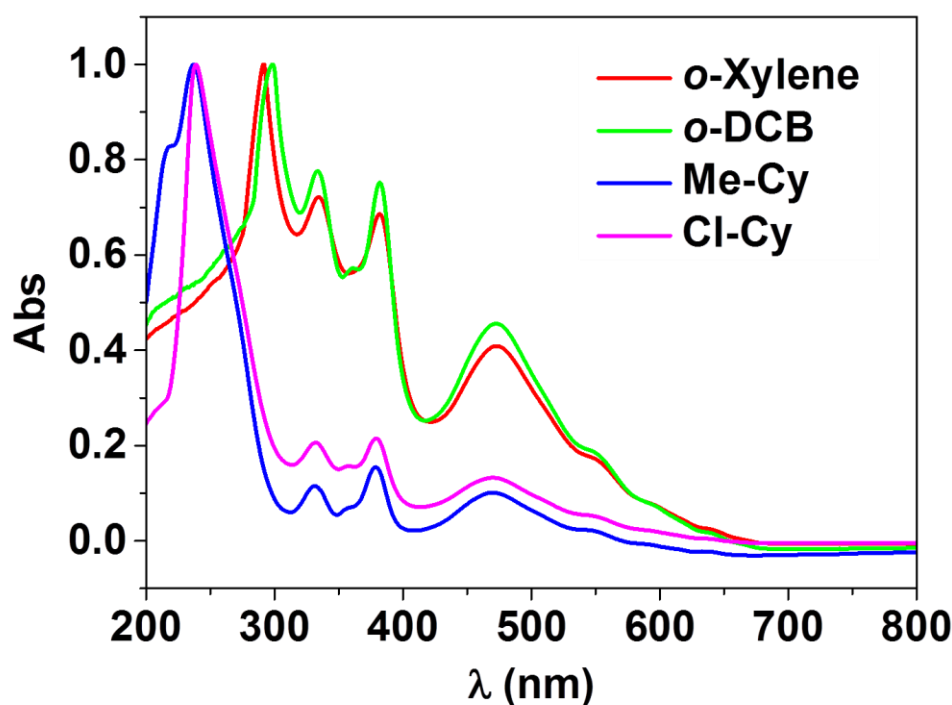The strong bathochromic effect that can be seen for the highest energy band in aromatic solvents has particular interest, pointing out a charge-transfer interaction between fullerene and solvent molecule. C_{70} has high electron affinity;[15] therefore, it can establish relevant charge-transfer interactions with an aromatic solvent.[16] Indeed, fullerenes and their excited state may be stabilized through solvent-solute π-stacking. In this regard, strong solute-solvent interactions may compete with solute-solute interactions that produce aggregation of fullerenes. In the case of aromatic solvents, more negative enthalpy values are achieved, leading to a greater solvation and thus less aggregation of fullerene molecules.[17] Therefore, stronger interactions of *o*-xylene and *o*-DCB with this carbon allotrope may be possible due to the π-delocalization all over the C_{70}-ball.

Interestingly, very significant differences in the UV-vis absorption spectra of C_{70} DMF solution were detected when aromatic cosolvents were used (Figures 4.11a-b). The relative position of the absorption peaks of the DMF:cosolvent mixture versus to the ones of pure DMF and cosolvent may provide insights into which solvent is promoting

more significant changes in the electronic structure (i.e. in energy diagram too) of C_{70} when interacting with it. Therefore, if the absorption features in the 4:1 mixture are closer in wavelength position to pure cosolvent rather than to pure DMF, then the cosolvent may be the main component responsible for solvation of C_{70} in the mixture. The C_{70} strongest absorbing band position in these spectra was detected closer to its position in pure solutions of cosolvent when mixtures of DMF:aromatic were used but was found closer to its position in DMF when aliphatic cosolvents were used (Figure 4.11c). This suggests that in these 4:1 mixtures C_{70} experiences major effects in the energy diagram for aromatic cosolvents, but less important ones with aliphatic ones, which agrees with the higher solvation of C_{70} with aromatic cosolvents proposed before.[17]
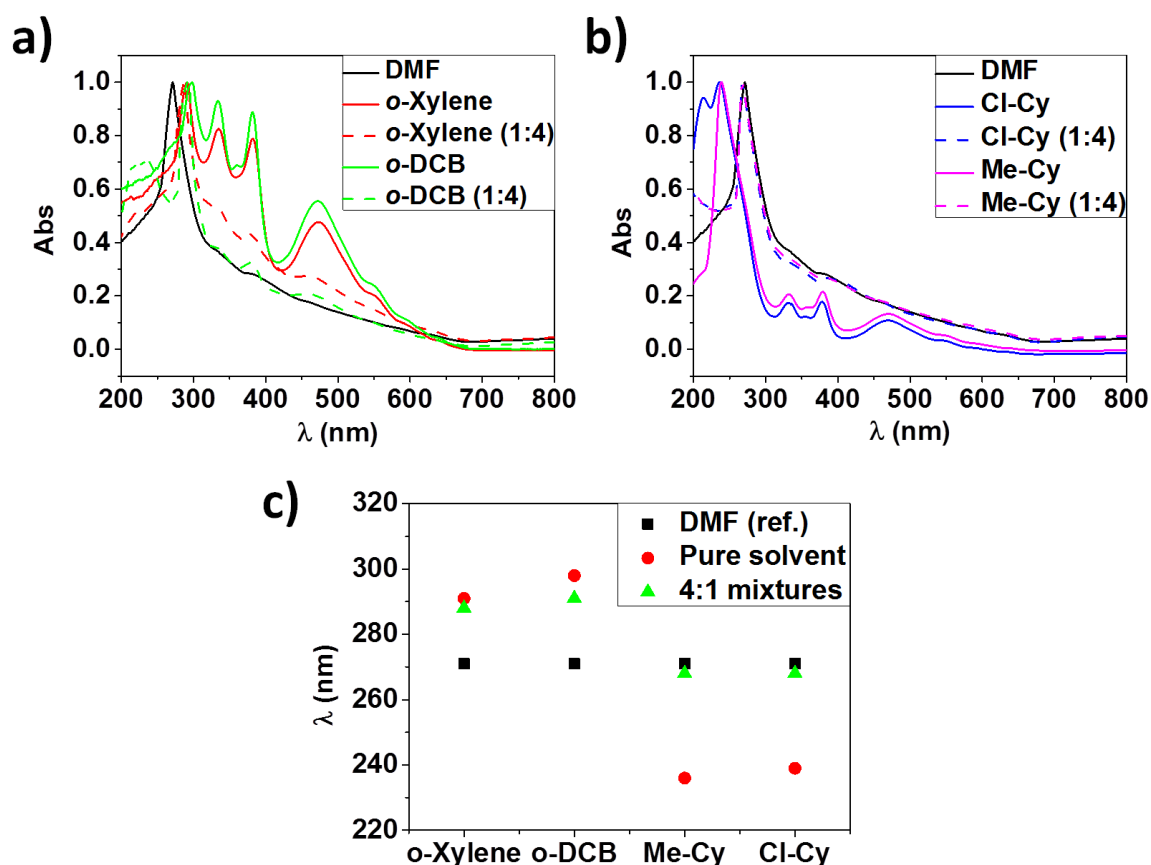

Figure 4.11. UV-vis absorption spectra for C_{70} dissolved in 0.008 mg mL^{-1} concentration in the studied a) aromatic and b) aliphatic solvents. c) Wavelength position for the strongest UV-vis absorbing band for DMF, pure cosolvents, and 4:1 mixtures.

It is noted that the emission spectra of C_{70} solutions also change depending on the cosolvent (Figure 12). Excitation at low-energy wavelength values when C_{70} is dissolved in *o*-xylene (i.e. aromatic) led to very little emission in comparison to the case for Me-Cy (i.e. aliphatic). The relatively minor emission may be due to stronger electronic interactions between aromatic cosolvents and fullerene, making possible nonradiative pathways for the excited-state fullerene electrons.
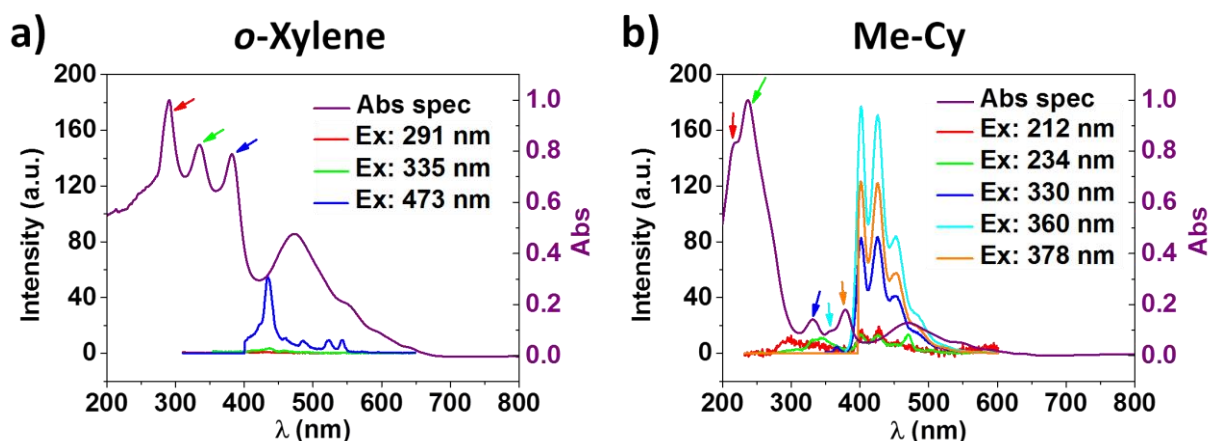
Figure 4.12. Absorbance and emission spectra of C_{70} at selected excitation wavelength values in a) *o*-xylene and b) Me-Cy. The colour of the emission spectra refers to the colour excitation at the frequency value of the same colour arrow. The emission spectra belong to the excitation at the frequency of the absorbance peak with the arrow of the same colour.

The EELS data carried out in collaboration with Andrey Chuvilin (CIC nanoGUNE) supports the hypothesis presented in this chapter. Significant peak broadening is observed for C_{70} crystals obtained from the solutions of the solvents used in this study when compared to the spectra of the sublimated film (Annex 4.1a).[14] This finding indicates that the electron structure of C_{70} is significantly influenced by these solvents, which in turn means a strong interaction of the fullerene cages with the solvent molecules even in the crystalline state. Furthermore, XRD characterization revealed the formation of different crystal structures when fullerenes were crystallized from the different solvents (Annex 4.1b).[14] This finding may point to inclusion of substantial amount of solvent into the crystals due to strong interaction of solvent molecules with C_{70}.

4.3.4 Cosolvent effect on perovskite:C_{70} morphology

The above characterization of the fullerene solutions and processed solid material pointed out the existence of significant interactions between C_{70} and the studied solvents, with major effects on the optoelectronic properties for the aromatic solvents. The effects of these interactions on the perovskite:fullerene film properties were also analyzed.

Figure 4.13 compares the top-view FE-SEM micrographs of the perovskite:C_{70} blend films processed with the different cosolvents. The micrographs do not show relevant differences in the morphology of the perovskite, but show the pinhole density varies from cosolvent to cosolvent. The pinhole-free morphology detected in films processed from formulations including *o*-xylene and *o*-DCB suggests that aromatic cosolvents helped to achieve very homogeneous perovskite layers, whereas aliphatic ones led to a high density of pinholes. The pinhole-free nature may indeed be one of the main origins of FF improvement in the solar cells.
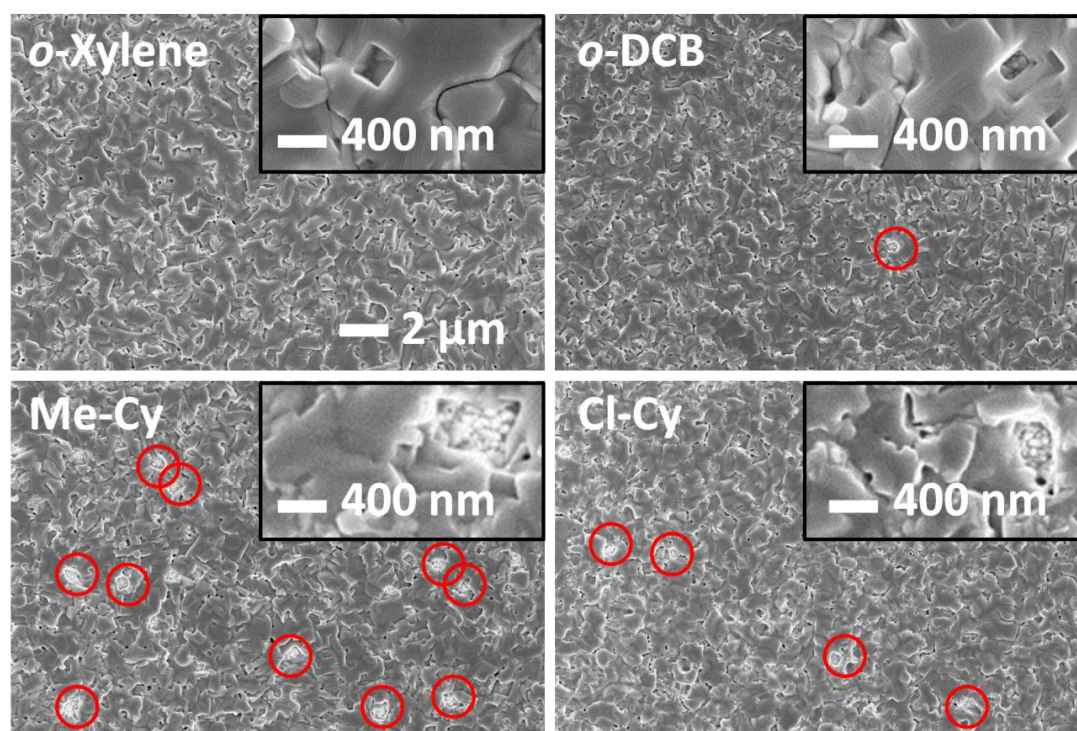
Figure 4.13. Top-view FE-SEM micrographs of MAPbI$_3$:C_{70} blend films processed by using studied cosolvents. An inset zooming in on the pinholes has been included for each cosolvent.

The AFM topography and phase images were recorded simultaneously in small pinhole-free regions by our collaborator Elisa Palacios-Lidón (Universidad de Murcia), providing

additional insights on the effect of cosolvents.[14] First, the overall grain morphology is basically independent of the cosolvent nature (Figure 4.14a). However, as it can be seen in Figure 4.14b, the corresponding phase images reveal important differences. Aromatic cosolvents (i.e. *o*-xylene and *o*-DCB) induced the formation of small island-like phase regions, of a few nanometers, randomly distributed within the grains. The phase contrast can be correlated with different chemical surface compositions,[18-20] indicating that the C_{70} concentration is not homogeneously distributed within the perovskite matrix. On the contrary, aliphatic cosolvents led to homogeneous phase-island-free grains and bright phase contrast at the stepped edges.

Figure 4.14. AFM results showing differences in a) low-magnification topography images (lateral size 4 $\mu m \times 4$ μm and z scale = 600 nm) and b) high-magnification phase images of perovskite:C_{70} blend layers processed with each studied cosolvent (top panels 2 $\mu m \times 2$ μm and bottom panels 500 nm $\times$ 375 nm). Further information is available in reference [21].

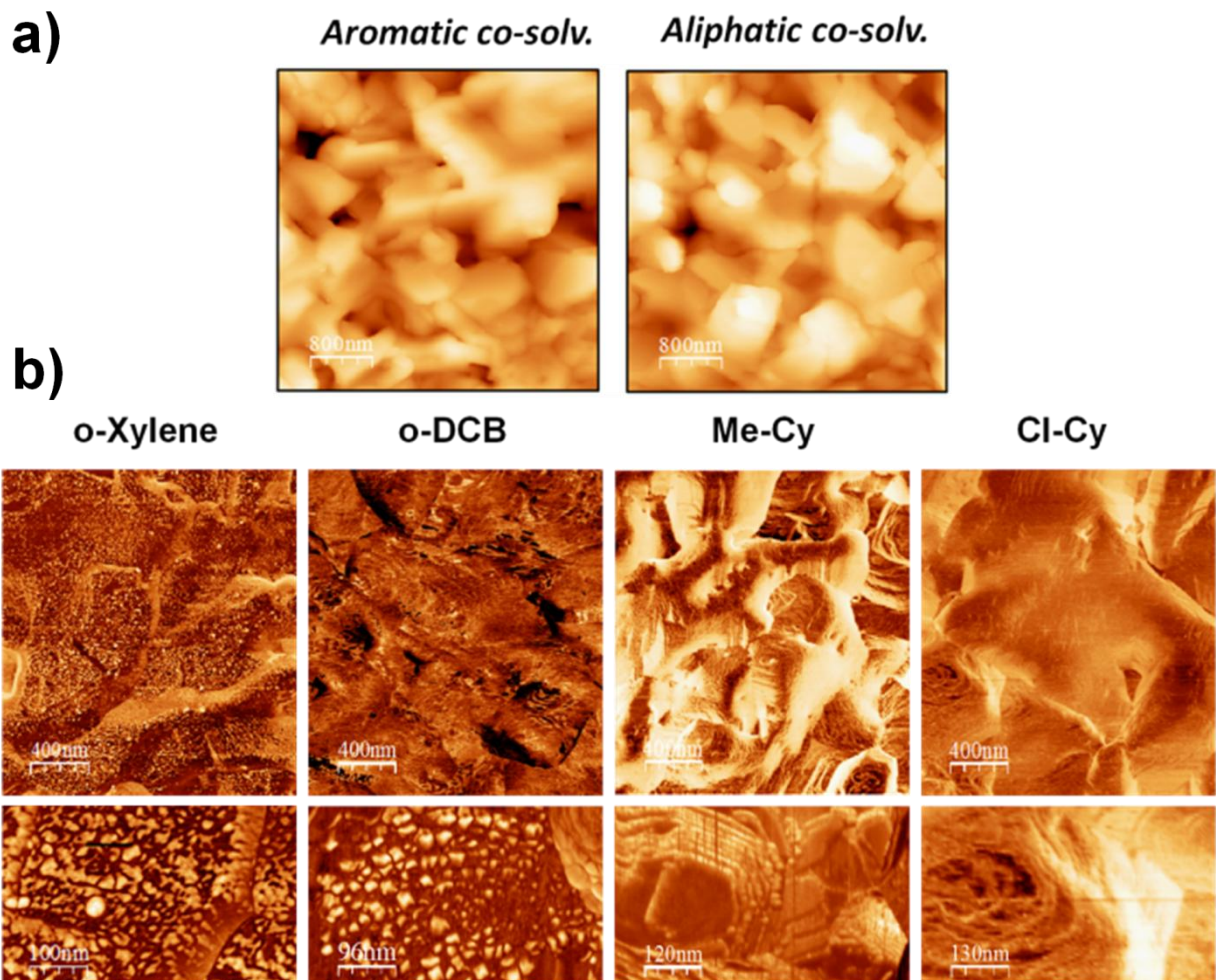This can be explained with a homogeneous distribution of C_{70} within the perovskite grains, even though slightly higher concentration at the bright phase contrast steps cannot be ruled out. Although the quantitative chemical composition of each region is not directly obtained from the AFM phase data, we can conclude that the cosolvent nature strongly affects C_{70} distribution.

AFM results are particularly interesting, because they explain the relevance of the aromaticity of the cosolvent among other properties such as vapor pressure. In this sense, it might be thought that a higher value of vapor pressure would promote migration of C_{70} to the surface. Still, the same nanoislands appear in AFM samples for solvents with such different vapor pressures at 100°C (i.e. the annealing temperature used for obtaining $MAPbI_3$:C_{70} films) as o-xylene (198 mmHg) and o-DCB (63 mmHg).

In this work STEM-EELS characterization was also carried out by our co-worker Andrey Chuvilin (CIC nanoGUNE). Perovskite:C_{70} blend films revealed significant differences in the C_{70} distribution as a function of the processing solvents (Figure 4.15). Briefly, when DMF was used as a solvent, C_{70} was not clearly identified in the STEM-EELS carbon map micrographs, although higher C-K signal was clearly detected in the EELS spectra (inset Figure 4.15), suggesting that fullerene may be integrated inside the crystalline structure of perovskite. However, when o-xylene was used as a cosolvent, STEM-EELS carbon maps showed a different distribution for C_{70}, leaving it visible, probably laying along the grain boundaries (Figure 7.4b). These results were in accordance with the micrographies obtained by AFM means (Figure 7.4c), for which a different distribution of the fullerene in the perovskite layer was observed.
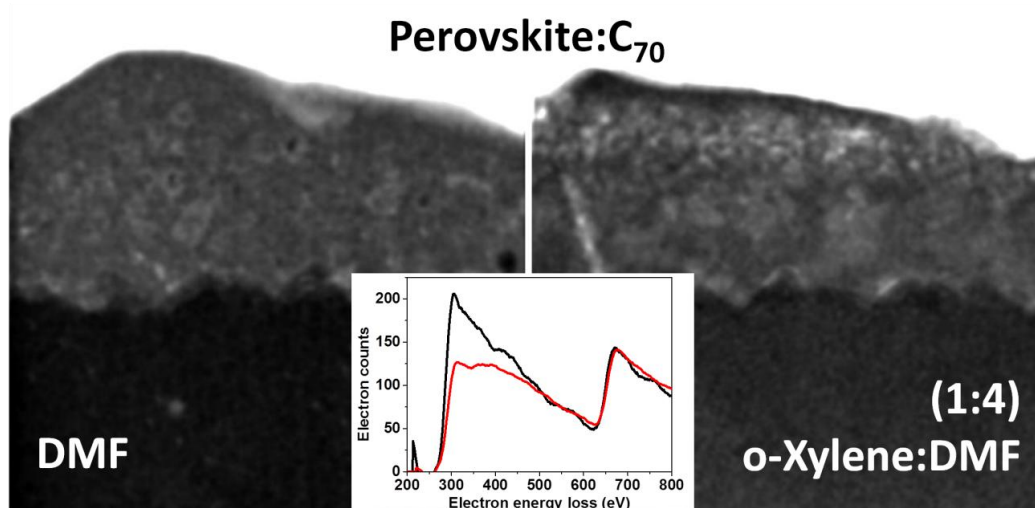
Figure 4.15. HAADF STEM micrographs and composition maps obtained by EELS of C K and I M edges of cross sections of solar cells based on perovskite:C_{70} films processed with and without *o*-xylene, while the inset in the center shows a comparison of EELS spectra from perovskite:C_{70} blend films with (red) and without *o*-xylene (black). Further information is available in reference [21].

4.4   Conclusions

The beneficial effect of the use of aromatic cosolvents for the processing of MAPbI$_3$:C_{70} blend films for their use in ETL-free solar cells are provided. The first trials with o-xylene led to enhanced PV performance with reproducible PCE values higher than 13%. Moreover, the comparison of two aromatic and two aliphatic cosolvents showed that the beneficial effect was unique to the aromatic ones. Interestingly, the positive effect was only seen when they were used for MAPbI$_3$:C_{70} blend films processing, while not having any influence on fullerene-free MAPbI$_3$ films. The reason for the relevance of the aromaticity in the cosolvent structure is unraveled by spectroscopic and microscopic techniques. UV-vis spectra reveal clear differences in band intensities and wavelength values, suggesting stronger optoelectronic impact of solute-solvent interactions for aromatic cosolvents through π-stacking. Microscopic methods also indicated differences in perovskite layers depending on the studied processing conditions. First, FE-SEM results showed a decrease in the number of pinholes for perovskite layers processed with aromatic cosolvents. Also, important morphological variations are seen by AFM means, suggesting distinct fullerene distributions in the perovskite layer that might be due to the

differences in the fullerene-cosolvent interactions, which was in agreement with EELS results. In conclusion, the present chapter provides an optimized protocol for the fabrication of efficient and reproducible MAPbI$_3$:C$_{70}$-based ETL-free PSCs through the introduction of strategy involving cosolvents. Furthermore, insights on the origin of the beneficial effect of combining C$_{70}$ and aromatic cosolvents are provided, paving the way for further improving the processing of fullerenes for their use in PSCs.

4.5   References

[1]   J. Pascual, I. Kosta, N. Tuyen, A. Chuvilin, G. Cabanero, H. J. Grande, E. M. Barea, I. Mora-Seró, J. L. Delgado, R. Tena-Zaera. Electron Transport Layer-Free Solar Cells Based on Perovskite-Fullerene Blend Films with Enhanced Performance and Stability. *ChemSusChem* **2016**, *9*, 2679.

[2]   J. K. J. van Duren, X. Yang, J. Loos, C. W. T. Bulle-Lieuwma, A. B. Sieval, J. C. Hummelen, R. A. J. Janssen. Relating the Morphology of Poly(p-phenylene vinylene)/Methanofullerene Blends to Solar-Cell Performance. *Adv. Funct. Mater.* **2004**, *14*, 425.

[3]   S. Cook, H. Ohkita, Y. Kim, J. J. Benson-Smith, D. D. C. Bradley, J. R. Durrant. A Photophysical Study of PCBM Thin Films. *Chem. Phys. Lett.* **2007**, *445*, 276.

[4]   F. C. Jamieson, E. B. Domingo, T. McCarthy-Ward, M. Heeney, N. Stingelin, J. R. Durrant. Fullerene Crystallisation as a Key Driver of Charge Separation in Polymer/Fullerene Bulk Heterojunction Solar Cells. *Chem. Sci.* **2012**, *3*, 485.

[5]   J-W. Lee, S.-H. Bae, N. De Marco, Y.-T. Hsieh, Z. Dai, Y. Yang. The Role of Grain Boundaries in Perovskite Solar Cells. *Mater. Today Energy* **2018**, *7*, 149.

[6]   Y. Shao, Z. Xiao, C. Bi, Y. Yuan, J. Huang. Origin and Elimination of Photocurrent Hysteresis by Fullerene Passivation in CH$_3$NH$_3$PbI$_3$ Planar Heterojunction Solar Cells. *Nat. Commun.* **2014**, *5*, 5784.

[7]   J. Xu, A. Buin, A. H. Ip, W. Li, O. Voznyy, R. Comin, M. Yuan, S. Jeon, Z. Ning, J. J. McDowell, P. Kanjanaboos, J.-P. Sun, X. Lan, L. N. Quan, D. H. Kim, I. G. Hill, P. Maksymovych, E. H. Sargent. Perovskite-Fullerene Hybrid Materials Suppress Hysteresis in Planar Diodes. *Nat. Commun.* **2015**, *6*, 7081.

[8]   C. Ran, Y. Chen, W. Gao, M. Wang, L. Dai. One-Dimensional (1D) [6,6]-Phenyl-C$_{61}$-Butyric Acid Methyl Ester (PCBM) Nanorods as Efficient Additive for Improving the Efficiency and Stability of Perovskite Solar Cells. *J. Mater. Chem. A* **2016**, *4*, 8566.

[9]   N. J. Jeon, J. H. Noh, Y. C. Kim, W. S. Yang, S. Ryu, S. I. Seok. Solvent Engineering for High-Performance Inorganic-Organic Hybrid Perovskite Solar Cells. *Nat. Mater.* **2014**, *13*, 897.

[10] H. Chen, Z. Wei, H. He, X. Zheng, K. S. Wong, S. Yang. Solvent Engineering Boosts the Efficiency of Paintable Carbon-Based Perovskite Solar Cells to Beyond 14%. *Adv. Energy Mater.* **2016**, *6*, 1502087.

[11] Y. Rong, Z. Tang, Y. Zhao, X. Zhong, S. Venkatesan, H. Graham, M. Patton, Y. Jing, A. M. Guloy, Y. Yao. Solvent Engineering towards Controlled Grain Growth in Perovskite Planar Heterojunction Solar Cells. *Nanoscale* **2015**, *7*, 10595.

[12] Y. Tu, J. Wu, X. He, P. Guo, T. Wu, H. Luo, Q. Liu, K. Wang, J. Lin, M. Huang, Y. Huang, Z. Lan, S. Li. Solvent Engineering for Forming Stonehenge-Like PbI_2 Nano-Structures towards Efficient Perovskite Solar Cells. *J. Mater. Chem. A* **2017**, *5*, 4376.

[13] K. N. Semenov, N. A. Charykov, V. A. Keskinov, A. K. Piartman, A. A. B. Aleksei, A. Kopyrin. Solubility of Light Fullerenes in Organic Solvents. *J. Chem. Eng. Data* **2010**, *55*, 13.

[14] J. Pascual, I. Kosta, E. Palacios-Lidon, A. Chuvilin, G. Grancini, Md. K. Nazeeruddin, H. J. Grande, J. L. Delgado, R. Tena-Zaera. Co-Solvent Effect in the Processing of the Perovskite:Fullerene Blend Films for Electron Transport Layer-Free Solar Cells. *J. Phys. Chem. C* **2018**, *122*, 2512.

[15] N. O. Mchedlov-Petrossyan. Fullerenes in Liquid Media: An Unsettling Intrusion into the Solution Chemistry. *Chem. Rev.* **2013**, *113*, 5149.

[16] I. Renge. Solvent Effects on the Absorption Maxima of Fullerenes C_{60} and C_{70}. *J. Phys. Chem.* **1995**, *99*, 15955.

[17] S. H. Gallagher, R. S. Armstrong, P. A. Lay, C. A. Reed. Solvent Effects on the Electronic Spectrum of C_{60}. *J. Phys. Chem.* **1995**, *99*, 5817.

[18] R. Garcia, R. Magerle, R. Perez. Nanoscale Compositional Mapping with Gentle Forces. *Nat. Mater.* **2007**, *6*, 405.

[19] W. W. Scott, B. Bhushan. Use of Phase Imaging in Atomic Force Microscopy for Measurement of Viscoelastic Contrast in Polymer Nanocomposites and Molecularly Thick Lubricant Films. *Ultramicroscopy* **2003**, *97*, 151.

[20] D. Raghavan, M. van Landingham, X. Gu, T. Nguyen. Characterization of Heterogeneous Regions in Polymer Systems Using Tapping Mode and Force Mode Atomic Force Microscopy. *Langmuir* **2000**, *16*, 9448.

[21] J. Pascual, J. L. Delgado, R. Tena-Zaera. Physicochemical Phenomena and Application in Solar Cells of Perovskite:Fullerene Films. *J. Phys. Chem. Lett.* **2018**, *9*, 2893.

5   Perovskite:fullerene derivative blends for ETL-free perovskite solar cells

5.1   Introduction

As presented in Chapter 1, fullerenes are very chemically versatile molecules. They are easy to functionalize and can bear many different groups that can be tailored in order to achieve certain properties.[1-3] In respect to this thesis, just C_{70} fullerene was used in the previous chapters, therefore no functionalized fullerenes were employed for the ETL-free purpose. Yet, C_{70} proved itself as a very promising molecule. In Chapter 3 $MAPbI_3$:C_{70} blend films were presented as improved light-absorbing layers for ETL-free PSCs.[4] The presence of fullerene in the perovskite matrix helped achieving enhanced performance and stability, paving the way towards efficient ETL-free solar cells. Additionally, the potential of C_{70} in these systems was enhanced even more with the cosolvent approach presented in Chapter 4.[5] With the addition of a small fraction of an aromatic cosolvent, very efficient (i.e. >13%) and reproducible ETL-free PSCs were achieved. Furthermore, the relevance of the interactions between fullerenes and solution solvents was explained, identifying the key processing parameters in order to achieve improved fullerene distribution throughout the perovskite layer. Taking all these results into account, it would still be required to investigate the effect of chemical functionalization of fullerenes on cell performance. In fact, in literature fullerene derivatives are usually the preferred ones for perovskite:fullerene blend films preparation. Functionalized fullerenes like PCBM[6] or a highly-substituted fullerene with carboxylic acid groups[7] led to very satisfactory results. In fact, many works reported during this thesis point out that fullerene derivatives might be more appealing for perovskite:fullerene blend purposes.[8-12] Testing fullerenes bearing different functional groups would prove the versatility and scope of the methods proposed in Chapters 3 and 4. Furthermore, certain functionalizations can be selected in order to provide the fullerene with a specific chemical or electronic character, in order to see the effect of this change in perovskite:fullerene blend films-based PSCs.

In this chapter perovskite:fullerene blend films with a variety of new fullerene derivatives endowed with different organic addends and with tailored electronic properties are studied and incorporated into ETL-free PSCs. New fullerene materials, synthesized and fully characterized by our collaborators Rafael Sandoval-Torrientes, Inés García-Benito and Nazario Martín (Universidad Complutense de Madrid and Imdea Nanociencia),[13] displaying tailored electron-accepting properties are here investigated to develop perovskite:fullerene blend films to be used in ETL-free PSCs. In addition to the unambiguous proof of universality and versatility of perovskite:fullerene blend films to obtain efficient ETL-free PSCs, new knowledge about innovative fullerenes in the PSC field is provided. Furthermore, the application of the cosolvent approach used presented in Chapter 4 for the best performing fullerene derivative allowed achieving highly efficient and reproducible devices of up to 14.3%. It is also worth noting that all fullerene derivatives here investigated showed much larger stability than that one for the fullerene-free device.

5.2   Experimental Section

5.2.1   Materials

The materials used in this chapter were obtained from commercial suppliers in high purity and used without further purification: glass/FTO (TEC15, Hartford Glass), MAI (DYESOL), $PbCl_2$ (98%, Sigma-Aldrich), spiro-OMeTAD (99%, Feiming Chemicals Limited), LiTFSI (99.9%, Solvionic), *tert*-butylpyridine (96%, Sigma-Aldrich), DMF (extra pure, Scharlab), 2-propanol (synthetic grade, Scharlab), acetone (technical grade, Scharlab), chlorobenzene (99.8%, Sigma-Aldrich) and acetonitrile (UV HPLC grade, Scharlab).

5.2.2   Device fabrication

The perovskite solution was prepared by dissolving MAI (7.71 mmol) and $PbCl_2$ (2.57 mmol) (molar ratio 3:1) in DMF (3 mL) and stirring overnight. Prior to deposition, the perovskite solution was saturated with the corresponding fullerene material (i.e. **IS1**,

IS2, **PI2**, **DPM-6**, and **PCBM**). It is noted that fullerene solubility in the perovskite solution was around 0.3 mg mL^{-1} for all of them. The resulting solution was spin coated on the substrates following a two-step protocol, which consisted of a first step of 500 rpm for 5 s followed by a second step of 2000 rpm for 45 s. Subsequently, the samples were annealed at 100°C for 2 h to ensure complete perovskite formation. Spiro-OMeTAD and Au layers were deposited on top of perovskite layer as described in Chapter 2.

5.2.3   Device characterization

The *J-V* chracteristics of the solar cells were measured under simulated solar light by using the setup decribed in chapter 2. The EQE spectra of the devices were also obtained from the home-made specific setup and methodology described in chapter 2.

5.3   Results and Discussion

5.3.1   Fullerene derivatives

The fullerene-based materials include two novel pyrazolino[60]fullerene derivatives (**PI1** and **PI2**),[18-22] two new isoxazolino[60]fullerene derivatives (**IS1** and **IS2**),[23] and two methano[60]fullerene derivatives (**DPM-6**[14,15] and **PCBM**). These fullerene derivatives are shown in Figure 5.1.

It is important to underline that pyrazolino[60]fullerenes and isoxazolino[60]fullerenes have never been previously used in PSCs. Therefore, to the best of our knowledge, this study represents the first attempt of using them in PSCs. In the case of methano[60]fullerenes, the most employed fullerene derivative in PSCs is by far **PCBM**.[16,17] However, the related **DPM-6** endowed with two aryl groups in the cyclopropane ring remains unexplored in regular or inverted PSCs. Therefore, in addition to the unambiguous proof of universality and versatility of perovskite:fullerene blend films to obtain efficient ETL-free PSCs, new knowledge about innovative fullerenes in the PSC field is provided.
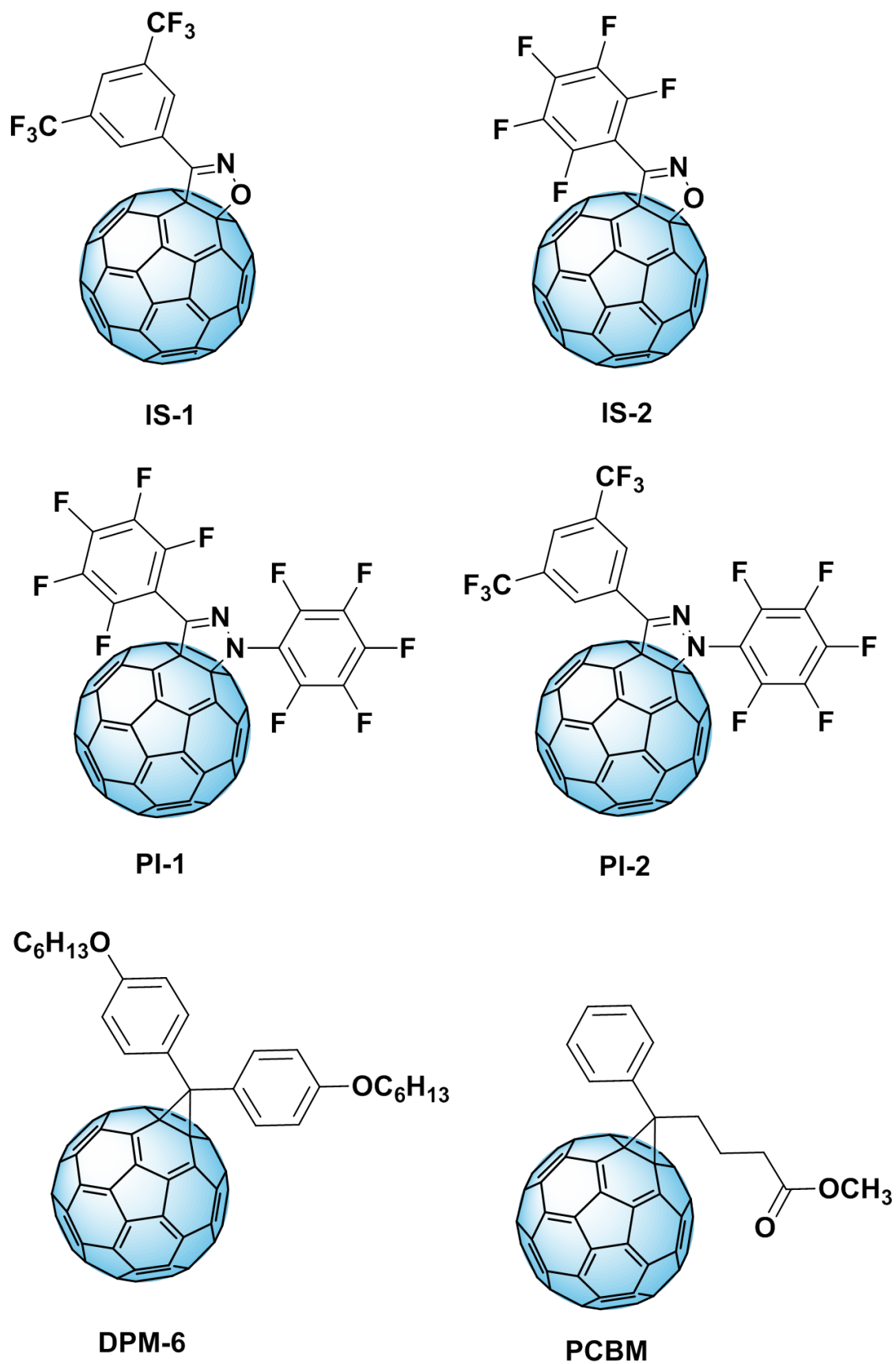
Figure 5.1. Fullerene derivatives tested in this chapter.

96

Owing to the presence of a heteroatom directly connected to the fullerene cage, pyrazolino[60]fullerenes and isoxazolino[60]fullerenes display better electron-accepting properties than methano[60]fullerenes.[24,25] Moreover, the presence of highly electron withdrawing fluorine atoms on the phenyl rings of pyrazolino[60]fullerenes and isoxazolino[60]fullerenes also contribute to the enhancement of these electron-accepting properties.[26]

5.3.2 Perovskite:fullerene blend films

The perovskite:fullerene blend film morphology was investigated for a fullerene of each new type of derivatization (i.e. isoxazoline **IS2** and a pyrazoline **PI2**). The top-view FE-SEM images of perovskite:fullerene blends did not show major differences other than the elimination of a big amount of pinholes, as occurred in perovskite:C_{70} blend films in Chapter 3[4] (Figure 5.2). However, some effect of the fullerene derivative on the blend film roughness cannot be fully figured out.

5.3.3 ETL-free solar cells

To evaluate the synthesized fullerene derivatives in ETL-free PSCs, perovskite:fullerene derivative blend films were prepared as in Chapter 3 and 4.[4,5] Prior to deposition, each fullerene derivative (**IS1**, **IS2**, **PI2**, **DPM-6**, and **PCBM**) was added to the perovskite solution to prepare the solar cells. It is noted that **PI1** was not used in this PV study because of its lack of solubility in DMF. However, the solubility of the other fullerene derivatives was around $0.3 \, \mathrm{mg \, mL^{-1}}$ (i.e. significantly higher than that of pristine C_{60}: $0.1 \, \mathrm{mg \, mL^{-1}}$). The blend films resulting from the use of the five different fullerene derivatives were used to fabricate solar cells in the following configuration glass/FTO/MAPbI$_3$:fullerene derivative/spiro-OMeTAD/Au. Solar cells based on perovskite films with pristine fullerene (i.e. glass/FTO/MAPbI$_3$:C_{60}/spiro-OMeTAD/Au) and without fullerene (i.e. glass/FTO/MAPbI$_3$/spiro-OMeTAD/Au) were also prepared for comparison. Figure 5.3 shows the *J-V* curves of the best devices under AM 1.5G simulated sunlight.
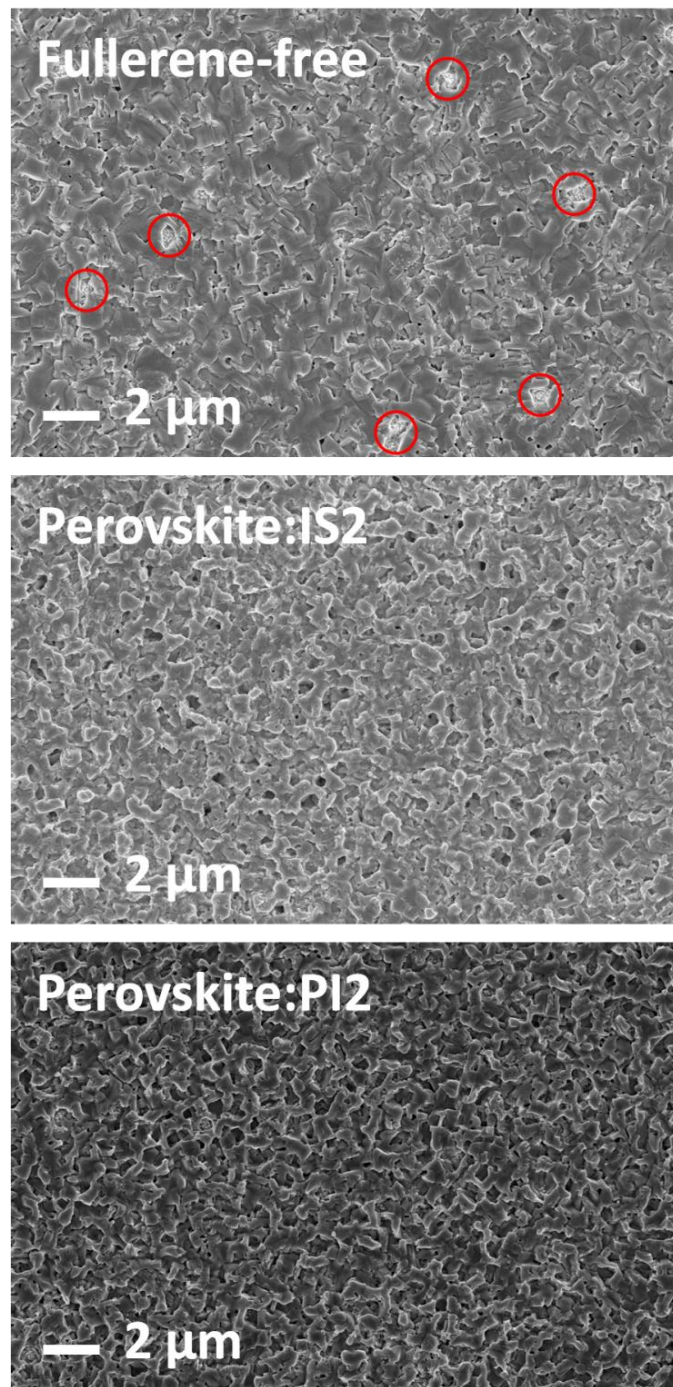
Figure 5.2. FE-SEM top view micrographies of perovskite layers without fullerene, with **IS2** and with **PI2**. Red circles point out pinholes in the layer.
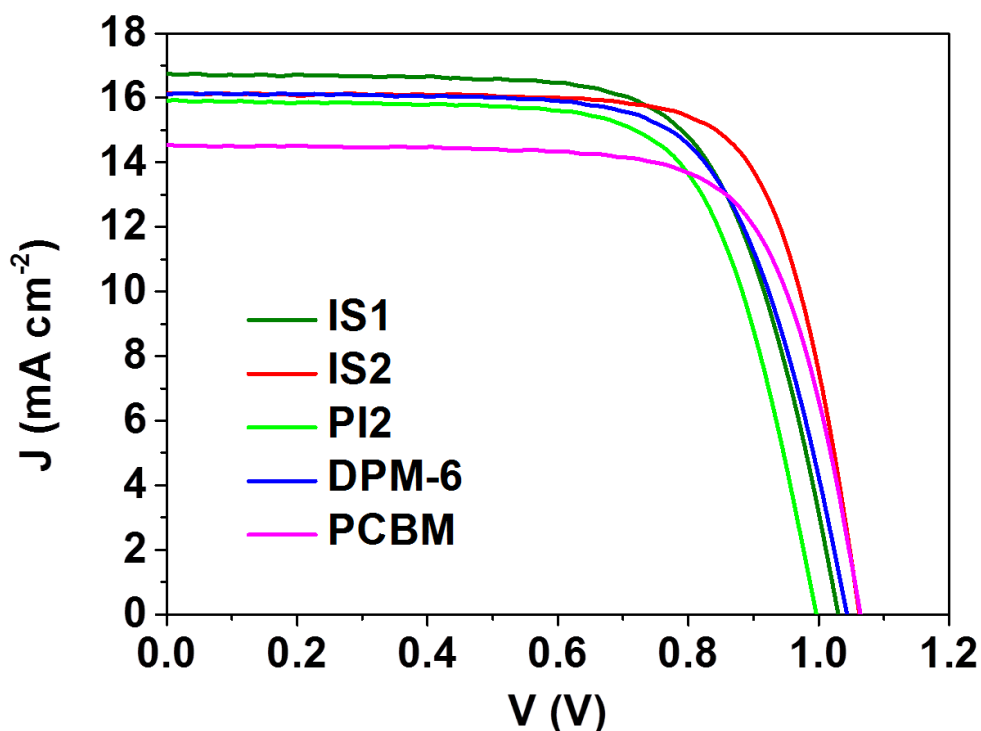
Figure 5.3. *J-V* curves of the most efficient ETL-free solar cells based on MAPbI$_3$:fullerene blends.

The PV parameters extracted from the *J-V* curves are summarized in Table 5.2. It is noted that, additionally to the best values, the mean ones (i.e. extracted from the full series, see statistical analysis in Figure 5.4) are also included in the table. As it can be seen, the PCE of the solar cells prepared with blend films including fullerene or derivatives is significantly higher than the reference device (i.e. with fullerene-free perovskite). Furthermore, the performance of solar cells based on perovskite:fullerene blend films is better than the analogue with pristine fullerene. This finding suggests that all the chemical modifications on the fullerenes studied here have a beneficial impact for their use in perovskite:fullerene blend films for PV applications.

Interestingly, the main improvement over the devices with pristine fullerene was found for the *J$_{sc}$*. This may be due to the better solubility in DMF exhibited by the fullerene derivatives, making possible to prepare processing solutions with fullerene/PbCl$_2$ ratios of 1:7200 (i.e. close to the optimum concentration from the studies in Chapter 3 with C$_{70}$).[4] However, further comparative analysis of the PV parameters indicates that, in general, the open circuit voltage (*V$_{oc}$*) increases in the following order: pyrazolino[60]fullerenes < isoxazolino[60]fullerenes < methano[60]fullerenes, following

a similar trend to that observed for the E_{LUMO} estimated by electrochemistry in collaboration with Rafael Sandoval-Torrientes, Inés García-Benito and Nazario Martín (Universidad Complutense de Madrid).[13]
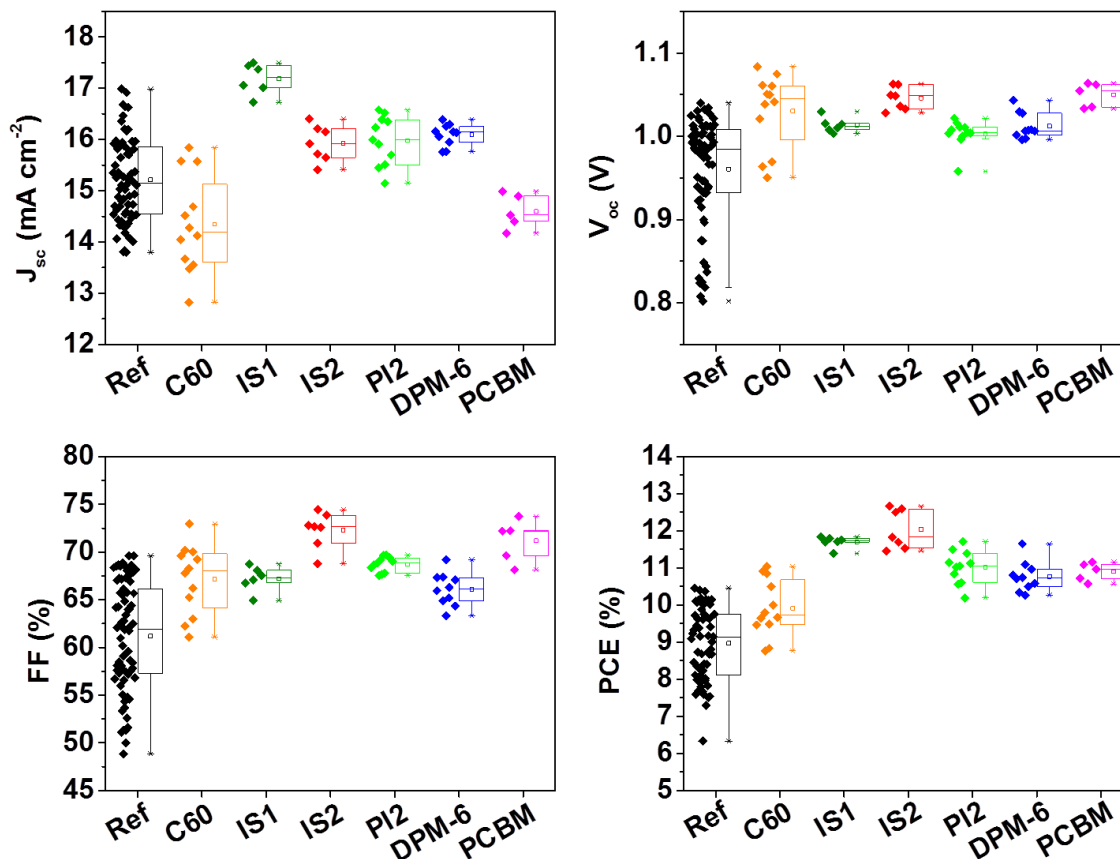
Figure 5.4. PV parameters for MAPbI$_3$:fullerene derivative blends-based ETL-free PSCs.

Table 5.1. PV parameters for the MAPbI$_3$:fullerene derivative blends-based ETL-free PSCs.[a]

Fullerene derivative	J_{sc} (mA cm^{-2})	V_{oc} (V)	FF (%)	PCE (%)
IS1	17.2 (16.7)	1.01 (1.03)	67.2 (68.7)	11.7 (11.8)
IS2	15.9 (16.1)	1.05 (1.06)	72.3 (73.8)	12.0 (12.7)
PI2	16.0 (16.5)	1.00 (1.02)	68.7 (69.4)	11.0 (11.7)
DPM-6	16.1 (16.1)	1.01 (1.04)	66.1 (69.2)	11.8 (10.6)
PCBM	14.6 (14.5)	1.05 (1.06)	71.2 (72.2)	10.9 (11.2)
C$_{60}$	14.3 (14.5)	1.03 (1.08)	67.2 (70.2)	9.9 (11.0)
fullerene-free	15.2 (17.0)	0.95 (1.04)	61.2 (69.6)	9.0 (10.5)

[a] Numbers in brackets correspond to values of the most efficient device of each type.

Table 5.2 is taken from the reported data in that work, showing the electrochemical properties of **IS1**, **IS2**, **PI1**, **PI2**, **DPM-6**, and **PCBM**, which were determined by means of cyclic voltammetry. **DPM-6** and **PCBM** showed a lower electron-accepting ability than pyrazolino[60]fullerenes and isoxazolino[60]fullerenes, being isoxazolino[60]fullerenes **IS1** and **IS2** a moderate electron-accepting nature and **PI1** and **PI2** the highest one. The fact that the V_{oc} of the cells depends on the E_{LUMO} of the inserted fullerene suggests that, additionally to the increase of fullerene solubility, the chemical functionalization may play a significant role in the solar cell performance. In particular, it seems that the use of less electron-accepting fullerenes within these blends results in an increase in the V_{oc}. Although further device characterization is required to determine the involved mechanisms, this finding may provide some useful practical guidelines for selecting fullerene derivatives for their use in PSCs. Another relevant aspect to bear in mind is the functionalization of the fullerenes. In particular, the isoxazolino moiety might represent a binding site for a better interaction with perovskite.

Table 5.2. Reduction potentials (from cyclic voltammetry) and energy levels of LUMO for the fullerene materials **IS1**, **IS2**, **PI1**, **PI2**, **DPM-6**, **PCBM**, and C_{60}.[13]

Fullerene derivative	$E_{red}^{1/2}$ **(V)**[a]	E_{LUMO} **(eV)**[b]
IS1	-0.347	-4.055
IS2	-0.352	-4.048
PI1	-0.322	-4.078
PI2	-0.316	-4.084
DPM-6	-0.430	-3.970
PCBM	-0.450	-3.950
C_{60}	-0.349	-4.050

[a] V vs $Ag/AgNO_3$; cyclic voltammograms for compounds **IS1**, **IS2**, **PI1**, **PI2**, **DPM-6**, and **PCBM** were recorded at a scan rate of 100 mV s^{-1}; glassy carbon as working electrode; reduction potentials were measured in o-DCB/MeCN (4:1) solution (Bu_4NPF_6 0.1 M as supporting electrolyte) at room temperature; all potentials are reported with reference to an internal standard of the Fc/Fc$^+$ couple. [b] The energetic level of the LUMO for each fullerene material was estimated using the following equation $E_{LUMO} = -(E_{red}^{1/2} + 4.4)$.

Since the best PCE was obtained for devices based on MAPbI$_3$:**IS2** blend films, the cosolvent approach from Chapter 4 was applied for them.[4] In particular, *o*-xylene was added to the perovskite precursors solution in 1:4 ratio in relation to DMF. As a result, solar cells with improved PV performance were obtained. In particular, Figure 5.5a shows a micrograph of the cross section of the best device, which showed a J_{sc} of 17.3 mA cm^{-2}, V_{oc} of 1.08 V and FF of 77.6% and a PCE of 14.3% (Figure 5.5b). In addition, this formulation leads to highly reproducible devices, with rather narrow PCE dispersion as seen in Figure 5.5c. Good agreement was found between the measured J_{sc} and value estimated from the EQE spectrum (Figure 5.6).
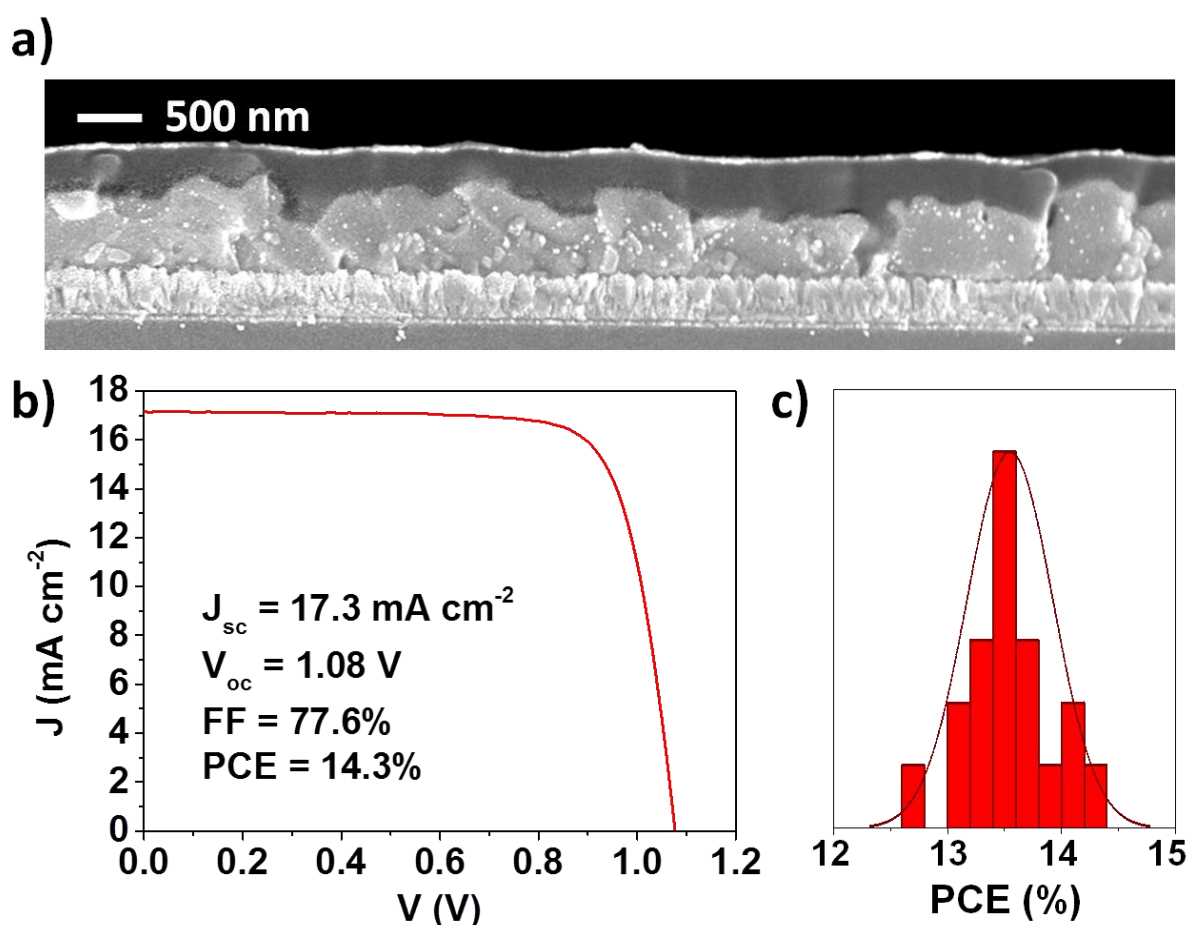

Figure 5.5. a) Cross-section micrograph obtained by FESEM and b) *J-V* curve and PV parameters for the best MAPbI$_3$:**IS2** blend film-based solar cell. c) Distribution of the best device PCE values, pointing out its reproducibility.
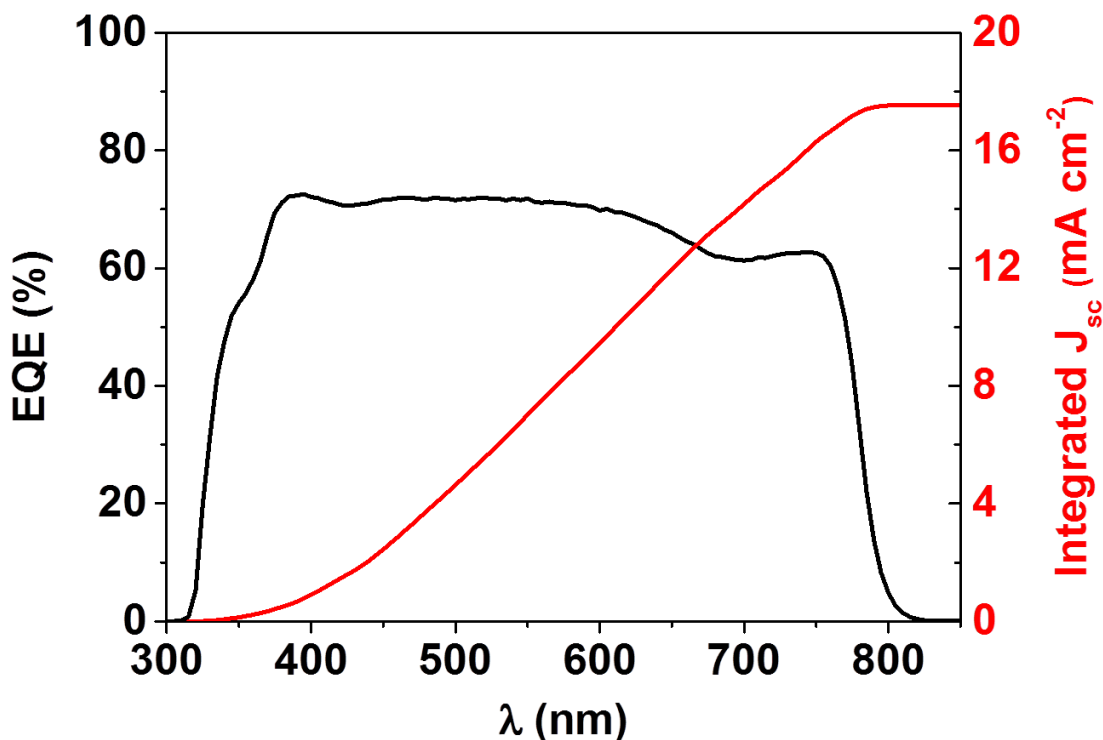
Figure 5.6. EQE spectrum and integrated current density of the best MAPbI$_3$:**IS2** blend film-based device.

5.3.4 Photostability of devices

As seen in Chapter 3 with C$_{70}$ and in other related published works, the photostability of the PSCs is highly improved when using perovskite:fullerene blend films.[4,18-22] Therefore, the effect of the different fullerene derivatives on the photostability of the non-encapsulated PSCs was also investigated. Figure 5.7 shows the evolution of PV parameters versus time under continuous AM 1.5G simulated sunlight for solar cells based on blend films including the best-performing fullerene from each derivative family (i.e. **IS2**, **PI2** and **DPM-6**). No clear differences can be seen, concluding that all fullerenes have similar beneficial impact on the photostability of the device. It is noted that FF is the most relevant parameter concerning photostability as V_{oc} and J_{sc} did almost not vary with exposure time. This finding suggests the fullerene core (i.e. irrespectively of the chemical modification) as the main cause of the stability enhancement. The contact angle of water drops on perovskite:fullerene derivative blend films were also

analyzed, exhibiting similar water contact angle (Table 5.3). These results point out similar behavior against moisture, therefore fullerenes might not have any effect in this sense, even though bearing F atoms.
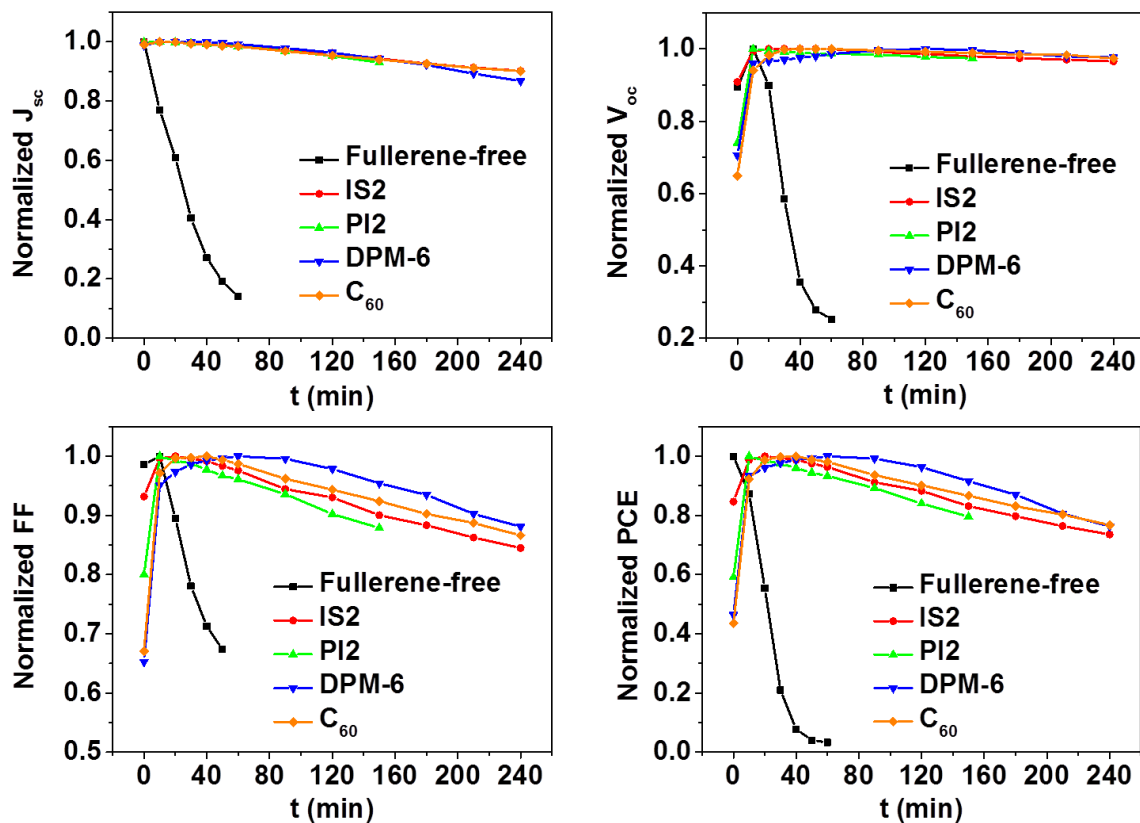
Figure 5.7. Evolution of PV parameters (normalized values) versus time under AM 1.5 simulated sunlight for non-encapsulated solar cells containing the best working fullerene for each type of derivatization.

Table 5.3. Contact angle for MAPbI$_3$:fullerene derivatives blend films.

Perovskite layer	Contact angle (°)
MAPbI$_3$	57 ± 6
MAPbI$_3$:**C$_{70}$**	59 ± 1
MAPbI$_3$:**IS1**	61 ± 2
MAPbI$_3$:**IS2**	57 ± 1
MAPbI$_3$:**PI2**	57 ± 1

5.4   Conclusions

A variety of novel (**IS1**, **IS2**, **PI1**, **PI2**) and well-known fullerene materials (**DPM-6, PCBM**) showing different electron-accepting capabilities were applied in MAPbI$_3$:fullerene blend films in order to study the effect of their electronic properties over the PV performance of ETL-free PSCs. The use of fullerene derivatives showed that the great improvement achieved for MAPbI$_3$:C$_{70}$ blend films could be enhanced with functionalized molecules, demonstrating the beneficial impact of the fullerene chemical modification. In particular, 14.3% power conversion efficiency was obtained for the ETL-free PSCs based on MAPbI$_3$:isoxazolino[60] derivative blend films using the cosolvent approach presented in Chapter 4,[4] placing this functional group in an advantageous position versus the very well-known **PCBM**. Furthermore, an interesting experimental correlation between the open circuit voltage value of the devices and the LUMO energy level of the fullerene material, which may be very helpful in future materials design for PSCs, has been found out as well. Furthermore, an interesting experimental correlation between the open circuit voltage value of the devices and the LUMO energy level of the fullerene material, which may be very helpful in future materials design for PSCs, has been found out as well. All in all, the current PV study, which includes ETL-free PSCs based on a large variety of perovskite:fullerene derivative blends, allows us to confirm the universality of using solution-processed perovskite:fullerene blend films as light absorber material for ETL-free solar cells. Yet, why better performances obtained with the derivatized fullerenes is still unclear, and therefore there is need for further research aiming to fully understand the role of fullerenes and their chemical functionalization in perovskite:fullerene blend films.

5.5   References

[1]   D. M. Guldi, N. Martín. Fullerenes: From Synthesis to Optoelectronic Properties. Kluver Academic Publishers, Dordrecht, Netherlands, 2002.

[2]   A. Hirsch. The Chemistry of Fullerenes. Wiley-VCH, Weinheim, Germany, 2005.

[3]   F. Langa, J.-F. Nierengarten. Fullerenes. Principles and Applications, Royal Society of Chemistry, Cambridge, United Kingdom, 2007.

[4] J. Pascual, I. Kosta, N. Tuyen, A. Chuvilin, G. Cabanero, H. J. Grande, E. M. Barea, I. Mora-Seró, J. L. Delgado, R. Tena-Zaera. Electron Transport Layer-Free Solar Cells Based on Perovskite-Fullerene Blend Films with Enhanced Performance and Stability. *ChemSusChem* **2016**, *9*, 2679.

[5] J. Pascual, I. Kosta, E. Palacios-Lidon, A. Chuvilin, G. Grancini, Md. K. Nazeeruddin, H. J. Grande, J. L. Delgado, R. Tena-Zaera. Co-Solvent Effect in the Processing of the Perovskite:Fullerene Blend Films for Electron Transport Layer-Free Solar Cells. *J. Phys. Chem. C* **2018**, *122*, 2512.

[6] J. Xu, A. Buin, A. H. Ip, W. Li, O. Voznyy, R. Comin, M. Yuan, S. Jeon, Z. Ning, J. J. McDowell, P. Kanjanaboos, J.-P. Sun, X. Lan, L. N. Quan, D. H. Kim, I. G. Hill, P. Maksymovych, E. H. Sargent. Perovskite-Fullerene Hybrid Materials Suppress Hysteresis in Planar Diodes. *Nat. Commun.* **2015**, *6*, 7081.

[7] K. Wang, C. Liu, P. Du, J. Zheng, X. Gong. Bulk Heterojunction Perovskite Hybrid Solar Cells with Large Fill Factor. *Energy Environ. Sci.* **2015**, *8*, 1245.

[8] M. Li, Y.-H. Chao, T. Kang, Z.-K. Wang, Y.-G. Yang, S.-L. Feng, Y. Hu, X.-Y. Gao, L.-S. Liao, C.-S. Hsu. Enhanced Crystallization and Stability of Perovskites by a Cross-Linkable Fullerene for High Performance Solar Cells. *J. Mater. Chem. A* **2016**, *4*, 15088.

[9] M. Li, Y.-G. Yang, Z.-K. Wang, T. Kang, Q. Wang, S.-H. Turren-Cruz, X.-Y. Gao, C.-S. Hsu, L.-S. Liao, A. Abate. Perovskite Grains Embraced in a Soft Fullerene Network Make Highly Efficient Flexible Solar Cells with Superior Mechanical Stability. *Adv. Mater.* **2019**, 1901519.

[10] S. Collavini, M. Saliba, W. R. Tress, P. J. Holzhey, S. F. Völker, K. Domanski, S. H. Turren-Cruz, A. Ummadisingu, S. M. Zakeeruddin, A. Hagfeldt, M. Grätzel, J. L. Delgado. Poly(ethylene glycol)-[60]Fullerene-Based Materials for Perovskite Solar Cells with Improved Moisture Resistance and Reduced Hysteresis. *ChemSusChem* **2018**, *11*, 1032.

[11] X. Liu, F. Lin, C.-C. Chueh, Q. Chen, T. Zhao, P.-W. Liang, Z. Zhu, Y. Sun, A. K.-Y. Jen. Fluoroalkyl-Substituted Fullerene/Perovskite Heterojunction for Efficient and Ambient Stable Perovskite Solar Cells. *Nano Energy* **2016**, *30*, 417.

[12] C. Ran, Y. Chen, W. Gao, M. Wang, L. Dai. One-Dimensional (1D) [6,6]-Phenyl-C_{61}-Butyric Acid Methyl Ester (PCBM) Nanorods as an Efficient Additive for Improving the Efficiency and Stability of Perovskite Solar Cells. *J. Mater. Chem. A* **2016**, *4*, 8566.

[13] R. Sandoval-Torrientes, J. Pascual, I. García-Benito, S. Collavini, I. Kosta, R. Tena-Zaera, N. Martín, J. L. Delgado. Modified Fullerenes for Efficient Electron Transport Layer-Free Perovskite/Fullerene Blend-Based Solar Cells. *ChemSusChem* **2017**, *10*, 2023.

[14] J. L. Delgado, P. de la Cruz, V. Lopez-Arza, F. Langa, D. B. Kimball, M. M. Haley, Y. Araki, O. Ito, Cyclization of 1-(2-Alkynylphenyl)-3,3-dialkyltriazenes:

A Convenient, High-Yield Synthesis of Substituted Cinnolines and Isoindazoles. *J. Org. Chem.* **2004**, *69*, 2661.

[15] J. L. Delgado, F. Oswald, F. Cardinali, F. Langa, N. Martín. On the Thermal Stability of [60]Fullerene Cycloadducts: Retro-Cycloaddition Reaction of 2-Pyrazolino[4,5:1,2][60]fullerenes. *J. Org. Chem.* **2008**, *73*, 3184.

[16] J. L. Delgado, F. Cardinali, E. Espíldora, M. R. Torres, F. Langa, N. Martín. Oxidation of 3-Alkyl-Substituted 2-Pyrazolino[60]fullerenes: A New Formyl-Containing Building Block for Fullerene Chemistry. *Org. Lett.* **2008**, *10*, 3705.

[17] J. L. Delgado, S. Osuna, P.-A. Bouit, R. Martínez-Alvarez, E. Espíldora, M. Solá, N. Martín. Competitive Retro-Cycloaddition Reaction in Fullerene Dimers Connected through Pyrrolidinopyrazolino Rings. *J. Org. Chem.* **2009**, *74*, 8174.

[18] J. L. Delgado, N. Martín, P. de la Cruz, F. Langa. Pyrazolinofullerenes: A Less Known Type of Highly Versatile Fullerene Derivatives. *Chem. Soc. Rev.* **2011**, *40*, 5232.

[19] J. L. Delgado, S. Filippone, F. Giacalone, M. A. Herranz, B. Illescas, E. M. Pérez, N. Martín. Buckyballs. *Top. Curr. Chem.* **2013**, *350*, 1.

[20] G. Garcia-Belmonte, P. P. Boix, J. Bisquert, M. Lenes, H. J. Bolink, A. La Rosa, S. Filippone, N. Martín. Influence of the Intermediate Density-of-States Occupancy on Open-Circuit Voltage of Bulk Heterojunction Solar Cells with Different Fullerene Acceptors. *J. Phys. Chem. Lett.* **2010**, *1*, 2566.

[21] H. J. Bolink, E. Coronado, A. Forment-Aliaga, M. Lenes, A. La Rosa, S. Filippone, N. Martín. Polymer Solar Cells Based on Diphenylmethanofullerenes with Reduced Sidechain Length. *J. Mater. Chem.* **2011**, *21*, 1382.

[22] M. R. Lilliedal, A. J. Medford, M. V. Madsen, K. Norrman, F. C. Krebs. The Effect of Post-Processing Treatments on Inflection Points in Current-Voltage Curves of Roll-to-Roll Processed Polymer Photovoltaics. *Sol. Energy Mater. Sol. Cells* **2010**, *94*, 2018.

[23] P. Docampo, J. M. Ball, M. Darwich, G. E. Eperon, H. J. Snaith. Efficient Organometal Trihalide Perovskite Planar-Heterojunction Solar Cells on Flexible Polymer Substrates. *Nat. Commun.* **2013**, *4*, 2761.

[24] F. Langa, P. de la Cruz, J. L. Delgado, M. J. Gómez-Escalonilla, A. González-Cortés, A. de la Hoz, V. López-Arza. The Importance of the Linking Bridge in Donor-C_{60} Electroactive Dyads. *New J. Chem.* **2002**, 26, 76.

[25] C. Villegas, J. L. Delgado, P.-A. Bouit, B. Grimm, W. Seitz, N. Martín, D. M. Guldi. Powering Reductive Charge Shift Reactions-Linking Fullerenes of Different Electron Acceptor Strength to Secure an Energy Gradient. *Chem. Sci.* **2011**, *2*, 1677.

[26] J. L. Delgado, P. de la Cruz, V. López-Arza, F. Langa, Z. Gan, Y. Araki, O. Ito. Synthesis and Photoinduced Intermolecular Electronic Acceptor Ability of Pyrazolo[60]fullerenes vs Tetrathiafulvalene. *Bull. Chem. Soc. Jpn.* **2005**, *78*, 1500.

6 Perovskite-fullerene interactions and implications in devices

6.1 Introduction

In Chapter 5 the ability of functionalized fullerenes to form perovskite:fullerene blend films for improved PSCs in comparison to non-functionalized C_{60} and C_{70} was proven.[1] Reproducible ETL-free PSCs with improved power conversion efficiency (i.e. 14.3 %) were achieved in chapter 5 by combining the knowledge gained in Chapters 3 and 4 with the application of a new isoxazoline-derivatized fullerene.[2,3] However, the reasons for the better performance of this molecule are still to be discovered. Behind these reasons there could be an enhanced role of the fullerene inside the perovskite layer, when derivatized. In literature, plenty of benefits on PSCs have been claimed for these carbon allotropes prior to this thesis and during it. Improvements in FF,[4-6] stability[2,4,5,7-9] and hysteresis suppression[4,7,10-14] have been supported on the different roles of fullerenes in perovskite devices. One of their fundamental properties is the ability for passivating trap states as they can bind uncoordinated atoms at the grain boundaries, as it has been widely claimed by several research groups.[4-6,15-20] Their chemical nature (e.g. symmetry, non-polarity, spherical shape) has also made them a perfect candidate as frames for the growth of perovskite crystals, leading to improved morphologies and increased grain sizes.[21] In fact, published fullerene derivatives applied in PSCs have led to devices with improved performance.[1,4,5,7,8,10,11] Nevertheless, if fullerenes are to be used in future protocols for PSC design, structurally-optimized fullerene derivatives would be required, in order to maximize their ability to passivate trap states or improve the perovskite crystallization, for instance.

Therefore, further insights on the physicochemical implications of fullerenes in perovskites are required, which would allow designing new generation fullerenes with advanced properties and shed light on current issues like the origin of FF increase or hysteresis suppression. A focused and straightforward approach that could shed light on this subject would be the study of these systems from their solution state with spectroscopical techniques and correlation with the final solar cell performance, taking a

look at all the interactions playing a role in solution and their effects on layer and device physico-chemical properties. In this respect, various spectroscopic techniques have already been applied separately for the study of certain perovskite formulations, not yet with fullerenes. In particular, Fourier-transform infrared spectroscopy (FTIR) has been extendedly used for the evaluation of the bonds that are being broken and established in the perovskite complex formation between the different precursors.[22-28] Not only that but ^{1}H-NMR was also applied in the work by Yavary and co-workers for understanding the chemical role of carbon nanoparticles in perovskite solutions.[29]

Considering fullerenes, their electronegative nature is particularly relevant for understanding how they would behave in a blend together with perovskite. This chemical nature strongly influences their chemical compatibility and thus the species which they will preferentially bind, being reported studies completely coherent with this. In this sense, several works have proved, before and during the present thesis, the establishment of intermolecular bonds between arenes and anions through anion-π interactions[30-35] and, more in particular, between fullerenes and halides.[10,14,36,37] This finding suggests that fullerenes would show certain preference towards halide-rich sites in the perovskite film and, in this line, Xu and co-workers found out the passivating role of PCBM for Pb-I antisites in the perovskite layer while studying the anion-π interaction.[10] Taking into account the ability of fullerenes to interact with perovskite, studying these interactions and how to modulate them would open a wide range of possibilities for the design, synthesis and application of new fullerenes with optimized structure for the enhancement of certain properties such as defect passivation.

In this Chapter evidence on the formation of specific interactions between fullerenes and perovskite precursors in solution is reported. To prove this fact, a novel combination of spectroscopic techniques was used on perovskite precursor solutions doped with fullerenes of different structural nature. NMR and IR spectra provided insightful data on the atoms and functional groups involved in the new complex formed. The alterations generated by the insertion of fullerenes could be linked later to microstructural properties of the perovskite layer by AFM means, carried out by our co-worker Elisa Palacios-Lidón (Universidad de Murcia).[38] However, the conclusions taken from this work do not intend to claim that the interactions observed in solution will be seen in the film

scenario, but just to confirm that improved performance devices can be achieved by controlling the characteristics of the perovskite solution. To further confirm the benefits of fullerene addition to PSCs, devices of various configurations were fabricated, all of them suggesting the FF as the main source of improvement in the performance. Furthermore, based on the chemical knowledge on perovskite:fullerene mixtures, a novel fullerene was synthesized, which led to PSCs of improved performance with PCE values up to 18.3%.

6.2   Experimental Section

6.2.1   Materials

The materials used in the photovoltaic study were obtained from commercial suppliers in high purity and used without further purification: glass/FTO (TEC15, Hartford Glass), MAI (DYESOL), FAI (DYESOL) $PbCl_2$ (98%, Sigma-Aldrich), $PbBr_2$ (TCI Chemicals), spiro-OMeTAD (99%, Feiming Chemicals Limited), LiTFSI (99.9%, Solvionic), *tert*-butylpyridine (96%, Sigma-Aldrich), FK209 (Sigma-Aldrich), DMF (extra pure, Scharlab), DMSO (Acros Organics), 2-propanol (synthetic grade, Scharlab), acetone (technical grade, Scharlab), chlorobenzene (99.8%, Sigma-Aldrich) and acetonitrile (UV HPLC grade, Scharlab). For the fabrication of p-i-n devices, anhydrous DMSO, DMF, ethyl acetate and toluene were purchased from Sigma-Aldrich. PTAA, bathocuproine (BCP) and C_{60} (99.9%) were purchased from Sigma-Aldrich. Cu turnings were purchased from Alfa Aesar. MAI was purchased from Dyenamo and PbI_2 from TCI. Patterned ITO glass substrates (25 x 25 mm, 15 Ω sq^{-1}) were purchased from Automatic Research GmbH.

6.2.2   Characterization

The morphological properties of the films were analyzed with an ULTRA plus ZEISS FE-SEM. FTIR spectra were obtained with a Nicolet 6700, recording 32 scans with a resolution of 2 cm^{-1} using a liquid cell of 0.1 mm path length with AgCl windows. NMR spectra were recorded on a Bruker Avance 300 (^{1}H: 300.2 MHz, ^{19}F: 376.4 MHz) at

room temperature. The chemical shift (δ) is quoted in ppm relative to the internal standard tetramethylsilane (TMS).

Fullerene-containing perovskite thin films for AFM measurement were transferred from vacuum darkness conditions to the humidity controlled AFM chamber to avoid degradation. AFM measurements were carried out under N_2 controlled atmosphere (RH<10%) at room temperature using a Nanotec S.L microscope operated in tapping mode with silicon tips (OMCL-C240TS-R3, nominal $k = 3$ N m^{-1} and $f = 70$ kHz). Freely available WSxM software has been used for mage acquisition and processing.[39]

6.2.3   Device fabrication

ETL-free device fabrication

All the spin-coating layer deposition steps were conducted in a nitrogen atmosphere. The perovskite solution was prepared by dissolving 7.71 mmol of MAI and 2.57 mmol of $PbCl_2$ (molar ratio 3:1) in 3 mL of DMF and stirring overnight. Prior to deposition, perovskite solution was saturated with the corresponding fullerene. The resulting solution was spin coated on the substrates following a two-step protocol, which consisted of a first step of 500 rpm for 5 s followed by a second step of 2000 rpm for 45 s. Subsequently, the samples were annealed at 100°C for 2 h.

n-i-p device fabrication

Glass/FTO 10 Ω sq^{-1} is cleaned by sonication in 2% Hellmanex water solution for 30 min. After rinsing with water, the substrates are further sonicated with ethanol for another 30 min and, after drying, with acetone for the same amount of time. After a 15 min UV-O$_3$ treatment, a TiO_2 compact layer is deposited on FTO via spin-coating from a 2 M $TiCl_4$ solution in H_2O. After a 5000 rpm/20 s spin-coating program, the substrates are sintered at 100°C for 10 min. Then, a mesoporous TiO_2 layer is deposited by spin coating for 10 s at 4000 rpm with a ramp of 2000 rpm s^{-1}, using 30 nm particle paste (Dyesol 30 NR-D) diluted in ethanol to achieve 150-200 nm thick layer. After the spin

coating, the substrates are sintered with a heating ramp up to 450°C, at which they are left for 30 min under dry air flow. Li-doping of mesoporous TiO_2 is obtained by spin coating a 10 mg mL^{-1} solution of LiTFSI in acetonitrile at 3000 rpm for 10 s. The substrate with Li-doped mesoporous TiO_2 is completed with a second sintering process, the same as before. After cooling down to 150°C the substrates are immediately transferred in a nitrogen atmosphere glove box for deposition of the perovskite films.

The perovskite films are deposited from a freshly prepared precursor solution, containing PbI_2:MAI, 1:1 mol/mol, 1.2 M in anhydrous DMSO, either pure or fullerene-saturated. The perovskite solution is spin coated following a two step-program at 1000 and 6000 rpm for 10 and 30 s respectively. During the second step, 150 μL of chlorobenzene are dripped onto the spinning substrate 5 s prior the end of the program. The substrates are then annealed at 100°C for 30 min.

After the perovskite annealing the substrates are allowed to cool down for few minutes and 50 μL spiro-OMeTAD solution (70 mmol in chlorobenzene) are spun at 4000 rpm for 20 s. The HTM solution is doped with *tert*-butylpyridine (3.3 mol/mol with respect to spiro-OMeTAD), LiTFSI (1.8 M in acetonitrile, 0.5 mol/mol with respect to spiro-OMeTAD) and FK209 (0.25 M in acetonitrile, 0.03 mol/mol in respect to Spiro-OMeTAD). Finally, 80 nm gold top electrode is thermally evaporated using a Quorum Q150T, under around 5 x 10^{-5} mbar, through an appropriate shadow mask (0.25 cm^2 pixel).

p-i-n device fabrication

Glass/ITO samples were cleaned by the following procedure: the samples were sonicated in distilled water with soap for 5 min, rinsed thoroughly with distilled water, dried, and sonicated in acetone and 2-propanol for 15 min in each solvent. After that, directly before HTM deposition, substrates were treated in an UV-O$_3$ cleaner for 15 min.

All the spin-coating layer deposition steps were conducted in a nitrogen atmosphere. PTAA (2 mg mL^{-1} in toluene) was spin-coated (4000 rpm for 30 s) and annealed for 10 min at 100°C on glass/ITO substrates. MAPbI$_3$ perovskite 1.2 M solution was obtained

by preparing a 1.5 M nominal MAI solution in DMF:DMSO (6:1 volume ratio) as stock solution and adding the corresponding volume to PbI_2. For perovskite:fullerene blend film preparation, DMF:DMSO mixtures for MAI stock solution contained the corresponding fullerene in 0.05 mg mL^{-1} concentration. A volume of 100 μL of perovskite solution was spread on the substrate one step spin-coating process (4000 rpm for 35 s) was carried out. A volume of 500 μL of ethyl acetate was dripped on the substrate 20 s after the start of the spin-coating process. Subsequently, the samples were annealed at 100°C for 1 h.

The substrates were covered by thermally evaporated layers of C_{60} (380°C, 0.15 A s^{-1}) and BCP (140°C, 0.15 A s^{-1}), with a thickness of 23 nm and 8 nm, respectively. Finally, 80 nm thick Cu metal frame was evaporated as a top contact, defining the active area of 0.144 cm^2.

6.2.4   Device characterization

ETL-free device characterization

The *J-V* chracteristics of the solar cells were measured under simulated solar light by using the setup decribed in chapter 2. The EQE spectra of the devices were also obtained from the home-made specific setup and methodology described in chapter 2.

n-i-p device characterization

The solar cells performances were measured using a Solixon A-20 Solar Simulator. Current-voltage characteristics of the cells were obtained by applying an external voltage bias while measuring the current response with a digital source meter (Keithley 2400). The employed voltage scan rate was 10 mV s^{-1} and no device preconditioning was applied before starting the measurement, such as light soaking or forward voltage bias applied for long time. The cells were masked with a black metal mask (0.16 cm^2) to estimate the active area and reduce the influence of the scattered light.

p-i-n device characterization

Current-voltage characteristics under 1 sun equivalent illumination were recorded using an Oriel LCS-100 class ABB solar simulator in a N_2-filled glovebox, calibrated with a Silicon reference cell from Fraunhofer ISE. The *J-V* curve was acquired with 0.1 V s^{-1} scan rate and a voltage step of 10 mV. EQE spectra were measured as a function of wavelength from 300 to 850 nm with a step of 10 nm using a home-built small-spot EQE system. A Stanford Research SR830 Lock-In amplifier is used to measure the electrical response of the device under test and evaluated in TracQ-Basic software.

6.3   Results and discussion

6.3.1   Spectroscopic analysis

Considering the currently open questions around the influence of perovskite-fullerene interactions on the device performance, this chapter aims to study the relevance of structural characteristics of fullerenes on this by different spectroscopic methods. The analysis was focused on certain selected fullerenes for a suitable comparison. In particular, considering the results in Chapters 3 and 5, **IS2**,[1] a C_{60} functionalized with an isoxazoline group, and the non-functionalized C_{60} and C_{70}[2] were chosen. **IS2**, particularly appealing as it provided very nice performance for ETL-free devices,[1] holds a characteristic functionalization that could help understanding possible working mechanisms. Since **IS2** contains fluorine atoms, we decided to perform ^{19}F-NMR experiments on 4:1 dimethylformamide:dimethyl sulfoxide (DMF:DMSO). As it can be seen in Figure 6.1a, the five fluorine atoms of this material show up only in three different signals (F_A at 161.0 ppm, F_B at 138.9 ppm and F_C at 150.0 ppm), where the fluorine atoms in *ortho* and *meta* positions F_A and F_B integrate both for two fluorine atoms due to their magnetic equivalence. Nevertheless, when the same experiment was carried out in the presence of $MA_{0.15}FA_{0.85}PbBr_{0.15}I_{0.85}$ (MAFA perovskite, where MA and FA stand for methylammonium and formamidinium, respectively) perovskite solution, the three signals were split into five, changing the relative values of what they integrate for. Since the aim was to see any possible effect of any perovskite amine on **IS2**, MAFA and not $MAPbI_3$ perovskite was used for this experiment. In the first case

where **IS2** is alone in solution, both sides of the aromatic ring are magnetically equivalent, explaining the integration for each of the fluorine atoms. However, the presence of perovskite precursors in solution suppresses this equivalency and new signals are found. The origin of these could be due to the fact that new chemical species is being formed, in which the shift and multiplicity of the NMR signals is therefore altered. One possible explanation could be the formation of hydrogen bonds between the N or O atoms of the **IS2** isoxazoline, which could act as Lewis bases, and perovskite amine or lead iodide. Due to the existence of a new non-coordinative bond through the isoxazoline moiety, the atoms in the aromatic ring would experience stronger electronic repulsions coming from the coordinating perovskite precursors. Therefore, the magnetic environment of fluorine atoms is changed, and so their chemical shift in the NMR spectrum. This hypothesis is also supported by the fact that fluorine atom in *para* position F_C at 150.0 ppm is the less affected one in the aromatic ring, as it would be the furthest one in space from this potential coordinative bond. These results point out the presence of some kind of interaction between the fullerene and perovskite precursors, but not specific bond formations. In order to tackle this issue, we thought of trying the same experiment but with each perovskite precursor individually (i.e., **IS2**:FAI and **IS2**:PbI$_2$). The ^{19}F-NMR spectra in Figure 6.1b show that the 3 signals remained unchanged for all of these solutions. This finding suggests that **IS2** might not be forming any complex with each precursor separately, as it might only participate in the complete perovskite complex. A representation of the possible complex being formed is shown in Figure 6.2.

Hence, these results suggest that **IS2** might be able to coordinate perovskite in some way, probably thanks to the isoxazoline group. If the potential of this functionalization is to be confirmed, a new fullerene should be designed. The idea was to combine the most successful molecules in Chapters 3 and 5 for ETL-free PSCs, C$_{70}$[2] and **IS2**,[1] hoping for a synergistic structural effect. The resulting fullerene **FU11** (Figure 6.3) is a C$_{70}$-cored **IS2** analogue, thus holding the same isoxazoline group. **FU11** was synthesized and fully characterized by Sebastian Völker (Polymat).[38] In the case of ^{19}F-NMR analysis it was not used, since the fluorine signals could not be properly resolved. This can be explained by the fact that C$_{70}$ derivatives are not a unique molecule but a mixture of various regioisomers, showing different NMR patterns. Thus its suitable detection and

assignment by ^{19}F-NMR is more complicated than in the case of **IS2**. This is an issue to deal with when working with C_{70} derivatives, widely reported in literature.[40-42]
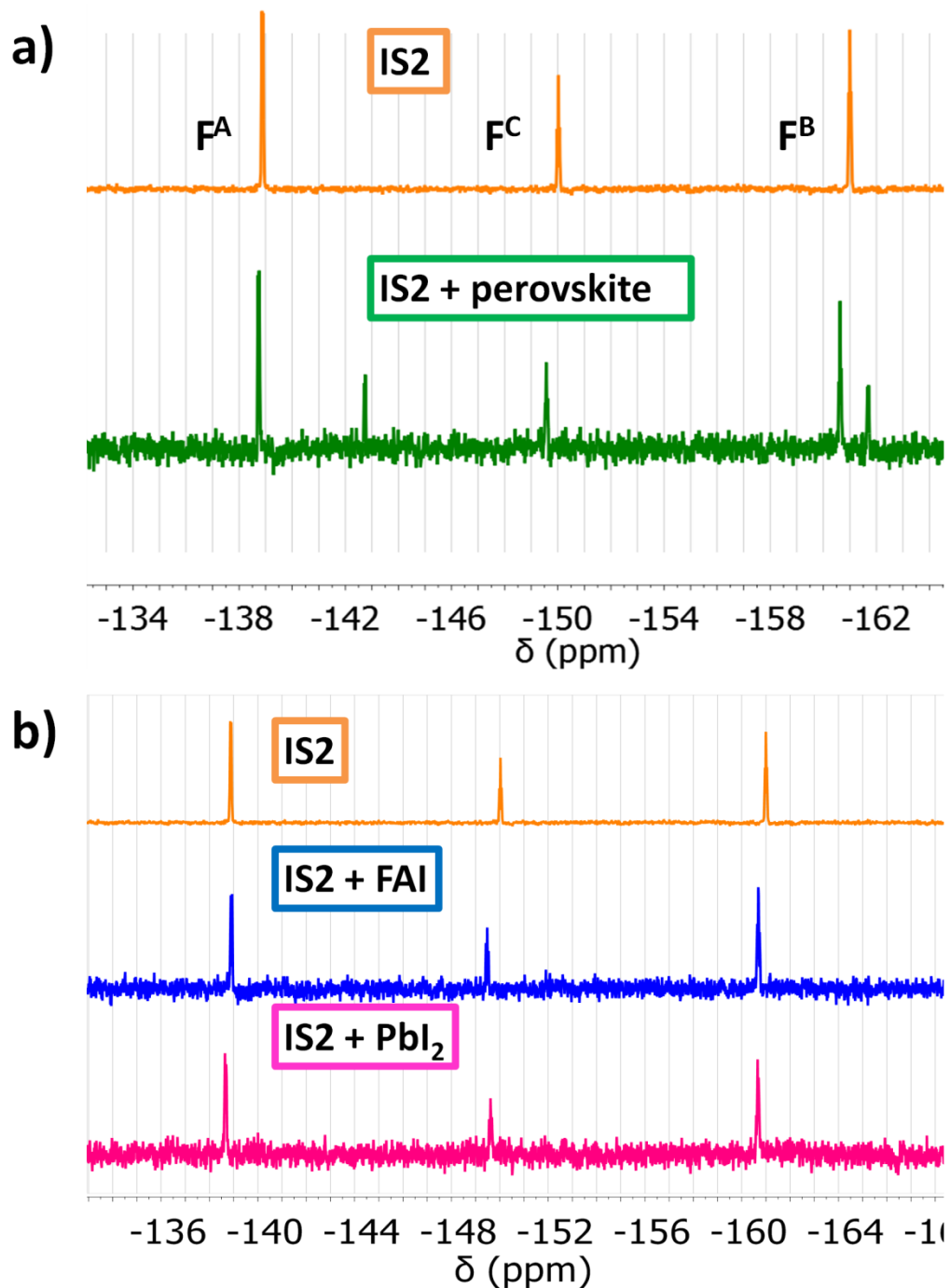
Figure 6.1. ^{19}F-NMR spectrum of **IS2**-saturated DMF:DMSO (4:1) solution with a) perovskite precursors together and b) separated at 1.2 M.
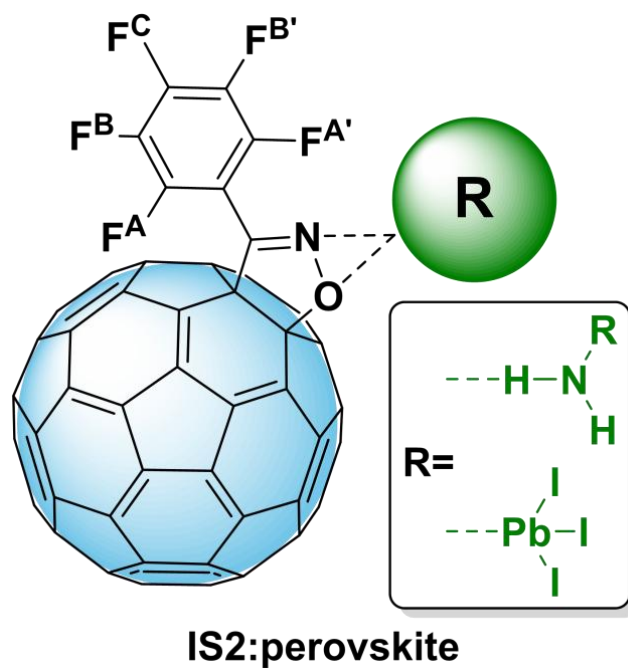
IS2:perovskite

Figure 6.2. ^{19}F-NMR spectra of **IS2**-saturated DMF:DMSO (4:1) solution and in presence of FAI and PbI$_2$ separately. Scheme of potential complexes to be formed between **IS2** and perovskite precursors.

FU11

Figure 6.3. Structure of **FU11**.

With the new fullerene **FU11** synthesized, the spectroscopic analysis could be carried out considering both fullerene core- and functional group-related structural changes.

Trying to find some kind of evidence on the bonds being formed between fullerenes and perovskite, solutions of MAPbI$_3$ at 1.2 M in DMSO with C$_{60}$, C$_{70}$, **IS2** and **FU11** were analyzed by FTIR spectroscopy means. This also repre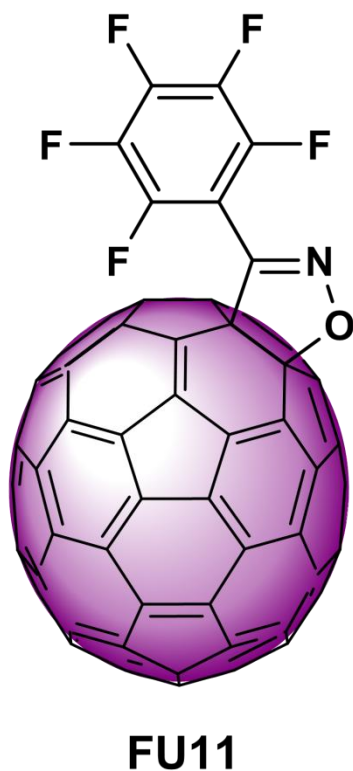sents the first study of perovskite complexes in solution by FTIR means, as every study done so far involved the preparation of perovskite powders where the interactions with fullerene derivatives may be significantly different. Due to the wide-absorbing range of the solvent (DMSO) in IR, N-H stretching vibration was the only character that could be studied, which typically appears in the 3500-3000 cm^{-1} region. As it can be seen in Figure 6.4a, the band for MAPbI$_3$:C$_{60}$ and MAPbI$_3$:C$_{70}$ remained in a comparable situation to the original pristine MAPbI$_3$ at 3145 cm^{-1}, but for **IS2** the band widened and shifted to higher wavenumber values (3164 cm^{-1}). For **FU11** signal the shift was quite moderate, but it also experienced widening. This is a sign of the formation of H-bonds, potentially coming from fullerene-MA interactions. However, the shift of the N-H stretching vibration to higher energy values means that the N-H bond is stronger, what could mean that the potential H-bond between **IS2** or **FU11** and the amine would be weaker than the original one in the perovskite. Nevertheless, both shift and widening of the N-H signal point out the existence of **IS2**-perovskite interactions that do not happen for the rest of the fullerenes. Additionally, these two phenomena (i.e. shift and widening) were not observed when studying lead-free MAI solutions in the presence of these fullerenes (Figure 6.4b). The spectra were identical for every MAI and MAI-fullerene solution, stressing out that fullerenes and methylammonium do not establish any interaction when PbI$_2$ is not in solution, even for the case of isoxazoline fullerenes. Overall, these results point in the same direction as the ones obtained by ^{19}F-NMR spectroscopy in Figure 6.1, as an interaction between **IS2** or **FU11** and perovskite can be observed, but only in the presence of the full perovskite complex. Additionally, FTIR shows for the first time the formation of H-bonds between functionalized fullerenes and perovskite amines, which might be the role of the Lewis bases that they hold.
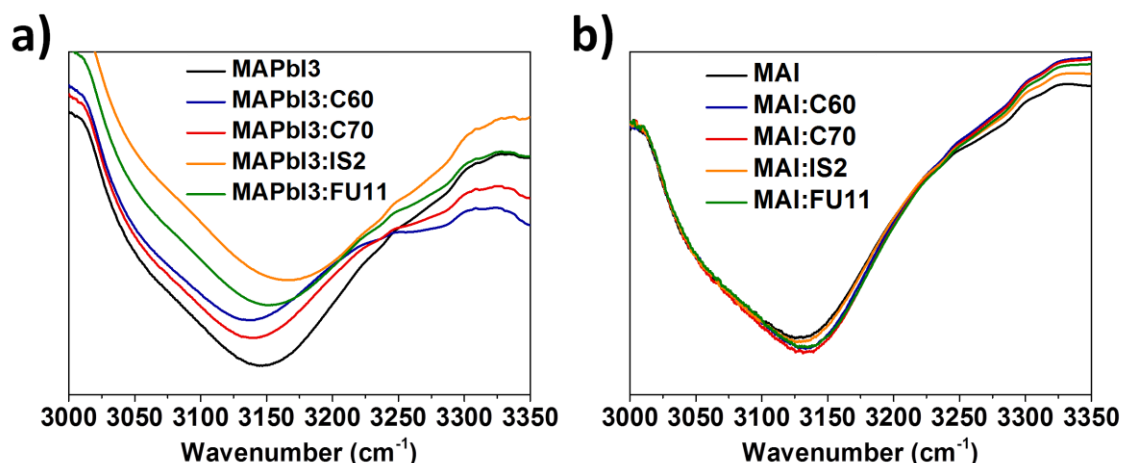
Figure 6.4. FTIR spectra of solutions containing C_{60}, C_{70}, **IS2** and **FU11** of a) MAPbI$_3$ and b) MAI at 1.2 M.

In order to further study the perovskite amine precursor, ^{1}H-NMR experiments were carried out to perovskite solution together with the studied fullerenes. Figure 6.5a shows how protons at 8.9 ppm belonging to FA were deshielded and split into higher multiplicities, independently of the fullerene nature. The reason why MAFA perovskite and not MAPbI$_3$ is being used for these experiments is because this splitting could only be seen for the protons belonging to FA and not for MA, due to the structure of the first one. FA protons can be differentiated in the shift value as there are two amine moieties in the same molecule, while MA contains only one, and the protonated form has resonance structures that hinder free rotation of C-N bonds. Following the same line as the previous experiments, when solutions without PbI$_2$ were measured (i.e. FAI:fullerenes), the effect of fullerenes vanished once again, showing in every case unaffected FA protons (Figure 6.5b). However, C_{60} and C_{70} lack of any functionalization that would allow them establishing any H-bond with perovskite amine groups. Therefore, fullerenes might have some influence on perovskite amine groups in an indirect way, probably through the establishment of anion-π coordinative bonds between the fullerene cage and iodide from PbI$_2$ in the perovskite complex. As pointed out earlier, this kind of bond has been characterized in the literature for very diverse arene-anion systems,[30-35] including fullerenes.[10,14,36,37]
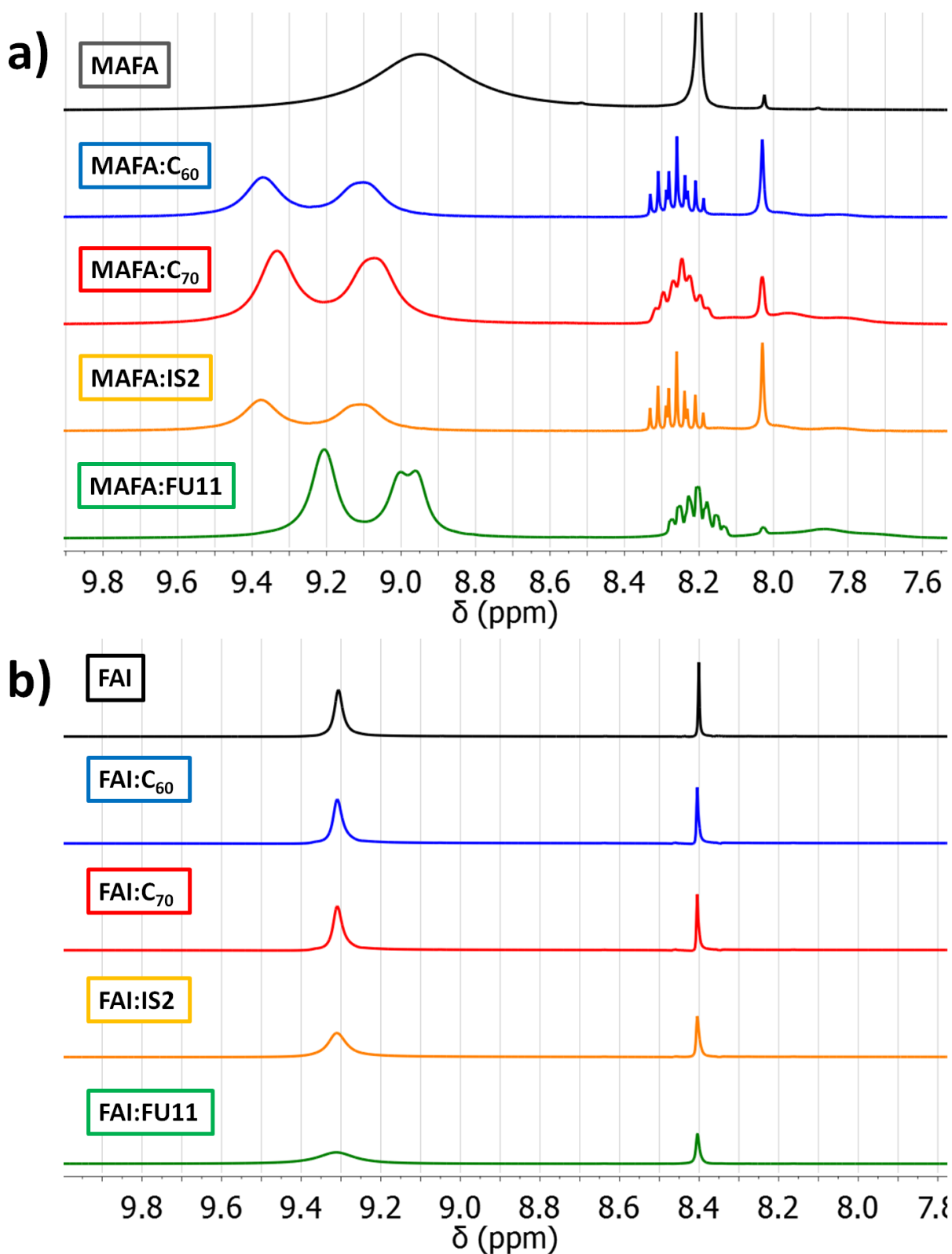
Figure 6.5. ^{1}H-NMR spectra of a) MAFA and b) FAI at 1.2 M in DMF:DMSO (4:1) in the presence of the different fullerenes.

In order to test the strength of the complexes that might be forming between perovskite and the different fullerenes, we decided to add a small fraction of toluene to mixtures

with perovskite:fullerene complexes. Fullerenes have high affinity for other aromatic molecules such as this solvent, as it was also shown for *o*-xylene or *o*-DCB in Chapter 4. Therefore it could be expected that toluene molecules solvate fullerenes and, in turn, the complex is broken, while monitoring all these changes by NMR. In this sense, the MAFA:fullerene solutions showed in Figure 6.5 were analyzed again by ^{1}H-NMR after the addition to the of a ¼ fraction of toluene-d8. As shown in Figure 6.6, for the non-substituted fullerenes C_{60} and C_{70} the splitting of the protons of FAI that the fullerene causes was no longer seen, whilst it remained for isoxazoline fullerenes **IS2** and **FU11**. These results point to the formation of a stronger complex with the perovskite when the fullerene has a second binding group such as the isoxazoline, as it does not disassemble when an aromatic cosolvent is added. In fact, all acquired spectroscopic data points out coherently the ability of functionalized fullerenes to form two-sided complexes with perovskite. This allows drawing a tentative structural representation of the interactions under study (not a claim of an exact perovskite-fullerene complex structure), which is shown in Figure 6.7. The present results suggest that non-functionalized C_{60} and C_{70} participate in the perovskite complex just through anion-π bonds with PbI_2 (Figure 6.7a), whilst the ones with Lewis base functional groups (**IS2** and **FU11**) can also establish H-bonds with perovskite amines (Figure 6.7b), leading to stronger complexes.
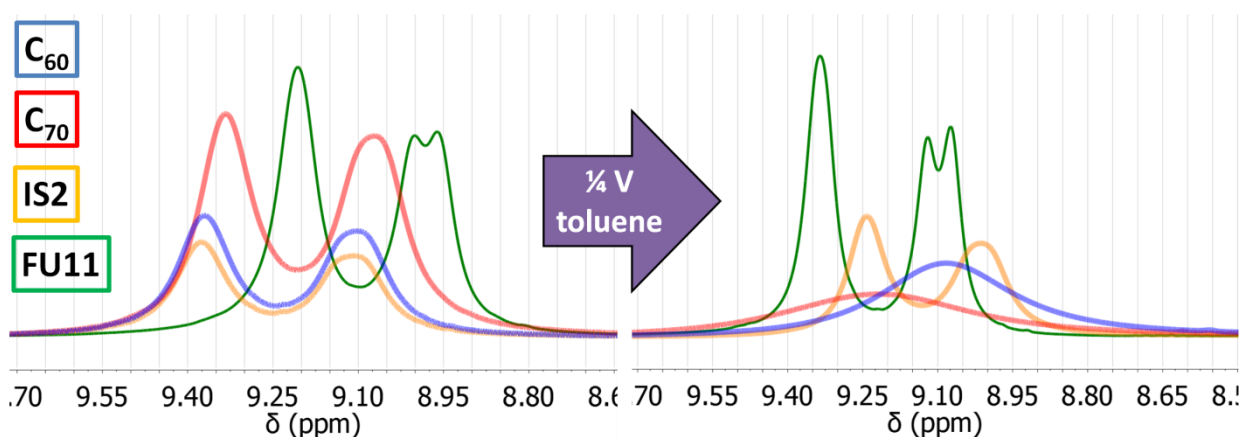

Figure 6.6. ^{1}H-NMR spectra of MAFA perovskite solution (1.2 M) containing C_{60}, C_{70}, **IS2** and **FU11** in DMF:DMSO (4:1) and after the addition of ¼ parts of toluene-d8.
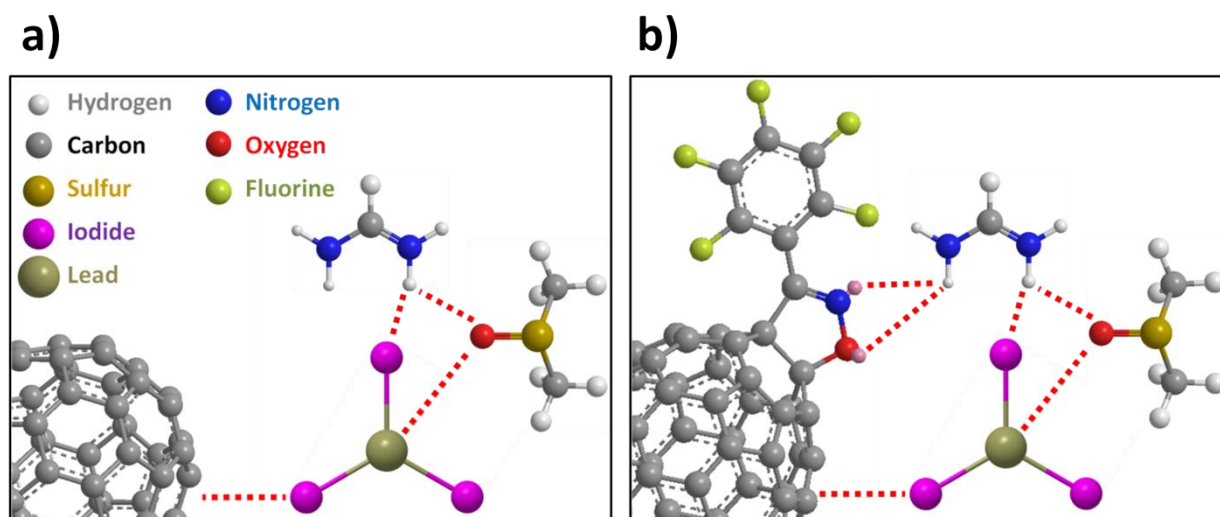
Figure 6.7. Tentative structural explanation of the interactions ongoing in the perovskite complexes with a) non-functionalized fullerenes and b) functionalized fullerenes.

As shown in Figure 6.8,[38] the AFM characterization (i.e carried out by the co-worker Dr. Elisa Palacios Lidón (Universidad de Murcia)) of the perovskite:fullerene films revealed a strong time-evolution divergence depending of the fullerene type. The gradual increase of the phase signal could be correlated with the diffusion of C_{70} to the surface, while the layers with **FU11** remained stable over time. This effect might be a result of the surface heating produced by the AFM instrument itself, but the results are in agreement with the existence of a stronger complex between perovskite and isoxazoline-containing fullerenes, and thus not diffusing to the surface. **FU11** could have two binding spots to perovskite in its structure as proposed previously, which is not the case for C_{70}, for which the complex with perovskite might not be strong enough and therefore migrates through the layer. This would mean that the strength in which perovskite and fullerene interact in solution might also be transferred to film scenario, and therefore fullerenes with more affinity to perovskite would potentially be able to, for example, passivate defects through more tight non-covalent bonds or complexes that may help the perovskite to crystallize into a higher quality layer.
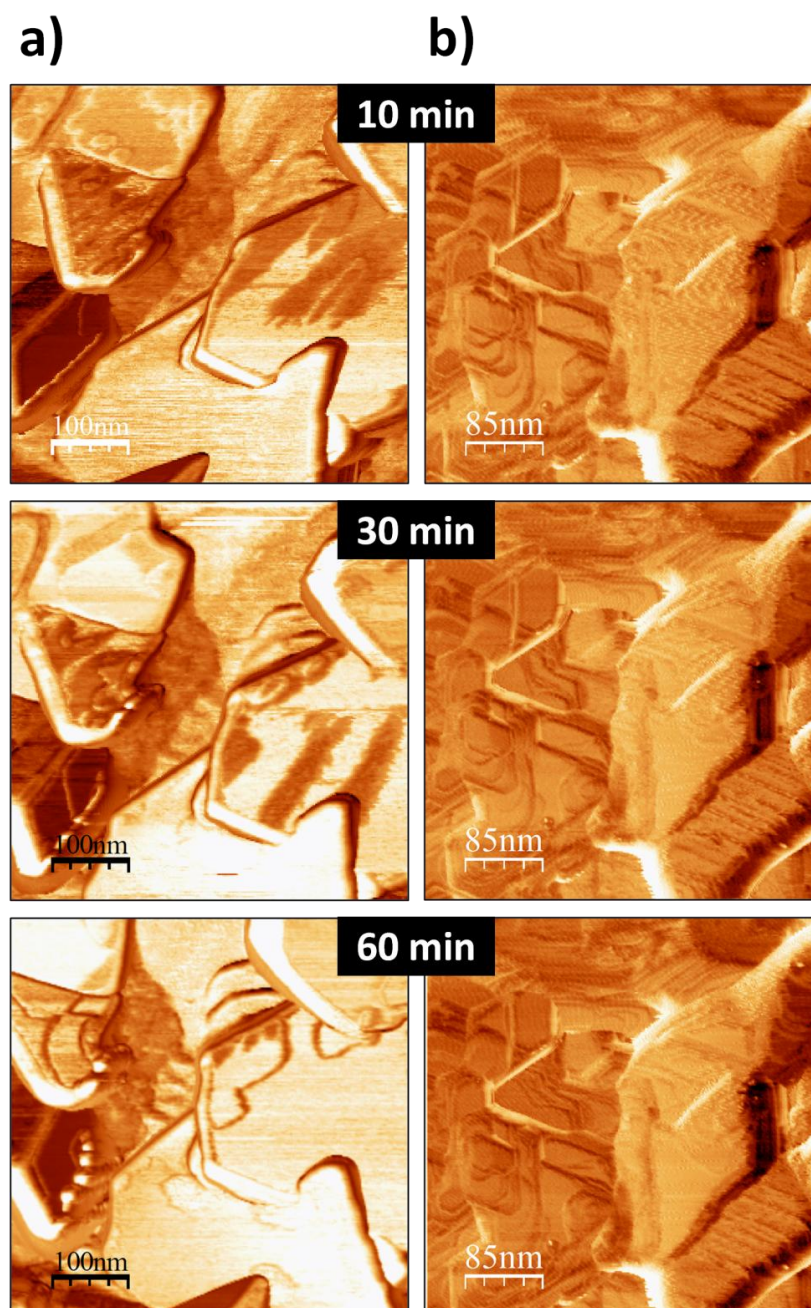
Figure 6.8. a) AFM phase images of MAPI:C$_{70}$ and b) MAPI:**FU11** films at different times.

6.3.2 Photovoltaic analysis

MAPbI$_3$ layers containing **FU11**, and C$_{70}$ for analyzing the effect of the functionalization, were applied in the fabrication of devices of diverse configurations. The device architectures chosen for this study considered also the ETL-free on, widely studied in the present thesis, but this chapter also aimed the universality, transferring the benefits of the developed perovskite:fullerene blends to n-i-p and p-i-n devices.

Considering this, first, MAPbI$_3$ layers containing C$_{70}$ and **FU11** were compared to the pristine perovskite in ETL-free devices on FTO substrates, with spiro-OMeTAD as HTL and Au as top contact. The whole structure can be seen in the cross-section micrograph acquired by FE-SEM means in Figure 6.9a. As seen in Chapter 3, the use of C$_{70}$ helped achieving better PCE values, an effect that was enhanced when applying **FU11**.
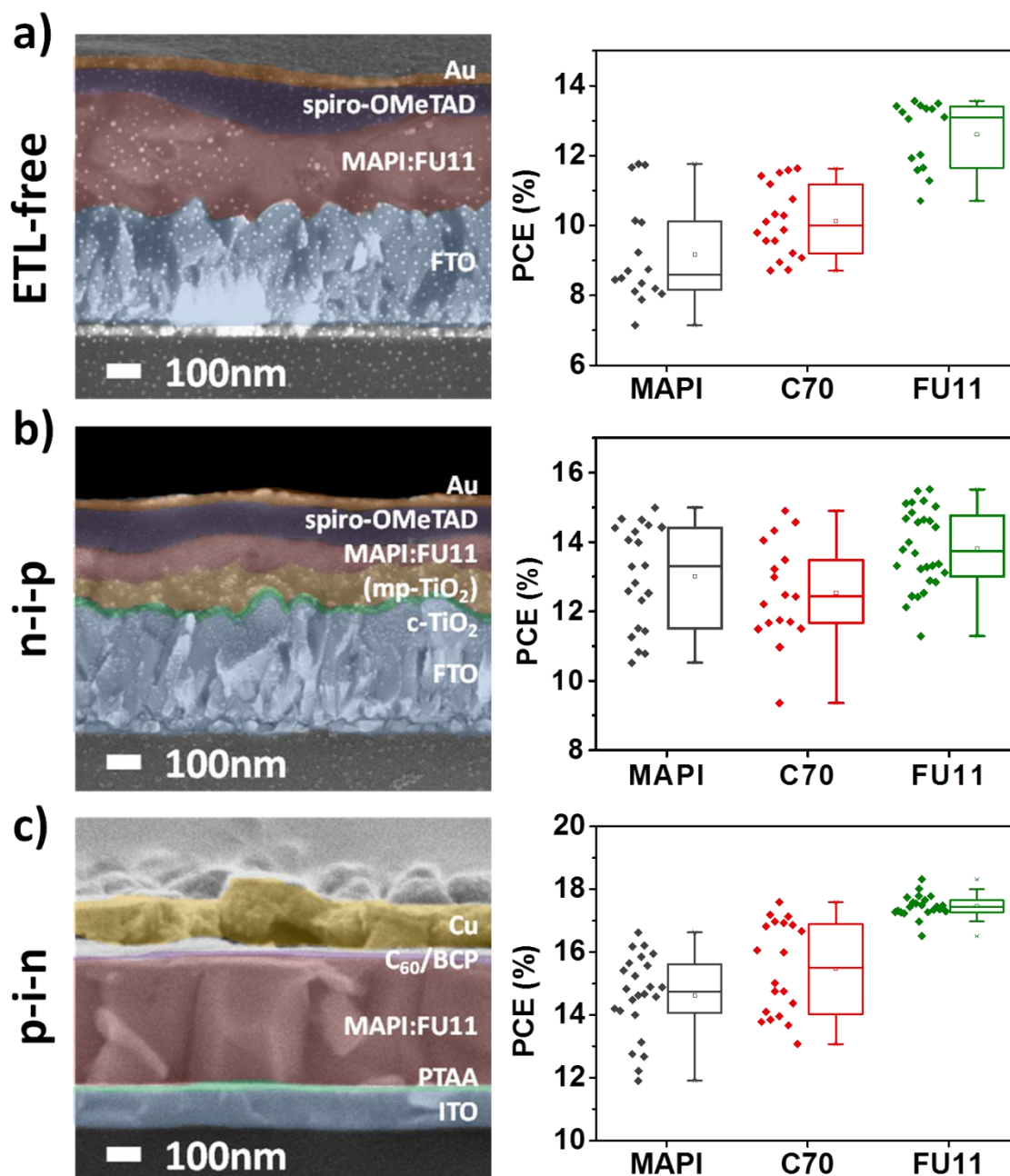
Figure 6.9. a) Cross-section micrographies by FE-SEM means and PCE values distribution of ETL-free devices on FTO, b) n-i-p devices on FTO/c-TiO$_2$/mp-TiO$_2$ and c) p-i-n devices on ITO/PTAA of MAPbI$_3$ perovskite with C$_{70}$ and **FU11** fullerenes.

This outcome was tried to be reproduced in n-i-p devices with compact and mesoporous TiO$_2$ (c- and mp-TiO$_2$, respectively) as ETL (Figure 6.9b), but there was not such an improvement but just a slight increase in the maximum PCE. Nevertheless, the improvement in the FF was particularly impressive, achieving excellent values up to 81.8% with the use of **FU11** (Figure 6.10), which is in agreement with most of perovskite:fullerene blend applications in literature.[4-6]

Table 6.1. Average and highest PCE cells PV parameter values of the devices in each of the configurations with MAPbI$_3$, MAPbI$_3$:C$_{70}$ and MAPbI$_3$:**FU11** blend layers.[a]

Configuration	Perovskite layer	J_{sc} (mA cm^{-2})	V_{oc} (V)	FF (%)	PCE (%)
ETL-free	MAPbI$_3$	14.4 (16.2)	1.01 (1.08)	62.4 (67.4)	9.2 (11.8)
	MAPbI$_3$:C$_{70}$	15.0 (15.1)	1.03 (1.06)	65.5 (73.0)	10.1 (11.6)
	MAPbI$_3$:**FU11**	16.6 (16.9)	1.05 (1.07)	72.2 (75.1)	12.6 (13.6)
n-i-p (mp-TiO$_2$)	MAPbI$_3$	17.4 (19.0)	1.03 (1.03)	72.3 (77.0)	13.0 (15.0)
	MAPbI$_3$:C$_{70}$	17.0 (19.2)	1.02 (1.04)	72.6 (74.7)	12.5 (14.9)
	MAPbI$_3$:**FU11**	17.3 (18.9)	1.04 (1.04)	77.0 (78.8)	13.8 (15.5)
p-i-n (PTAA)	MAPbI$_3$	21.0 (21.7)	0.98 (1.05)	70.7 (73.1)	14.6 (16.6)
	MAPbI$_3$:C$_{70}$	21.5 (21.9)	0.99 (1.03)	72.6 (77.9)	15.5 (17.6)
	MAPbI$_3$:**FU11**	22.1 (22.3)	1.04 (1.06)	76.1 (77.3)	17.5 (18.3)

[a] Numbers in brackets correspond to values of the most efficient device of each type.

Finally, these fullerenes were tried in p-i-n devices, precisely on ITO/PTAA substrates and with C$_{60}$/BCP/Cu as top contact (Figure 6.9c). Cells improved with both fullerenes,

moderately with C_{70}-containing films, but with **FU11** a narrow distribution of excellent PCE values was obtained. A record device with a PCE value of 18.3% was obtained, with a J_{sc} of 22.32 mA cm^{-2}, a V_{oc} of 1.06 V and a FF of 77.3%. These results, which mainly come from the improvement of FF, could have their origin in the possibility of fullerenes to passivate defects. The enhanced ability of **FU11** could be related to the stronger complex that we have earlier proposed that it forms with perovskite. The possibility for **FU11** to bind tightly to perovskite precursors might also favor binding potential defects in the perovskite at the grain boundaries. In this sense, the way in which fullerene interacts with perovskite in the precursor solution might have a great importance, as it might influence the efficiency in which it can improve the film characteristics in terms of defect suppression. In Table 1 the average and maximum values are shown and the distribution of PV parameter values for each of the device configurations is available in Figure 6.10.
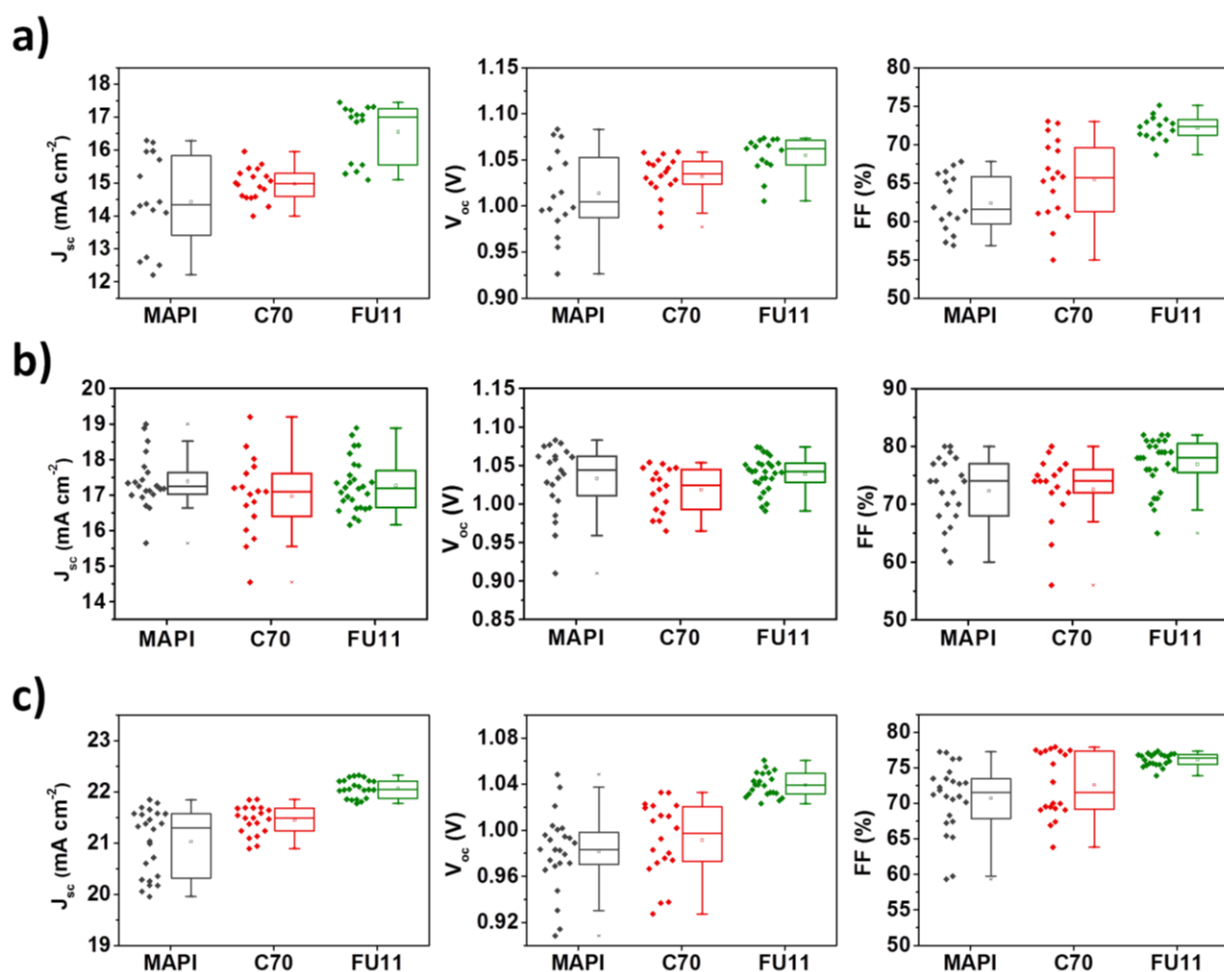

Figure 6.10. PV parameters (i.e. J_{sc}, V_{oc} and FF) for MAPbI$_3$:C$_{70}$ and :**FU11** blend films-based PSCs and without fullerene (MAPI) with a) ETL-free, b) n-i-p and c) p-i-n configurations.

Fullerene **FU11** worked particularly well in p-i-n devices and showed the highest efficiency values among the different device architectures. The microstructural properties of MAPbI$_3$:**FU11** layers on PTAA were analyzed and, as Figure 6.11a shows in the top-view and cross-section (in the inset) micrographs, a flat layer with good morphology was achieved, with large grain size distribution of 100-300 nm. Figure 6.11b shows the *J-V* curve of the best device for each type of MAPbI$_3$ film, showing again the improvement that the fullerenes bring to p-i-n configuration. Small hysteresis could be observed, which was unchanged for every type of MAPbI$_3$ film, in contrast to what has been claimed in various works in literature for perovskite:fullerene blend films-based PSCs.[6,10] The maximum power point tracking that we can be seen in Figure 6.11c revealed a stabilized 18.3% after 2 min at 1 sun of illumination, being a stable value as identical to the original value. In Figure 6.11d we present the EQE spectrum of the best cell. The *J$_{sc}$* value that we could integrate from it was 22.22 mA cm^{-2}, which is in perfect agreement with the *J$_{sc}$* value of 22.32 mA cm^{-2} obtained from the *J-V* curve.

6.4   Conclusion

As a summary, by using a novel combination of spectroscopic techniques, further insights into the working mechanism in which fullerene participates in the perovskite complex in solution were provided, and how its functionalization affects the final outcome in the layer and device properties. Searching for a fullerene with enhanced ability to form stronger complexes with perovskite, a new one was designed and proved in blends with perovskite for their use in devices. The devices bearing this novel fullerene showed improved performance for ETL-free PSCs with a main enhancement of FF, pointing out the potential of isoxazoline-containing fullerenes. This strategy was furthermore proven to be universal for many types of devices of different configuration, reaching efficiency values of up to 18.3%. Deepening in the understanding of the working mechanisms of fullerenes and the relevance of their chemical nature in solution allowed controlling the system from the solution state to device fabrication, going through film properties. Although there is still a lot to understand about these carbon nanomaterials for perovskite applications, this work stresses out the relevance of the

strength of the complexes formed in solution between perovskite and fullerene and the need to control and optimize them in order to further improve these devices.
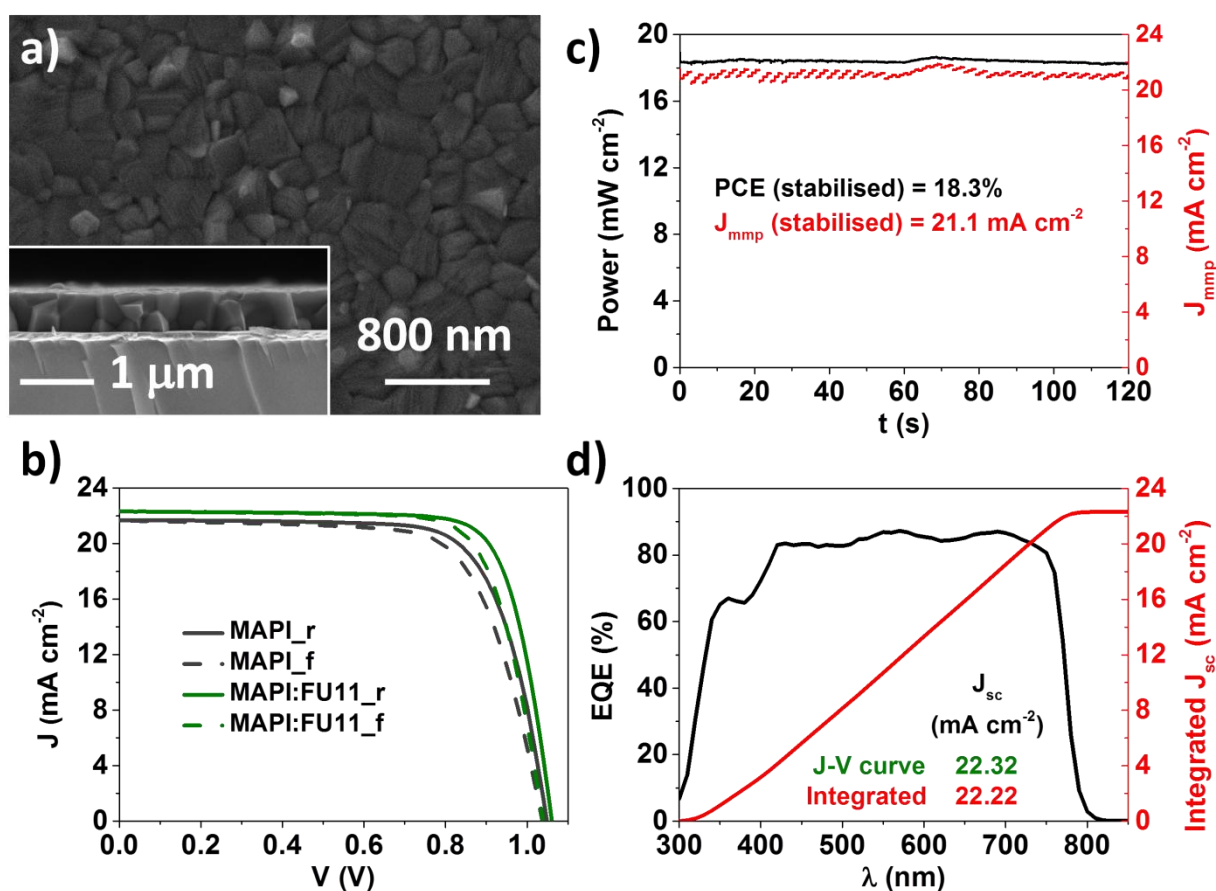
Figure 6.11. a) Top-view FE-SEM micrograph of MAPbI$_3$:**FU11** layer on ITO/PTAA and cross-section in the inset. b) Best *J-V* curves in reverse (r) and forward (f) scan for MAPbI$_3$ and MAPbI$_3$:**FU11** in p-i-n devices. c) Stabilized power output and *J$_{mmp}$* for record device. d) EQE spectrum and integrated current curve for record device. A comparison between the integrated *J$_{sc}$* and the one taken from the *J-V* curve is given.

6.5   References

[1]   R. Sandoval-Torrientes, J. Pascual, I. García-Benito, S. Collavini, I. Kosta, R. Tena-Zaera, N. Martín, J. L. Delgado. Modified Fullerenes for Efficient Electron Transport Layer-Free Perovskite/Fullerene Blend-Based Solar Cells. *ChemSusChem* **2017**, *10*, 2023.

[2]   J. Pascual, I. Kosta, N. Tuyen, A. Chuvilin, G. Cabanero, H. J. Grande, E. M. Barea, I. Mora-Seró, J. L. Delgado, R. Tena-Zaera. Electron Transport Layer-Free

Solar Cells Based on Perovskite-Fullerene Blend Films with Enhanced Performance and Stability. *ChemSusChem* **2016**, *9*, 2679.

[3] J. Pascual, I. Kosta, E. Palacios-Lidon, A. Chuvilin, G. Grancini, Md. K. Nazeeruddin, H. J. Grande, J. L. Delgado, R. Tena-Zaera. Co-Solvent Effect in the Processing of the Perovskite:Fullerene Blend Films for Electron Transport Layer-Free Solar Cells. *J. Phys. Chem. C* **2018**, *122*, 2512.

[4] X. Liu, F. Lin, C.-C. Chueh, Q. Chen, T. Zhao, P.-W. Liang, Z. Zhu, Y. Sun, A. K.-Y. Jen. Fluoroalkyl-Substituted Fullerene/Perovskite Heterojunction for Efficient and Ambient Stable Perovskite Solar Cells. *Nano Energy* **2016**, *30*, 417.

[5] F. Zhang, W. Shi, J. Luo, N. Pellet, C. Yi, X. Li, X. Zhao, T. J. S. Dennis, X. Li, S. Wang, Y. Xiao, S. M. Zakeeruddin, D. Bi, M. Grätzel. Isomer-Pure Bis-PCBM-Assisted Crystal Engineering of Perovskite Solar Cells Showing Excellent Efficiency and Stability. *Adv. Mater.* **2017**, *29*, 1606806.

[6] Y. Shao, Z. Xiao, C. Bi, Y. Yuan, J. Huang. Origin and Elimination of Photocurrent Hysteresis by Fullerene Passivation in $CH_3NH_3PbI_3$ Planar Heterojunction Solar Cells. *Nat. Commun.* **2014**, *5*, 5784.

[7] K. Wang, C. Liu, P. Du, J. Zheng, X. Gong. Bulk Heterojunction Perovskite Hybrid Solar Cells with Large Fill Factor. *Energy Environ. Sci.* **2015**, *8*, 1245.

[8] S. Collavini, M. Saliba, W. R. Tress, P. J. Holzhey, S. F. Völker, K. Domanski, S. H. Turren-Cruz, A. Ummadisingu, S. M. Zakeeruddin, A. Hagfeldt, M. Grätzel, J. L. Delgado. Poly(ethylene glycol)-[60]Fullerene-Based Materials for Perovskite Solar Cells with Improved Moisture Resistance and Reduced Hysteresis. *ChemSusChem* **2018**, *11*, 1032.

[9] Y. Zhao, J. Wei, H. Li, Y. Yan, W. Zhou, D. Yu, Q. A. Zhao. A Polymer Scaffold for Self-Healing Perovskite Solar Cells. *Nat. Commun.* **2016**, *7*, 10228.

[10] J. Xu, A. Buin, A. H. Ip, W. Li, O. Voznyy, R. Comin, M. Yuan, S. Jeon, Z. Ning, J. J. McDowell, P. Kanjanaboos, J.-P. Sun, X. Lan, L. N. Quan, D. H. Kim, I. G. Hill, P. Maksymovych, E. H. Sargent. Perovskite-Fullerene Hybrid Materials Suppress Hysteresis in Planar Diodes. *Nat. Commun.* **2015**, *6*, 7081.

[11] M. Li, Y.-H. Chao, T. Kang, Z.-K. Wang, Y.-G. Yang, S.-L. Feng, Y. Hu, X.-Y. Gao, L.-S. Liao, C.-S. Hsu. Enhanced Crystallization and Stability of Perovskites by a Cross-Linkable Fullerene for High-Performance Solar Cells. *J. Mater. Chem. A* **2016**, *4*, 15088.

[12] Z. Xiao, C. Bi, Y. Shao, Q. Dong, Q. Wang, Y. Yuan, C. Wang, Y. Gao, J. Huang. The Origin of High Efficiency in Low-Temperature Solution-Processable Bilayer Organometal Halide Hybrid Solar Cells. *Energy Environ. Sci.* **2014**, *7*, 2619.

[13] H. J. Snaith, A. Abate, J. M. Ball, G. E. Eperon, T. Leijtens, N. K. Noel, S. D. Stranks, J. T.-W. Wang, K. Wojciechowski, W. Zhang. Anomalous Hysteresis in Perovskite Solar Cells. *J. Phys. Chem. Lett.* **2014**, *5*, 1511.

[14] X. Sun, L. Y. Ji, W. W. Chen, X. Guo, H. H. Wang, M. Lei, Q. Wang, Y. F. Li. Halide Anion-Fullerene π Noncovalent Interactions: N-Doping and a Halide Anion Migration Mechanism in p-i-n Perovskite Solar Cells. *J. Mater. Chem. A* **2017**, 5, 20720.

[15] H. Azimi, T. Ameri, H. Zhang, Y. Hou, C. O. R. Quiroz, J. Min, M. Hu, Z.-G. Zhang, T. Przybilla, G. J. Matt, E. Spiecker, Y. Li, C. J. Brabec. A Universal Interface Layer Based on an Amine-Functionalized Fullerene Derivative with Dual Functionality for Efficient Solution Processed Organic and Perovskite Solar Cells. *Adv. Energy Mater.* **2015**, *5*, 1401692.

[16] C. Tian, K. Kochiss, E. Castro, G. Betancourt-Solis, H. Han, L. Echegoyen. A Dimeric Fullerene Derivative for Efficient Inverted Planar Perovskite Solar Cells with Improved Stability. *J. Mater. Chem. A* **2017**, *5*, 7326.

[17] Q. Xue, Y. Bai, M. Liu, R. Xia, Z. Hu, Z. Chen, X.-F. Jiang, F. Huang, S. Yang, Y. Matsuo, H.-L. Yip, Y. Cao. Dual Interfacial Modifications Enable High Performance Semitransparent Perovskite Solar Cells with Large Open Circuit Voltage and Fill Factor. *Adv. Energy Mater.* **2017**, *7*, 1602333.

[18] S. Collavini, I. Kosta, S. F. Völker, G. Cabanero, H. J. Grande, R. Tena-Zaera, J. L. Delgado. Efficient Regular Perovskite Solar Cells Based on Pristine [70]Fullerene as Electron-Selective Contact. *ChemSusChem* **2016**, *9*, 1263.

[19] W. Ke, D. Zhao, C. R. Grice, A. J. Cimaroli, J. Ge, H. Tao, H. Lei, G. Fang, Y. Yan. Efficient Planar Perovskite Solar Cells Using Room-Temperature Vacuum-Processed C_{60} Electron Selective Layers. *Mater. Chem. A* **2015**, *3*, 17971.

[20] Y. Li, Y. Zhao, Q. Chen, Y. M. Yang, Y. Liu, Z. Hong, Z. Liu, Y.-T. Hsieh, L. Meng, Y. Li, Y. Yang. Multifunctional Fullerene Derivative for Interface Engineering in Perovskite Solar Cells. *J. Am. Chem. Soc.* **2015**, *137*, 15540.

[21] C. Liu, W. Li, H. Li, C. Zhang, J. Fan, Y. Mai. C_{60} Additive-Assisted Crystallization in $CH_3NH_3Pb_{0.75}Sn_{0.25}I_3$ Perovskite Solar Cells with High Stability and Efficiency. *Nanoscale* **2017**, *9*, 13967.

[22] M. Jung, S.-G. Ji, G. Kim, S. I. Seok. Perovskite Precursor Solution Chemistry: From Fundamentals to Photovoltaic Applications. *Chem. Soc. Rev.* **2019**, *48*, 2011.

[23] N. Ahn, D.-Y. Son, I.-H. Jang, S. M. Kang, M. Choi, N.-G. Park. Highly Reproducible Perovskite Solar Cells with Average Efficiency of 18.3% and Best Efficiency of 19.7% Fabricated via Lewis Base Adduct of Lead(II) Iodide. *J. Am. Chem. Soc.* **2015**, *137*, 8696.

[24] J.-W. Lee, H.-S. Kim, N.-G. Park. Lewis Acid-Base Adduct Approach for High Efficiency Perovskite Solar Cells. *Acc. Chem. Res.* **2016**, *49*, 311.

[25] X. Guo, C. McCleese, C. Kolodziej, A. C. S. Samia, Y. Zhao, C. Burda. Identification and Characterization of the Intermediate Phase in Hybrid Organic-Inorganic $MAPbI_3$ Perovskite. *Dalton Trans.* **2016**, *45*, 3806.

[26] L. Zhi, Y. Li, X. Cao, Y. Li, X. Cui, L. Ci, J. Wei. Perovskite Solar Cells Fabricated by Using an Environmental Friendly Aprotic Polar Additive of 1,3-Dimethyl-2-imidazolidinone. *Nanoscale Res. Lett.* **2017**, *12*, 632.

[27] Q. Hu, L. Zhao, J. Wu, K. Gao, D. Luo, Y. Jiang, Z. Zhang, C. Zhu, E. Schaible, A. Hexemer, C. Wang, Y. Liu, W. Zhang, M. Grätzel, F. Liu, T. P. Russell, R. Zhu, Q. Gong. *In situ* dynamic observations of perovskite crystallisation and microstructure evolution intermediated from $[PbI_6]^{4-}$cage nanoparticles. *Nat. Commun.* **2017**, *8*, 15688.

[28] J.-W. Lee, Z. Dai, C. Lee, H. M. Lee, T.-H. Han, N. De Marco, O. Lin, C. S. Choi, B. Dunn, J. Koh, D. Di Carlo, J. H. Ko, H. D. Maynard, Y. Yang. Tuning Molecular Interactions for Highly Reproducible and Efficient Formamidinium Perovskite Solar Cells via Adduct Approach. *J. Am. Chem. Soc.* **2018**, *140*, 6317.

[29] M. Yavari, M. Mazloum-Arkadani, S. Gholipour, N. Marinova, J. L. Delgado, S.-H. Turren-Cruz, K. Domanski, N. Taghavinia, M. Saliba, M. Grätzel, A. Hagfeldt, W. Tress. Carbon Nanoparticles in High-Performance Perovskite Solar Cells. *Adv. Energy Mater.* **2018**, *8*, 1702719.

[30] B. L. Schottel, H. T. Chifotides, K. Dunbar. Anion-π Interactions. *Chem. Soc. Rev.* **2008**, *37*, 68.

[31] B. P. Hay, V. S. Bryantsev. Anion-Arene Adducts: C-H Hydrogen Bonding, Anion-π Interaction, and Carbon Bonding Motifs. *Chem. Commun.* **2008**, 2417.

[32] A. Frontera, P. Gamez, M. Mascal, T. J. Mooibroek, J. Reedijk. Putting Anion-π Interactions into Perspective. *Angew. Chem. Int. Ed.* **2011**, *50*, 9564.

[33] H. T. Chifotides, K. R. Dunbar. Anion-π Interactions in Supramolecular Architectures. *Acc. Chem. Res.* **2016**, *46*, 894.

[34] R. E. Dawson, A. Hennig, D. P. Weimann, D. Emery, V. Ravikumar, J. Montenegro, T. Takeuchi, S. Gabutti, M. Mayor, J. Mareda, C. A. Schalley, S. Matile. Experimental Evidence for the Functional Relevance of Anion-π Interactions. *Nat. Chem.* **2010**, *2*, 533.

[35] M. Giese, M. Albrecht, K. Rissanen. Experimental Investigation of Anion-π Interactions-Applications and Biochemical Relevance. *Chem. Commun.* **2016**, *52*, 1778.

[36] C.-Z. Li, C.-C. Chueh, F. Ding, H.-L. Yip, P.-W. Liang, X. Li, A. K.-Y. Jen. Doping of Fullerenes via Anion-Induced Electron Transfer and its Implication for Surfactant Facilitated High Performance Polymer Solar Cells. *Adv. Mater.* **2013**, *25*, 4425.

[37] X. Sun, W. Chen, L. Liang, W. Hu, H. Wang, Z. Pang, Y. Ye, X. Hu, Q. Wang, X. Kong, Y. Jin, M. Lei. Construction of Electron Transfer Network by Self-Assembly of Self-*n*-Doped Fullerene Ammonium Iodide. *Chem. Mater.* **2016**, *28*, 8726.

[38] J. Pascual, S. Collavini, S. F. Völker, N. Phung, E. Palacios-Lidon, L. Irusta, H.-J. Grande, A. Abate, J. L. Delgado, R. Tena-Zaera. Unravelling Fullerene-Perovskite Interactions Introduces Advanced Blend Films for Performance-Improved Solar Cells. *Submitted*.

[39] I. Horcas, R. Fernandez, J. M. Gomez-Rodriguez, J. Colchero, J. Gomez-Herrero, A. M. Baro. WSXM: A Software for Scanning Probe Microscopy and a Tool for Nanotechnology. *Rev. Sci. Instrum.* **2007**, *78*, 013705.

[40] J. L. Delgado, E. Espíldora, M. Liedtke, A. Sperlich, D. Rauh, A. Baumann, C. Deibel, V. Dyakonov, N. Martín. Fullerene Dimers (C_{60}/C_{70}) for Energy Harvesting. *Chem. Eur. J.* **2009**, *15*, 13474.

[41] C. Villegas, M. Wolf, D. Joly, J. L. Delgado, D. M. Guldi, N. Martín. Coordinating Electron Transport Chains to an Electron Donor. *Org. Lett.* **2015**, *17*, 5056.

[42] M. Wolf, C. Villegas, O. Trukhina, J. L. Delgado, T. Torres, N. Martín, T. Clark, D. M. Guldi. Mediating Reductive Charge Shift Reactions in Electron Transport Chains. *J. Am. Chem. Soc.* **2017**, *139*, 17474.

7   Summary and outlook

7.1   Summary

The most relevant findings from the present thesis are summarized below:

- C_{70} fullerene is an effective additive for the preparation of MAPbI$_3$:fullerene blend films for their use in ETL-free PSCs. The perovskite blends prepared with this fullerene led to films with almost complete elimination of pinholes, even considered the low quality of perovskite films usually obtained when depositing them directly on bare FTO. Devices containing these blends showed improved PV parameters, in particular FF, and photostability. These results stressed out the great potential of fullerenes for the fabrication of efficient and stable ETL-free PSCs.

- The effectiveness of fullerenes in MAPbI$_3$:fullerene blend films is highly affected by the characteristics of the perovskite solution. The addition of small fractions of aromatic solvents (e.g. *o*-xylene or *o*-DCB) to the fullerene-containing perovskite precursor solution leads to ETL-free devices with enhanced efficiency (i.e. cosolvent approach).
Furthermore, the cosolvent may be influencing the way in which fullerene is being distributed throughout the perovskite layer, as confirmed by microscopic techniques. Additionally, the aromatic cosolvents reduced the pinhole density more efficiently, in contrast to the aliphatic ones.
Spectroscopic techniques suggested the aromatic cosolvents (i.e. the best working ones) were preferentially interacting with fullerene molecules in contrast to the main solvent DMF, probably avoiding their aggregation and promoting a more homogeneous distribution.

- The derivatization of fullerenes and their application PSCs improves the performance in comparison to the non-functionalized ones. The use of an isoxazoline-functionalized fullerene led to very high and reproducible PCE values

(i.e. >14% in ETL-free PSCs) in combination with the cosolvent approach from Chapter 4.

The fullerene derivatives that were tested had been designed with tailored electronic properties. In this regard, a correlation was found between the electron-accepting nature of the fullerenes and the V_{oc} of the devices, suggesting an electronic role of the fullerenes. The latter has indeed been proved by TRPL pointing out electron-transfer from perovskite to fullerene molecules in the picoseconds scale.

The photostability increase was observed to be universal to every fullerene and comparable to the one for C_{60} and C_{70}, suggesting that it is the fullerene cage the responsible moiety for the stability improvement.

- Perovskite-fullerene interactions in the precursor solution have been identified through a set of spectroscopic techniques.

    - The fullerene cage might preferentially bind PbI_2, affecting the whole perovskite precursor complex in solution.
    - The functionalization of the fullerene cage with a group bearing Lewis bases allows fullerenes to bind at the same time to the protons of the perovskite amine precursors, leading to stronger perovskite-fullerene complexes.

The ability of fullerenes to form complexes of different strength with perovskite in solution has direct effects on morphological and device properties. In this sense, fullerenes forming the strongest complexes lead to the most efficient PSCs.

- The benefits of the strategy of using $MAPbI_3$:fullerene blend films for PSCs is proven to be universal to different types of configurations. The effect is much more positive when a fullerene with high complexing ability is used.

    - For ETL-free devices the use of perovskite:fullerene blends improves all PV parameters generally, as well as the reproducibility.
    - The improvement is not so evident in n-i-p devices, although a clear increase in FF is achieved (i.e. >80%)

- As for ETL-free devices, the effect in p-i-n devices is general to every PV parameter, in particular achieving very reproducible values (i.e. PCE >17.5%).

Considering all the achievements summarized above, it can be concluded that the present thesis has provided the field of perovskite photovoltaics with significant contributions in the development of efficient and stable ETL-free PSCs and the use of perovskite:fullerene blend films in them. Furthermore, this thesis contains not only the application of these blend films, but their optimization and the scope to fullerene derivatives as well. In particular, this work represents an excellent guideline for the obtainment of efficient, stable and reproducible ETL-free PSCs, a configuration of particular interest due to its facile, cheap and fast processing. Considering industrial processes, this thesis proves the feasibility to process a typical n-type semiconductor together with the light absorbing material in one step and still obtain great-performing devices. This work also provided deep insights on the origin of the beneficial effect of fullerenes and the relationship between their structure and the final device performance. All in all, this thesis paved the way towards the application of optimized perovskite:fullerene blend films in any type of solar cell configuration.

7.2 Outlook

At the beginning of this thesis the PSC scenario was still in its early stages. However, it was already enough time for perovskite materials to revolutionize the PV field,[1-3] eclipsing in a very short period of time other emerging technologies such as all-organic[4-6] or dye-sensitized solar cells in terms of performance.[7-9] This was the result of the unique optoelectronic properties and high versatility for processing of these hybrid materials.[10-13] Most of the research work had been carried out on the optimization of composition and deposition engineering of perovskite layers,[14,15] but also on the development of optimized charge transporting materials.[16-18]

In this sense, the materials applied in the present thesis, fullerenes, have played a prominent role in the development of PSCs, particularly as ETLs due to their electron-accepting character.[19-36] Nevertheless, they proved to hold much wider applicability in

this type of devices. In the context of this thesis, few trials had been made with perovskite:fullerene blends before its starting, being these an important source of motivation for this work.[37-40] In fact, the potential of these molecules promoted several other works during the elaboration of this thesis,[27,41-46] owing to the many benefits of perovskite:fullerene blends for PSCs, listed below.

- Easy and versatile processability
- PV parameters and stability improvement
- Morphology improvement
- Trap states passivation
- Fullerene chemical versatility: fullerene derivatives

As a summary, this outlook aims to address the main benefits claimed for perovskite:fullerene blend films, placing the contributions of the present thesis in the global scientific context, pointing out their interest for the community. In the same way, there are many aspects that still remain unexplained, and therefore the next stages of perovskite:fullerene blend films research are also proposed.

7.2.1   Processing of perovskite:fullerene blends

Perovskite:fullerene blends have been proven to be applicable in PSCs in very diverse ways. The first reported inclusion of fullerene in the perovskite layer can be found in the work by Shao and co-workers.[47] Inspired by the works from the groups of Jeng and Malinkiewicz,[48,49] they deposited PCBM on top of the perovskite layer as ETL in p-i-n architecture (Figure 7.1a). The authors suggested that the applied thermal annealing allowed fullerene to permeate along perovskite grain boundaries. Therefore, depositing a PCBM layer over the perovskite and promoting interpenetration of fullerene along active layer grains signified the first type of integration of fullerene in the perovskite film.

The other main way to introduce fullerene into the perovskite layer was based on much more direct, controllable approaches, by doping the perovskite layer during a certain step of its processing, forming a perovskite:fullerene film. PCBM was introduced in p-i-n devices by Wu et al.[37] by dissolving this fullerene in the toluene for the dripping step,

leading to the interpenetration of fullerene into the perovskite layer (Figure 7.1a). During the dripping process, a thin film of PCBM is also formed, thick enough to separate the active layer from the back metal electrode. By an alternative processing way based on adding PCBM to the perovskite precursors solution (i.e. formulating an "all-in-one" processing solution), Xu and co-workers[38] deposited a perovskite:fullerene film on top of the electron-transporting TiO$_2$ layer and prepared a n-i-p architecture, as shown in Figure 7.1b.

Moreover, dissolving a fullerene derivative in the perovskite solution (i.e. using "all-in-one" processing solutions)[38-45] allowed easily introducing a modified fullerene into the blend films without the use of toxic processing solvents like chlorobenzene or dichlorobenzene, generally used for the processing of fullerene as ETL. Due to the uncertainty of knowing about the actual distribution of fullerene within the perovskite matrix, the authors used used PCBM in high concentrations in order to promote their aggregation and observe where the fullerenes were distributing.[48] In fact, large aggregates of PCBM were clearly detected at grain boundaries in SEM micrographs of films processed from these solutions. Therefore, fullerene was suggested to be preferentially located at the perovskite grain boundaries.

The present thesis has provided significant contributions in terms of perovskite:fullerene blend films processing, both in solution engineering and devices configurations. This work represents the first optimized method for the processing of ETL-free PSCs by using perovskite:C$_{70}$ blend films. The C$_{70}$ was dissolved in the perovskite precursor solution and deposited in a very simple one-step process,[41] so as to achieve highly efficient ETL-free devices, an effect that was enhanced by using the advanced cosolvent strategy, which led to even more efficient cells with high reproducibility.[50] This configuration holds particular interest for industrial application, due to the easy-processing and cost effectiveness of removing production steps.

Apart from the two main processing ways mentioned above, it is worth mentioning that, without an initial intention of introducing fullerenes into the perovskite film, Collavini and co-workers[27] demonstrated the partial dissolution of the fullerene ETL in n-i-p devices when the perovskite film was processed by spinning DMF-based solutions. This

finding, in agreement with previous limitations found by Wojciechowski et al.,[51] may open some room for perovskite:fullerene films in n-i-p solar cells, which were initially not considered.
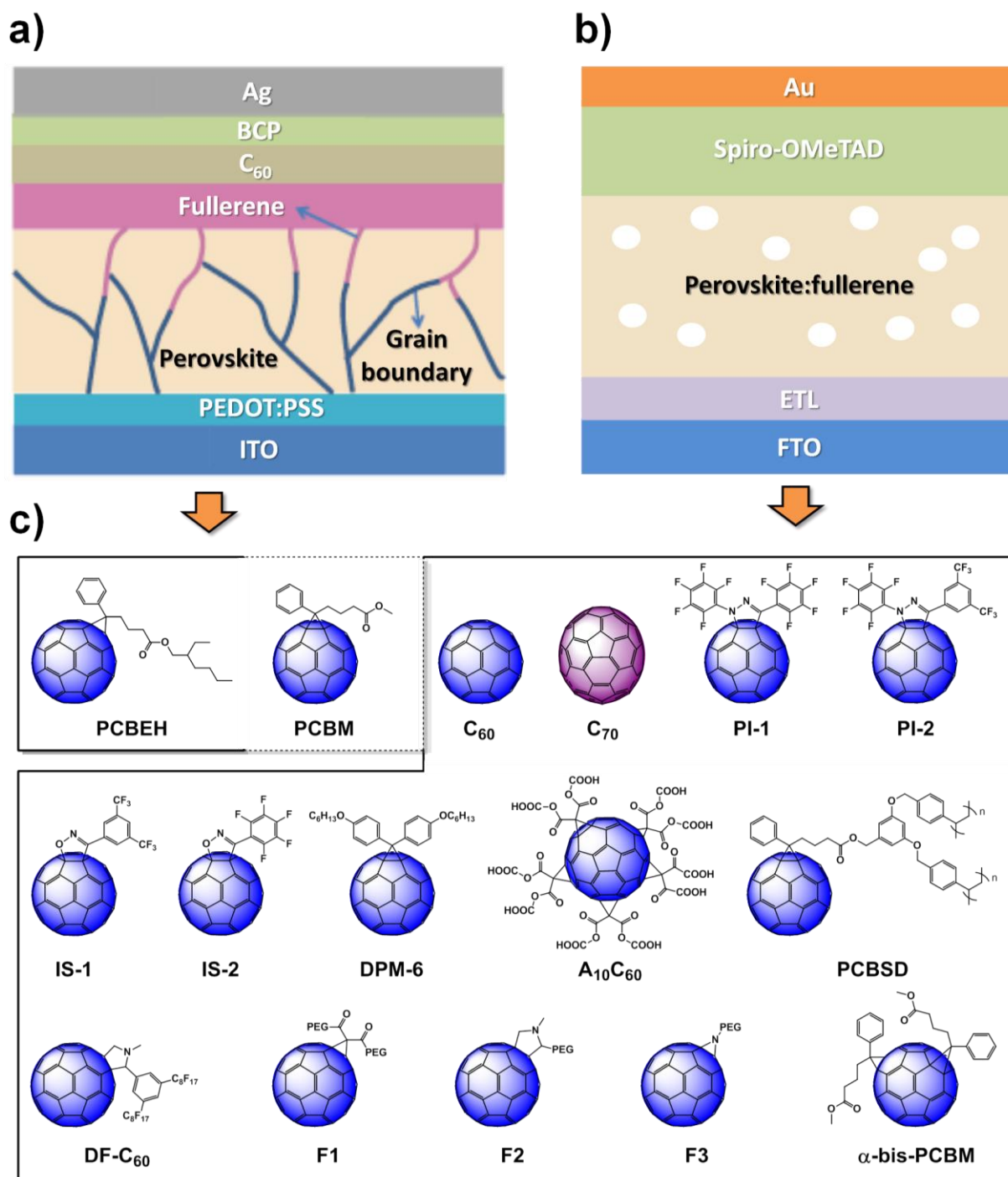
Figure 7.1. a) PSC with p-i-n architecture including perovskite:fullerene blend films, where "fullerene" means fullerene and derivatives.[47] b) PSC with n-i-p architecture including perovskite:fullerene films. It is noted that "fullerene" means fullerene and derivatives. c) Structure of fullerenes and derivatives introduced in perovskite films through interpenetration from ETL (top-left square) and by "all-in-one" methodology (bottom-right square). PCBM was used in both strategies.

140

Therefore, three different ways to obtain perovskite:fullerene blend films have been reported. However, the distribution of the fullerene may depend significantly on the processing method. Briefly, fullerene is expected to be only at the upper perovskite grain boundaries when added as an upper film in the solar cell fabrication. However, distribution in whole blend film is possible when added by using an "all-in-one" processing solution (Figure 7.1b), although further knowledge of the preferential sites for fullerenes and tailoring methods seem to be needed. A similar scenario may occur when the integration of the fullerene on the perovskite films occurs due to the partial dissolution of the fullerene ETL during the deposition of perovskite in n-i-p solar cells, although larger fullerene concentration at the bottom of the perovskite film might be expected.

7.2.2 PV parameters and stability improvement

Independently of the PSC architecture, the use of perovskite:fullerene layers has been clearly demonstrated to have a direct and positive impact on power conversion efficiency. In particular, notable improvements were seen in J_{sc} and V_{oc} values for the use of fullerene derivatives[39,40] and PCBM (Figure 7.2a),[37,38] which for J_{sc} were ascribed to the improved EQE spectrum as shown in the inset, suggesting better electron extraction from the perovskite.

The elimination of the photocurrent hysteresis was another benefit of using these systems. Previous studies suggest that this phenomenon originates from charge traps, ferroelectric properties of perovskites, and ion electromigration in perovskite layers.[52,53] A complete elimination could be found through the use of perovskite:PCBM blends, as shown in Figure 7.2b.[38] It is worth noting that elimination of the hysteresis phenomenon was also detected when blend films including fullerene derivatives $A_{10}C_{60}$[39] and PCBSD[40] (Figure 7.1c) were used. A reduction of hysteresis was also found for solar cells based on perovskite:fluoroalkyl-substituted fullerene DF-C_{60} (Figure 7.1c) films, and increased the stability of p-i-n devices as well.[42]

The same result can be found for solar cells not only based on perovskite:PCBM films,[37] but also when they were obtained by permeation of the PCBM along the perovskite grain boundaries by thermal annealing.[47] An increase in stability was also seen for a blend with pure isomer α-bis-PCBM (Figure 7.1c), achieving an excellent PCE of 20.8%.[43] Although the beneficial effect of fullerene is clear, it is worth noting that the record value of 20.8% is also due to the high PCE of the control device (18.8%).

Nevertheless, as it can be seen in Table 7.1, the main contributor to power conversion efficiency enhancement in solar cells based on perovskite:fullerene films is the increase in FF value. The highest increase for this parameter was achieved by Wang and co-workers[39] with a 10-carboxylic-acid-substituted fullerene $A_{10}C_{60}$ in a perovskite blend. Another derivative, the crosslinking fullerene PCBSD, also led to an improvement in FF in a perovskite blend by Li and co-workers.[40] This beneficial effect could also be seen for perovskite:PCBM blend-containing n-i-p devices, increasing FF from 66% to 74%, as shown in Figure 7.2b.[38]

Overall, the main effect of perovskite:fullerene films is the increase of device FF. In this sense, an answer regarding the role of the fullerene in the perovskite and its effect on this parameter is required, so as to understand these systems and exploit better perovskite:fullerene mixtures. In this sense, the effect of fullerenes on perovskite film morphology and trap states passivation needs to be addressed.

Table 7.1. PV parameters improvement for PSCs Based on perovskite:fullerene blends.

Fullerene	J_{sc} (mA cm^{-2})	V_{oc} (V)	FF (%)	PCE (%)
Ref	14.2	0.94	**61**	8.1
C_{60}[27,a]	15.1	1.00	**69**	10.4
Ref	14.3	0.96	**61**	8.4
C_{70}[27,a]	15.4	0.99	**75**	11.4
Ref	14.9	1.02	**70**	10.6
C_{70}[41,a]	17.4	1.06	**74**	13.6
Ref	17.9	0.93	**68**	11.3
PCBM[37]	22.0	1.08	**79**	18.8

Fullerene	J_{sc} (mA cm^{-2})	V_{oc} (V)	FF (%)	PCE (%)
Ref	14.4	0.98	**65**	8.1
PCBM[38,b]	18.0	1.09	**75**	14.4
Ref	17.0	1.04	**70**	10.5
PCBM[45,c]	14.5	1.06	**72**	11.2
IS1[45,c]	16.7	1.03	**69**	11.8
IS2[45,c]	17.3	1.08	**78**	14.3
PI2[45,c]	16.5	1.02	**69**	11.7
DPM-6[45,c]	16.1	1.04	**69**	11.6
Ref	17.3	0.86	**77**	11.5
A$_{10}$C$_{60}$[39]	19.4	0.88	**82**	14.0
Ref	18.7	0.95	**71**	12.6
C-PCBSD[40]	22.8	0.98	**77**	17.2
Ref	23.3	1.09	**71**	18.8
PCBM[43]	23.7	1.11	**73**	19.9
α-bis-PCBM[43]	24.0	1.13	**74**	20.8
Ref	19.4	1.07	**75**	15.7
DF-C$_{60}$[42]	21.1	1.09	**79**	18.1
Ref	21.2	1.10	**79**	18.4
F1[44]	20.7	1.09	**73**	16.4
F2[44]	17.8	1.06	**76**	15.1
F3[44]	18.5	1.07	**78**	16.4
Ref[d]	21.5	0.95	**75**	15.2
PCBEH[46,b]	22.1	0.95	**78**	16.3

[a] The ETL was made of the same fullerene. [b] Fullerene interpenetrated into the perovskite layer from the ETL in p-i-n architecture. [c] ETL-free, n-i-p architecture device. [d] Reference device made with PCBM.
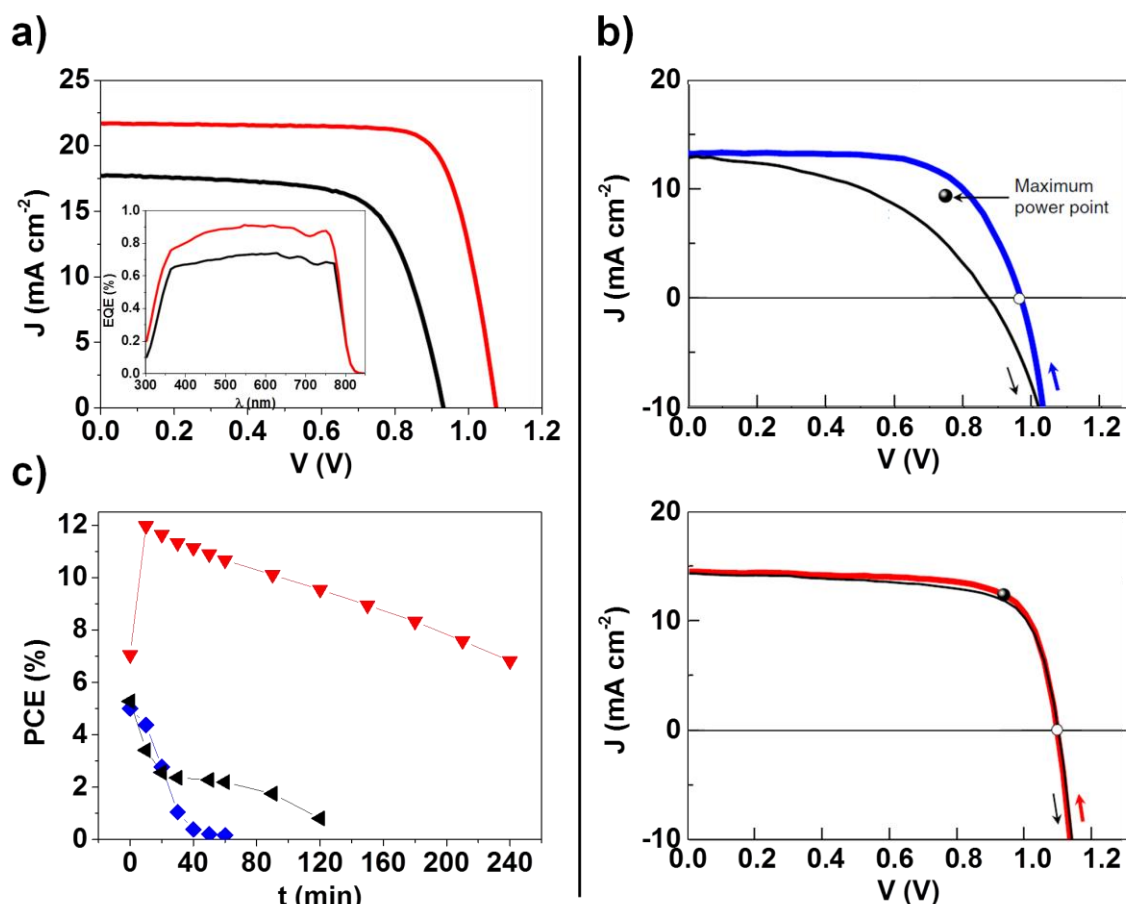
Figure 7.2. a) *J-V* curves and EQE spectra in the inset of fullerene-free (black) and interpenetrated PCBM-containing (red) PSCs.[37] b) Direct (black) and direct (colored) *J-V* curves of fullerene-free (blue) and PCBM-containing "all-in-one" methodology (red) PSCs.[38] c) Photostability of fullerene-free PSCs with TiO$_2$ as ETL (black) and without ETL (blue), and ETL-free C$_{70}$-containing "all-in-one" methodology (red) PSCs.[41]

7.2.3 Morphology

The use of "all-in-one" processing solutions may have a direct impact on the morphology of the deposited layer. As a clear example, the works in this thesis demonstrated that using C$_{70}$-containing "all-in-one" processing solution was a straightforward approach to improve the pinhole issue in perovskite films processed directly on FTO surfaces for ETL-free devices (Figure 7.3a),[41] which was previously identified as a highly challenging scenario.[54,55] It is also worth noting that Li and co-workers[40] found that the addition of cross-linking fullerene derivative PCBSD to the processing solution assisted in the consecution of perovskite:fullerene films with a

decreased density of pinholes on PEDOT:PSS surfaces as well, as it can be seen in FESEM micrographs. The IS analysis indeed showed an increased R_{sh} in devices based on perovskite:fullerene films, benefiting from the decreased pinhole density in these films. The IS characterization also revealed decreased R_s values, which were attributed to the larger grains (i.e. improved electron conductivity) in perovskite:fullerene films (Figure 7.3b). The improvement in resistance values was said to contribute to FF increase for devices based on perovskite:fullerene films. Impedance spectroscopy was also used by Wang et al.[39] for explaining the high FF value, finding that devices based on perovskite:$A_{10}C_{60}$ films show smaller charge-transfer resistance in comparison to those based on perovskite films (Figure 7.3c). These results were attributed to the larger interfacial area between perovskite and fullerene. However, fullerene percolation was assumed and, according to the TEM micrographs of perovskite:C_{70} films,[41] this does not necessarily occur in perovskite:fullerene blend films. Therefore, other phenomena affecting the charge transfer should not be ruled out. Indeed, Wang et al.[39] also found a large increase in the recombination resistance for devices based on perovskite:- fullerene films, suggesting other significant roles for fullerene as well. In this sense, Wu and co-workers[37] proposed the assistance of PCBM fullerene in the crystallization of perovskite, improving its structural quality and crystal size.

7.2.4   Trap states passivation

Apart from the morphology, trap states in perovskite may significantly affect FF of the solar cells. These are charge recombination sites that decrease the recombination resistance, leading to lower FF values,[56] apart from being a cause for perovskite degradation[57] and hysteresis.[58] The origin of trap states has been ascribed to the existence of sites with a higher concentration of uncoordinated Pb atoms,[59-61] as well as Pb-I antisites where the trimer PbI_3^- is formed, due to the occupation of a Pb site by I anion, as stated by Xu et al.[38] Furthermore, these authors clarify by density functional theory (DFT) DOS how trap states become shallower when PCBM binds defect sites, resulting in devices with larger FFs.
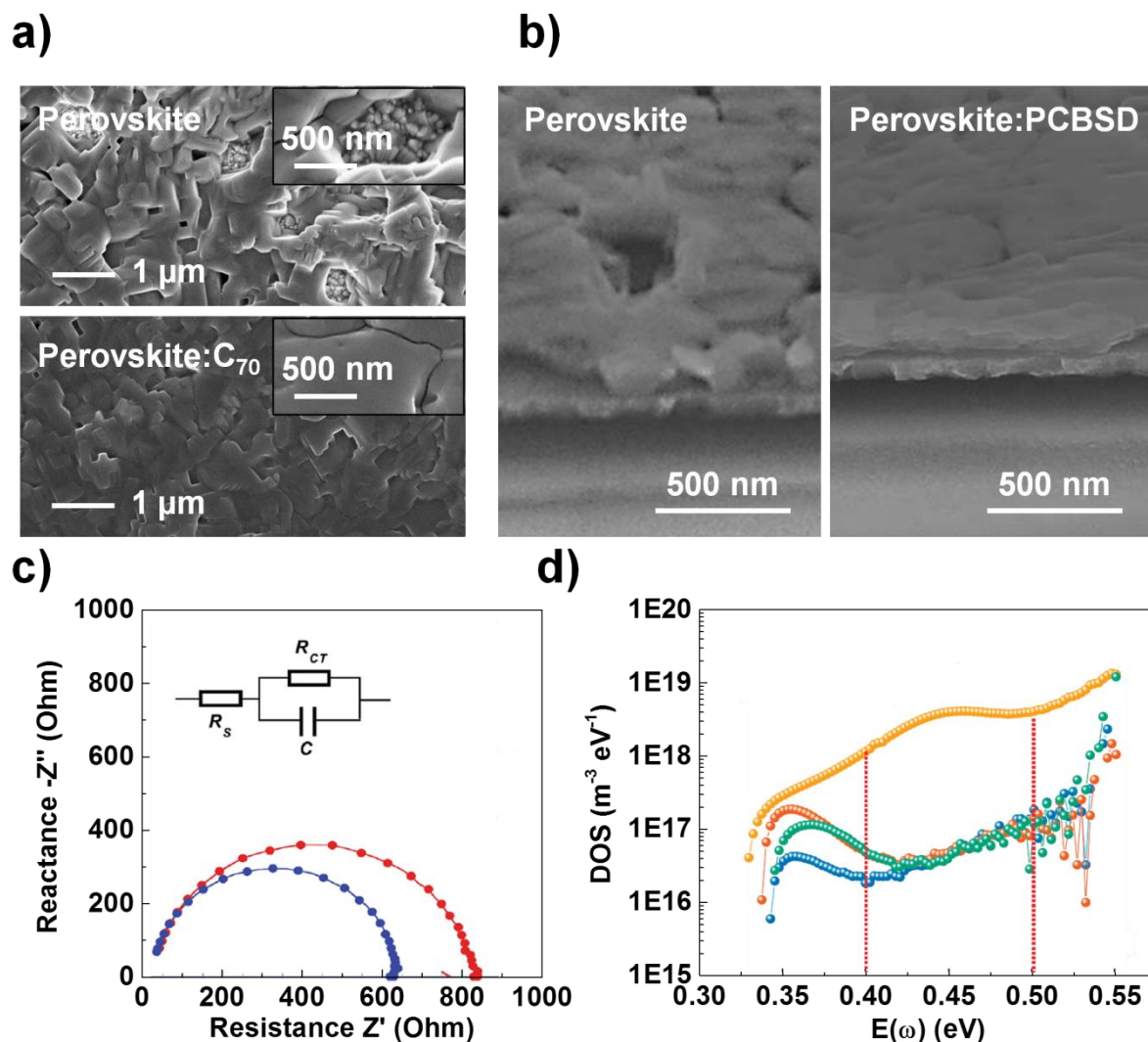
Figure 7.3. a) Top-view micrograph by FE-SEM means of the elimination of pinhole presence by the introduction of C_{70} in the perovskite film by "all-in-one" strategy.[41] b) SEM micrographs of the removal of large voids and pinholes by the use of perovskite:PCBSD "all-in-one" active layers.[40] c) Nyquist plots of fullerene-free (blue) and $A_{10}C_{60}$-containing (red) PSCs measured in the dark and at an applied voltage close to the V_{oc} of the PSC.[39] d) tDOS obtained by thermal admittance spectroscopy for devices without PCBM (orange), with PCBM but no thermal annealing (red), with 15 min thermal annealing PCBM (green) and with 45 min thermal annealing PCBM (blue).[47]

In the same line, Shao and co-workers[47] found in an experimental work that perovskites present a large density of defect states, from 10^{17} to 10^{19} m^{-3} without fullerene passivation (Figure 7.3d). After depositing PCBM, the tDOS over 0.40 eV of energy experienced a considerable decrease of almost 2 orders of magnitude, which was consistent with the decrease in the photocurrent hysteresis. Thus, after interpenetration of PCBM along perovskite grain boundaries by thermal annealing, they found a reduction

in the tDOS for trap states in the 0.35-0.40 eV range, pointing out that deeper (>0.4 eV) trap states on a perovskite surface can be passivated by PCBM without thermal annealing. However, thermal annealing is required to passivate inner shallow (0.35-0.40 eV) trap states located along grain boundaries, thus reaching maximized FFs. This passivation turns out to be particularly relevant for efficient device performance, since electron extraction at a cathode is highly affected by electron recombination on the perovskite surface. In fact, the smaller series resistance that was found for the devices in which PCBM was said to participate in passivation might have led to the increase in J_{sc} and FF. Therefore, these experimental results showed how PCBM is thermodynamically favored to bind these excess-halide-containing sites, avoiding the formation of traps. Reports on other fullerene derivatives, such as α-bis-PCBM[43] and DF-C$_{60}$,[42] also revealed their role in defect passivation and charge transport. In this sense, the FF improvement in perovskite:fullerene blends might be associated with the passivating role of fullerene. Hence, a deeper understanding of the fullerene-trap state system is required, so that the passivating nature of fullerenes can be maximized.

This thesis has provided several insights on the distribution of fullerenes throughout the perovskite layer and its dependence on perovskite-fullerene interactions, also identifying the latter ones. In particular, anion-π interactions have been proposed in Chapter 6 to exist between the fullerene cage and iodide anions of perovskite, affecting the characteristics of the perovskite precursors complex in solution.[66] With the use of NMR and FTIR techniques, functionalized fullerenes bearing a Lewis base were also found to form H-bonds with perovskite amines, leading to stronger complexes. Blend films formed from these mixtures were observed to have different morphological properties, as well as improved performance in PSCs of varied configurations. Tentative schemes of the possible complexes being formed between non-functionalized and isoxazoline-functionalized fullerenes are represented in Figure 7.4a. The interactions of fullerenes with the solvents of the perovskite solution were also found to be relevant in Chapter 4, when C$_{70}$ was used in "all-in-one" solutions for the preparation of efficient ETL-free devices.[50] The STEM-EELS characterization of the perovskite:C$_{70}$ blend films confirmed significant differences in the distribution of C$_{70}$ depending on the solvent mixture (Figure 7.4b). In particular, when *o*-xylene was used as a cosolvent, carbon

maps showed a different distribution for C_{70}, leaving it visible, probably laying along the grain boundaries (Figure 7.4b), being in accordance with the micrographies obtained by AFM means (Figure 7.4c), for which significantly different distribution patterns for fullerene were observed in the perovskite layer. While the film processed with pure DMF showed a homogeneous phase, the use of an aromatic cosolvent led to island-like regions of a few nanometers distributed along the grains. The improvement in PV parameters might be derived from the new distribution of fullerene along the boundaries, a preferred situation for trap passivation, as was also found in a previous work when Cu(thiourea)I was used as additive.[67] This probably happened since C_{70} integrated in the perovskite structure when it was dissolved with it in the precursor solution, a result that does not happen when an aromatic cosolvent was added, which could establish π-stacking interactions with the fullerene, weakening its affinity for perovskite and therefore distributing itself along the grain boundaries. The variation in affinity of fullerene for different nature cosolvents was proven by UV-vis spectra of solutions of C_{70} in the different cosolvents (Figure 7.4d). Apart from the higher absorption for higher energy bands that can be seen for aromatic cosolvents, the bathochromic effect that they experience was pointing out the presence of charge-transfer interactions. C_{70} shows a clear preference to be surrounded by aromatic cosolvent molecules, as the wavelength value of the main absorption band of the fullerene is determined mainly just by this cosolvent instead of DMF. Hence, the interactions between fullerene and perovskite are of particular relevance when determining its distribution throughout the active layer, especially the methodology (processing, fullerene modification, etc.) that allows dispersing these carbon nanostructures along perovskite grain boundaries, where they can passivate defects or participate in charge-transfer processes.

Therefore, perovskite:fullerene interactions have been proven to be essential for affording an efficient electron transfer and defect passivation in perovskite. In this context, the present thesis has made great contributions. The different affinity between perovskite and fullerenes does actually depend on the nature of the latter ones. In this sense, the preparation and application of fullerene derivatives might be a key point for optimizing the affinity for perovskite and, in the same line, maximizing their passivating character through their controlled distribution along grain boundaries.[35]
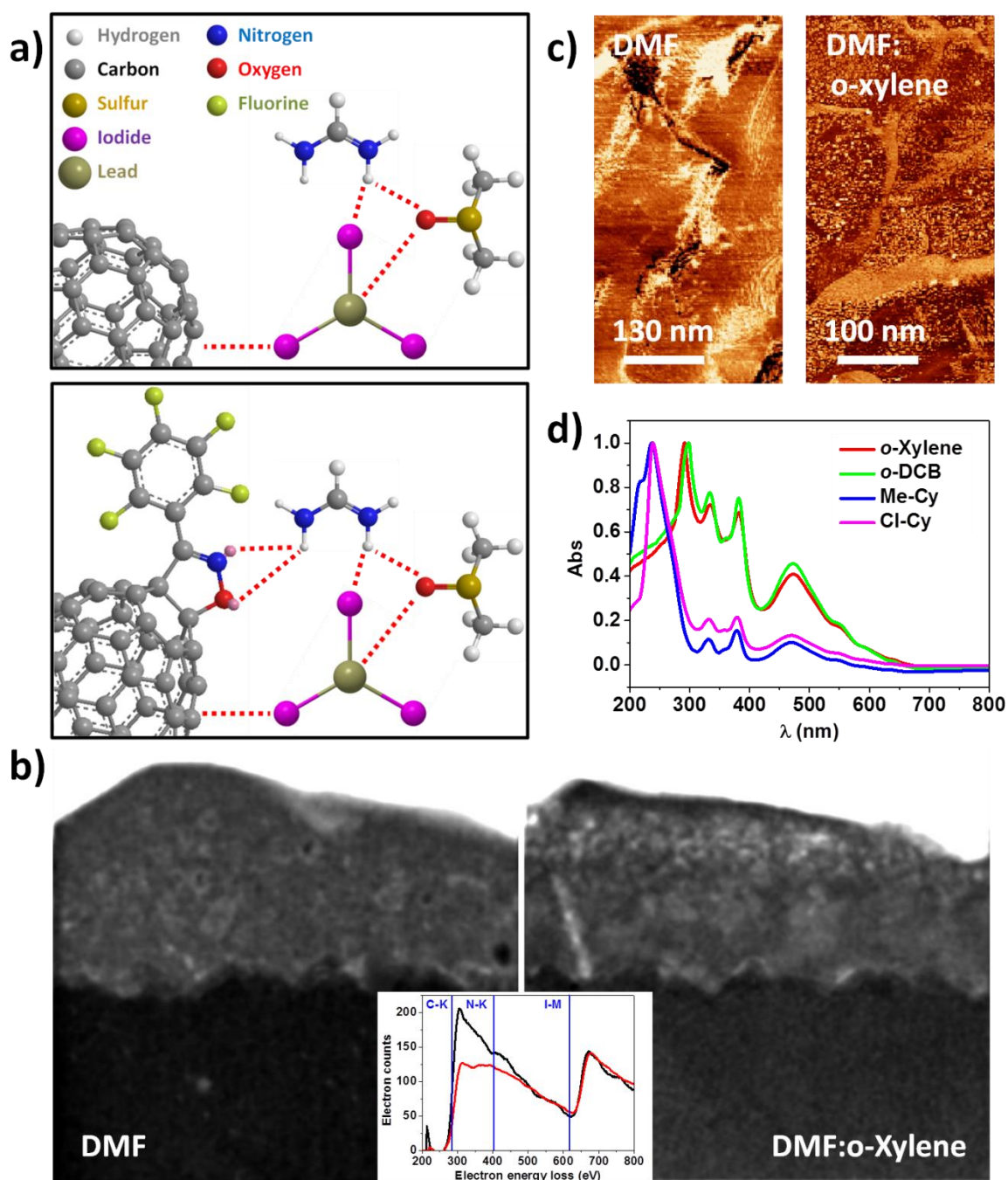
Figure 7.4. a) Tentative structural explanation of the interactions ongoing in the perovskite complexes with non-functionalized fullerenes and isoxazoline-functionalized fullerenes.[66] b) HAADF STEM micrographs and composition maps obtained by EELS of C K and I M edges of cross sections of solar cells based on perovskite:C_{70} films processed with and without *o*-xylene, while the inset in the center shows a comparison of EELS spectra from perovskite:C_{70} blend films with (red) and without *o*-xylene (black).[41] c) AFM results showing differences in high magnification phase images of perovskite:C_{70} layers processed with and without *o*-xylene.[50] d) UV-vis absorption spectra for C_{70} dissolved in different aromatic and aliphatic cosolvents.[50]

7.2.5 Fullerene chemical versatility: fullerene derivatives

Fullerenes are a family of compounds with a wide range of chemical possibilities. They allow plenty of modifications by which we can tune their properties, adapting them to a specific application. Therefore, they are presented as one of the most promising groups of compounds, not only due to their benefits and versatility in PSCs, but also to the opportunities for optimization that they offer. In general, fullerene derivatives have assisted the processing of perovskite layers with enhanced morphology quality, due to their passivating character, leading to enhanced PV parameters and stability. This is the case of the 10-carboxylic acid-containing fullerene $A_{10}C_{60}$ by Wang and co-workers,[39] which, even for the high degree of functionalization, had very similar LUMO and HOMO energy levels compared to PCBM, since the substituents did not change any optoelectronic property from C_{60} (Figure 7.1c). However, it was successfully modified for a significant increase in the resistance to moisture. Recently, based on previous studies about the stability to moisture through the employment of hygroscopic PEG in PSCs,[68] some fullerenes were derivatized (i.e. F1, F2, and F3) with these polymeric moieties by Collavini and co-workers (Figure 7.1c).[44] Although a little decrease in PCE was experienced for them (i.e. likely due to the decrease of charge mobility in the blend film caused by the polymeric moieties), the fullerenes were still successful in the enhancement of stability to moisture, as expected from their PEG functionalization.

By dissolving them in the perovskite precursor solution, the authors achieved a huge increase in the resistance to aging and moisture. Fullerene PCBSD also assisted in the resistance to moisture thanks to its cross-linking ability,[40] and fluorinated fullerene DF-C_{60} increased the ambient stability of the device.[42] Moreover, it helped in the passivation of pinholes in the perovskite layer. In a different way, Tian and co-workers[46] used a fullerene derivative with a long alkyl chain with enhanced solubility as an ETL in p-i-n architectures. The better solubility was claimed to allow fullerene to permeate deeper in the perovskite and distribute more efficiently along grain boundaries, passivating trap states and improving film morphology.

Considering the contributions of this thesis, a series of LUMO-tailored fullerene derivatives were tried in ETL-free devices, showing improved performance in comparison to non-functionalized fullerenes.[45] Based on the enhancement of the

electron-accepting character of fullerene, the authors synthesized a pair of isoxazolinofullerenes (IS1, IS2, Figure 7.1c) and pyrazolinofullerenes (PI1, PI2, Figure 7.1c) that showed, in ETL-free n-i-p PSCs, a trend between LUMO energy of the fullerene derivative and the resulting V_{oc} in the device. Furthermore, the use of the cosolvent approach in combination with the optimized IS2 fullerene allowed achieving highly efficient (PCE up to 14.3%) and reproducible devices. Furthermore, the insights in spectroscopic studies allowed designing and testing a novel C_{70}-based isoxazoline molecule (i.e. FU11), whose use in perovskite blends led to great improvement in performance in diverse PSC configurations.

7.3   Concluding remarks and next steps

The use of fullerenes in many diverse ways has been determining for the enormous development of PSCs. More in particular, their introduction in the perovskite layer has led to an exceptional enhancement of the PV parameters, being FF the most affected one. Additionally, hysteresis was largely decreased and stability of the devices increased in comparison to fullerene-free standard PSCs. This is mainly due to the increase in the quality of the perovskite layer through the inclusion of fullerene in it, leading to big improvements in the robustness of the layers. In this sense, we have pointed out the trap sites-passivating role of fullerenes as the source of their beneficial effects. In fact, fullerenes, and more in particular the ones with Lewis base-character, have shown a particular preference for these trap sites, as they have been claimed to coordinate with the different elements present in these defects, such as triiodide moieties or uncoordinated Pb. Therefore, controlling the fullerene-perovskite interactions in defects is required so as to maximize their positive effects in these systems. We have also discussed the potential importance of the location of fullerenes in the perovskite layer, since different results were obtained when fullerene was distributed inside or outside perovskite grains, suggesting that trap site-passivation can only occur when fullerene was distributed along the perovskite grain boundaries. Owing to the different compatibility that differently functionalized fullerenes could have with perovskite, many fullerene derivatives have been introduced in this layer. We have enumerated all of them

and indicated the relevance of their functionalization in their beneficial character. Considering these aspects, future works will continue studying the interactions that govern perovskite:fullerene systems, so that the factors that cause the different fullerene distribution and affinity for perovskite can be identified. It is desirable that the particular interactions between fullerene and perovskite moieties are studied, so that preferred functionalizations of fullerenes can be classified. Future strategically modified fullerenes will be consciously designed for enhanced trap states passivation by distributing them preferentially along grain boundaries. In addition, the mechanism in which fullerenes carry out this defect-passivation is not fully explained yet. All in all, there is still much work to do in the characterization of the perovskite:fullerene systems, and blend films in particular, to completely understand the role of these carbon nanomaterials in these devices, but unraveling this will lead to a new generation of molecules capable of enhancing PV parameters, as well as other benefits as hysteresis elimination or stability enhancement, through easy "all-in-one" procedures.

7.4   References

[1]   NRELBest Research-Cell Efficiencies: https://www.nrel.gov/pv/assets/pdfs/best-reserch-cell-efficiencies.pdf, accessed: June, 2019.

[2]   H. S. Jung, N.-G. Park. Perovskite Solar Cells: From Materials to Devices. *Small* **2015**, *11*, 10.

[3]   N. H. Tiep, Z. Ku, H. J. Fan. Recent Advances in Improving the Stability of Perovskite Solar Cells. *Adv. Energy Mater.* **2016**, *6*, 1501420.

[4]   S. M. Ryno, M. K. Ravva, X. Chen, H. Li, J.-L. Brédas. Molecular Understanding of Fullerene-Electron Donor Interactions in Organic Solar Cells. *Adv. Energy Mater.* **2017**, *7*, 1601370.

[5]   C. Cui, Y. Li, Y. Li. Fullerene Derivatives for the Applications as Acceptor and Cathode Buffer Layer Materials for Organic and Perovskite Solar Cells. *Adv. Energy Mater.* **2017**, *7*, 1601251.

[6]   J. L. Delgado, P. A. Bouit, S. Filippone, M. A. Herranz, N. Martín. Organic Photovoltaics: a Chemical Approach. *Chem. Commun.* **2010**, *46*, 4853.

[7]   A. Hagfeldt, G. Boschloo, L. Sun, L. Kloo, H. Pettersson. Dye- Sensitized Solar Cells. *Chem. Rev.* **2010**, *110*, 6595.

[8] S. Wenger, P.-A. Bouit, Q. Chen, J. Teuscher, D. Di Censo, R. Humphry-Baker, J. E. Moser, J. L. Delgado, N. Martín, S. M. Zakeeruddin, M. Grätzel. Efficient Electron Transfer and Sensitizer Regeneration in Stable π-Extended Tetrathiafulvalene-Sensitized Solar Cells. *J. Am. Chem. Soc.* **2010**, *132*, 5164.

[9] B. Xu, H. Tian, L. Lin, D. Qian, H. Chen, J. Zhang, N. Vlachopoulos, G. Boschloo, Y. Luo, F. Zhang, A. Hagfeldt, L. Sun. Integrated Design of Organic Hole Transport Materials for Efficient Solid-State Dye-Sensitized Solar Cells. *Adv. Energy Mater.* **2015**, *5*, 1401185.

[10] J. S. Manser, J. A. Christians, P. V. Kamat. Intriguing Optoelectronic Properties of Metal Halide Perovskites. *Chem. Rev.* **2016**, *116*, 12956.

[11] S. F. Völker, S. Collavini, J. L. Delgado. Organic Charge Carriers for Perovskite Solar Cells. *ChemSusChem* **2015**, *8*, 3012.

[12] M.-H. Li, P.-S. Shen, K.-C. Wang, T.-F. Guo, P. Chen. Inorganic p-Type Contact Materials for Perovskite-Based Solar Cells. *J. Mater. Chem. A* **2015**, *3*, 9011.

[13] S. Collavini, J. L. Delgado. Carbon Nanoforms in Perovskite-Based Solar Cells. *Adv. Energy Mater.* **2017**, *7*, 1601000.

[14] N. J. Jeon, J. H. Noh, W. S. Yang, Y. C. Kim, S. Ryu, J. Seo, S. I. Seok. Compositional Engineering of Perovskite Materials for High-Performance Solar Cells. *Nature* **2015**, *517*, 476.

[15] M. Saliba, T. Matsui, K. Domanski, J.-Y. Seo, A. Ummadisingu, S. M. Zakeeruddin, J.-P. Correa-Baena, W. R. Tress, A. Abate, A. Hagfeldt, M. Grätzel. Incorporation of Rubidium Cations into Perovskite Solar Cells Improves Photovoltaic Performance. *Science* **2016**, *354*, 206.

[16] A. Molina-Ontoria, I. Zimmermann, I. Garcia-Benito, P. Gratia, C. Roldán-Carmona, S. Aghazada, M. Grätzel, M. K. Nazeeruddin, N. Martín. Benzotrithiophene-Based Hole-Transporting Materials for 18.2% Perovskite Solar Cells. *Angew. Chem. Int. Ed.* **2016**, *55*, 6270.

[17] H. Li, K. Fu, P. P. Boix, L. H. Wong, A. Hagfeldt, M. Grätzel, S. G. Mhaisalkar, A. C. Grimsdale. Hole-Transporting Small Molecules Based on Thiophene Cores for High Efficiency Perovskite Solar Cells. *ChemSusChem* **2014**, *12*, 3420.

[18] M. A. Haque, A. D. Sheikh, X. Guan, T. Wu. Metal Oxides as Efficient Charge Transporters in Perovskite Solar Cells. *Adv. Energy Mater.* **2017**, *7*, 1602803.

[19] C.-Y. Chang, W.-K. Huang, Y.-C. Chang, K.-T. Lee, C.-T. Chen. A Solution-Processed n-Doped Fullerene Cathode Interfacial Layer for Efficient and Stable Large-Area Perovskite Solar Cells. *J. Mater. Chem. A* **2016**, *4*, 640.

[20] X. Liu, W. Jiao, M. Lei, Y. Zhou, B. Song, Y. Li. Crown-Ether Functionalized Fullerene as a Solution-Processable Cathode Buffer Layer for High Performance Perovskite and Polymer Solar Cells. *J. Mater. Chem. A* **2015**, *3*, 9278.

[21] P. Docampo, J. M. Ball, M. Darwich, G. E. Eperon, H. J. Snaith. Efficient Organometal Trihalide Perovskite Planar-Heterojunction Solar Cells on Flexible Polymer Substrates. *Nat. Commun.* **2013**, *4*, 2761.

[22] J. Y. Jeng, K. C. Chen, T. Y. Chiang, P. Y. Lin, T. D. Tsai, Y. C. Chang, T. F. Guo, P. Chen, T. C. Wen, Y. J. Hsu. Nickel Oxide Electrode Interlayer in $CH_3NH_3PbI_3$ Perovskite/PCBM Planar- Heterojunction Hybrid Solar Cells. *Adv. Mater.* **2014**, *26*, 4107.

[23] Y. Bai, Q. Dong, Y. Shao, Y. Deng, Q. Wang, L. Shen, D. Wang, W. Wei, J. Huang. Enhancing Stability and Efficiency of Perovskite Solar Cells with Crosslinkable Silane-Functionalized and Doped Fullerene. *Nat. Commun.* **2016**, *7*, 12806.

[24] H. Azimi, T. Ameri, H. Zhang, Y. Hou, C. O. R. Quiroz, J. Min, M. Hu, Z.-G. Zhang, T. Przybilla, G. J. Matt, E. Spiecker, Y. Li, C. J. Brabec. A Universal Interface Layer Based on an Amine-Functionalized Fullerene Derivative with Dual Functionality for Efficient Solution Processed Organic and Perovskite Solar Cells. *Adv. Energy Mater.* **2015**, *5*, 1401692.

[25] C. Tian, K. Kochiss, E. Castro, G. Betancourt-Solis, H. Han, L. Echegoyen. A Dimeric Fullerene Derivative for Efficient Inverted Planar Perovskite Solar Cells with Improved Stability. *J. Mater. Chem. A* **2017**, *5*, 7326.

[26] Q. Xue, Y. Bai, M. Liu, R. Xia, Z. Hu, Z. Chen, X.-F. Jiang, F. Huang, S. Yang, Y. Matsuo, H.-L. Yip, Y. Cao. Dual Interfacial Modifications Enable High Performance Semitransparent Perovskite Solar Cells with Large Open Circuit Voltage and Fill Factor. *Adv. Energy Mater.* **2017**, *7*, 1602333.

[27] S. Collavini, I. Kosta, S. F. Völker, G. Cabanero, H. J. Grande, R. Tena-Zaera, J. L. Delgado Efficient Regular Perovskite Solar Cells Based on Pristine [70]Fullerene as Electron-Selective Contact. *ChemSusChem* **2016**, *9*, 1263.

[28] W. Ke, D. Zhao, C. R. Grice, A. J. Cimaroli, J. Ge, H. Tao, H. Lei, G. Fang, Y. Yan. Efficient Planar Perovskite Solar Cells Using Room-Temperature Vacuum-Processed C_{60} Electron Selective Layers. *J. Mater. Chem. A* **2015**, *3*, 17971.

[29] Y. Li, Y. Zhao, Q. Chen, Y. M. Yang, Y. Liu, Z. Hong, Z. Liu, Y.-T. Hsieh, L. Meng, Y. Li, Y. Yang. Multifunctional Fullerene Derivative for Interface Engineering in Perovskite Solar Cells. *J. Am. Chem. Soc.* **2015**, *137*, 15540.

[30] Z. Wang, D. P. McMeekin, N. Sakai, S. van Reenen, K. Wojciechowski, J. B. Patel, M. B. Johnston, H. J. Snaith. Efficient and Air-Stable Mixed-Cation Lead Mixed-Halide Perovskite Solar Cells with n-Doped Organic Electron Extraction Layers. *Adv. Mater.* **2017**, *29*, 1604186.

[31] T. Gatti, E. Menna, M. Meneghetti, M. Maggini, A. Petrozza, F. Lamberti. The Renaissance of Fullerenes with Perovskite Solar Cells. *Nano Energy* **2017**, *41*, 84.

[32] K. Wojciechowski, I. Ramirez, T. Gorisse, O. Dautel, R. Dasari, N. Sakai, J. M. Hardigree, S. Song, S. Marder, M. Riede, G. Wantz, H. J. Snaith. Cross-Linkable

Fullerene Derivatives for Solution-Processed n-i-p Perovskite Solar Cells. *ACS Energy Lett.* **2016**, *1*, 648.

[33] L. L. Deng, S.-Y. Xie, F. Gao. Fullerene-Based Materials for Photovoltaic Applications: Toward Efficient, Hysteresis-Free, and Stable Perovskite Solar Cells. *Adv. Electron. Mater.* **2017**, 1700435.

[34] Y. Fang, C. Bi, D. Wang, J. Huang. The Functions of Fullerenes in Hybrid Perovskite Solar Cells. *ACS Energy Lett.* **2017**, *2*, 782.

[35] E. Castro, J. Murillo, O. Fernandez-Delgado, L. Echegoyen. Progress in Fullerene-Based Hybrid Perovskite Solar Cells. *J. Mater. Chem. C* **2018**, *6*, 2635.

[36] A.-N. Cho, N.-G. Park. Impact of Interfacial Layers in Perovskite Solar Cells. *ChemSusChem* **2017**, *10*, 3687.

[37] Y. Wu, X. Yang, W. Chen, Y. Yue, M. Cai, F. Xie, E. Bi, A. Islam, L. Han. Perovskite Solar Cells with 18.21% Efficiency and Area over 1 cm^2 Fabricated by Heterojunction Engineering. *Nat. Energy* **2016**, *1*, 16148.

[38] J. Xu, A. Buin, A. H. Ip, W. Li, O. Voznyy, R. Comin, M. Yuan, S. Jeon, Z. Ning, J. J. McDowell, P. Kanjanaboos, J.-P. Sun, X. Lan, L. N. Quan, D. H. Kim, I. G. Hill, P. Maksymovych, E. H. Sargent. Perovskite-Fullerene Hybrid Materials Suppress Hysteresis in Planar Diodes. *Nat. Commun.* **2015**, *6*, 7081.

[39] K. Wang, C. Liu, P. Du, J. Zheng, X. Gong. Bulk Heterojunction Perovskite Hybrid Solar Cells with Large Fill Factor. *Energy Environ. Sci.* **2015**, *8*, 1245.

[40] M. Li, Y.-H. Chao, T. Kang, Z.-K. Wang, Y.-G. Yang, S.-L. Feng, Y. Hu, X.-Y. Gao, L.-S. Liao, C.-S. Hsu. Enhanced Crystallization and Stability of Perovskites by a Cross-Linkable Fullerene for High Performance Solar Cells. *J. Mater. Chem. A* **2016**, *4*, 15088.

[41] J. Pascual, I. Kosta, N. Tuyen, A. Chuvilin, G. Cabanero, H. J. Grande, E. M. Barea, I. Mora-Seró, J. L. Delgado, R. Tena-Zaera. Electron Transport Layer-Free Solar Cells Based on Perovskite-Fullerene Blend Films with Enhanced Performance and Stability. *ChemSusChem* **2016**, *9*, 2679.

[42] X. Liu, F. Lin, C.-C. Chueh, Q. Chen, T. Zhao, P.-W. Liang, Z. Zhu, Y. Sun, A. K.-Y. Jen. Fluoroalkyl-Substituted Fullerene/ Perovskite Heterojunction for Efficient and Ambient Stable Perovskite Solar Cells. *Nano Energy* **2016**, *30*, 417.

[43] F. Zhang, W. Shi, J. Luo, N. Pellet, C. Yi, X. Li, X. Zhao, T. J. S. Dennis, X. Li, S. Wang, Y. Xiao, S. M. Zakeeruddin, D. Bi, M. Grätzel. Isomer-Pure Bis-PCBM-Assisted Crystal Engineering of Perovskite Solar Cells Showing Excellent Efficiency and Stability. *Adv. Mater.* **2017**, *29*, 1606806.

[44] S. Collavini, M. Saliba, W. R. Tress, P. J. Holzhey, S. F. Völker, K. Domanski, S. H. Turren-Cruz, A. Ummadisingu, S. M. Zakeeruddin, A. Hagfeldt, M. Grätzel, J. L. Delgado. Poly(ethylene glycol)-[60]Fullerene-Based Materials for Perovskite

Solar Cells with Improved Moisture Resistance and Reduced Hysteresis. *ChemSusChem* **2018**, *11*, 1032.

[45] R. Sandoval-Torrientes, J. Pascual, I. García-Benito, S. Collavini, I. Kosta, R. Tena-Zaera, N. Martín, J. L. Delgado. Modified Fullerenes for Efficient Electron Transport Layer-Free Perovskite/Fullerene Blend-Based Solar Cells. *ChemSusChem* **2017**, *10*, 2023.

[46] C. Tian, E. Castro, G. Betancourt-Solis, Z. Nan, O. Fernandez-Delgado, S. Jankuru, L. Echegoyen. Fullerene Derivative with a Branched Alkyl Chain Exhibits Enhanced Charge Extraction and Stability in Inverted Planar Perovskite Solar Cells. *New J. Chem.* **2018**, *42*, 2896.

[47] Y. Shao, Z. Xiao, C. Bi, Y. Yuan, J. Huang. Origin and Elimination of Photocurrent Hysteresis by Fullerene Passivation in $CH_3NH_3PbI_3$ Planar Heterojunction Solar Cells. *Nat. Commun.* **2014**, *5*, 5784.

[48] J.-Y. Jeng, Y.-F. Chiang, M.-H. Lee, S.-R. Peng, T.-F. Guo, P. Chen, T.-C. Wen. $CH_3NH_3PbI_3$ Perovskite/Fullerene Planar-Heterojunction Hybrid Solar Cells. *Adv. Mater.* **2013**, *25*, 3727.

[49] O. Malinkiewicz, A. Yella, Y. H. Lee, G. M. Espallargas, M. Grätzel, M. K. Nazeeruddin, H. J. Bolink. Perovskite Solar Cells Employing Organic Charge-Transport Layers. *Nat. Photonics* **2014**, *8*, 128.

[50] J. Pascual, I. Kosta, E. Palacios-Lidon, A. Chuvilin, G. Grancini, Md. K. Nazeeruddin, H. J. Grande, J. L. Delgado, R. Tena-Zaera. Co-Solvent Effect in the Processing of the Perovskite:Fullerene Blend Films for Electron Transport Layer-Free Solar Cells. *J. Phys. Chem. C* **2018**, *122*, 2512.

[51] K. Wojciechowski, T. Leijtens, S. Siprova, C. Schlueter, M. T. Hörantner, J. T.-W. Wang, C.-Z. Li, A. K.-Y. Jen, T.-L. Lee, H. J. Snaith. C_{60} as an Efficient n-Type Compact Layer in Perovskite Solar Cells. *J. Phys. Chem. Lett.* **2015**, *6*, 2399.

[52] Z. Xiao, C. Bi, Y. Shao, Q. Dong, Q. Wang, Q. Yuan, Y. Wang, C. Gao, Y. Huang. Efficient, High Yield Perovskite Photovoltaic Devices Grown by Interdiffusion of Solution-Processed Precursor Stacking Layers. *Energy Environ. Sci.* **2014**, *7*, 2619.

[53] H. J. Snaith, A. Abate, J. M. Ball, G. E. Eperon, T. Leijtens, N. K. Noel, S. D. Stranks, J. T.-W. Wang, K. Wojciechowski, W. Zhang. Anomalous Hysteresis in Perovskite Solar Cells. *J. Phys. Chem. Lett.* **2014**, *5*, 1511.

[54] D. Liu, J. Yang, T. L. Kelly. Compact Layer Free Perovskite Solar Cells with 13.5% Efficiency. *J. Am. Chem. Soc.* **2014**, *136*, 17116.

[55] L. Huang, Z. Hu, J. Xu, X. Sun, Y. Du, J. Ni, H. Cai, J. Li, J. Zhang. Efficient Planar Perovskite Solar Cells without a High Temperature Processed Titanium Dioxide Electron Transport Layer. *Sol. Energy Mater. Sol. Cells* **2016**, *149*, 1.

[56] M. M. Mandoc, F. B. Kooistra, J. C. Hummelen, B. de Boer, P. W. M. Blom. Effect of Traps on the Performance of Bulk Heterojunction Organic Solar Cells. *Appl. Phys. Lett.* **2007**, *91*, 263505.

[57] D. Song, J. Ji, Y. Li, G. Li, M. Li, T. Wang, D. Wei, P. Cui, Y. He, J. M. Mbengue. Degradation of Organometallic Perovskite Solar Cells Induced by Trap States. *Appl. Phys. Lett.* **2016**, *108*, 093901.

[58] S. Van Reenen, M. Kemerink, H. J. Snaith. Modeling Anomalous Hysteresis in Perovskite Solar Cells. *J. Phys. Chem. Lett.* **2015**, *6*, 3808.

[59] A. Abate, M. Saliba, D. J. Hollman, S. D. Stranks, K. Wojciechowski, R. Avolio, G. Grancini, A. Petrozza, H. J. Snaith. Supramolecular Halogen Bond Passivation of Organic-Inorganic Halide Perovskite Solar Cells. *Nano Lett.* **2014**, *14*, 3247.

[60] N. K. Noel, A. Abate, S. D. Stranks, E. S. Parrott, V. M. Burlakov, A. Goriely, H. J. Snaith. Enhanced Photoluminescence and Solar Cell Performance via Lewis Base Passivation of Organic-Inorganic Lead Halide Perovskites. *ACS Nano* **2014**, *8*, 9815.

[61] I. A. Shkrob, T. W. Marin. Charge Trapping in Photovoltaically Active Perovskites and Related Halogenoplumbate Compounds. *J. Phys. Chem. Lett.* **2014**, *5*, 1066.

[62] C. Tian, E. Castro, T. Wang, G. Betancourt-Solis, G. Rodriguez, L. Echegoyen. Improved Performance and Stability of Inverted Planar Perovskite Solar Cells Using Fulleropyrrolidine Layers. *ACS Appl. Mater. Interfaces* **2016**, *8*, 31426.

[63] M. F. N. Taufique, S. M. Mortuza, S. Banerjee. Mechanistic Insight into the Attachment of Fullerene Derivatives on Crystal Faces of Methylammonium Lead Iodide Based Perovskites. *J. Phys. Chem. C* **2016**, *120*, 22426.

[64] X. Sun, L. Y. Ji, W. W. Chen, X. Guo, H. H. Wang, M. Lei, Q. Wang, Y. F. Li. Halide Anion-Fullerene π Noncovalent Interactions: n-Doping and a Halide Anion Migration Mechanism in p-i-n Perovskite Solar Cells. *J. Mater. Chem. A* **2017**, *5*, 20720.

[65] C. Quarti, F. De Angelis, D. Beljonne. Influence of Surface Termination on the Energy Level Alignment at the $CH_3NH_3PbI_3$ Perovskite/C_{60} Interface. *Chem. Mater.* **2017**, *29*, 958.

[66] J. Pascual, S. Collavini, S. F. Völker, N. Phung, E. Palacios-Lidon, L. Irusta, H.-J. Grande, A. Abate, J. L. Delgado, R. Tena-Zaera. Unravelling Fullerene-Perovskite Interactions Introduces Advanced Blend Films for Performance-Improved Solar Cells. *Submitted*.

[67] S. Ye, H. Rao, Z. Zhao, L. Zhang, H. Bao, W. Sun, Y. Li, F. Gu, J. Wang, Z. Liu, Z. Bian, C. Huang. A Breakthrough Efficiency of 19.9% Obtained in Inverted Perovskite Solar Cells by Using an Efficient Trap State Passivator Cu(thiourea)I. *J. Am. Chem. Soc.* **2017**, *139*, 7504.

[68] Y. Zhao, J. Wei, H. Li, Y. Yan, W. Zhou, D. Yu, Q. Zhao. A Polymer Scaffold for Self-Healing Perovskite Solar Cells. *Nat. Commun.* **2016**, *7*, 10228.

8   Contributions

The results obtained from the research work developed in this thesis have been translated into 7 scientific papers and 4 oral communications in national and international congresses.

8.1   Publications

Electron Transport Layer-Free Solar Cells Based on Perovskite–Fullerene Blend Films with Enhanced Performance and Stability. *(Chapter 3)*

Jorge Pascual, Ivet Kosta, Thi Tuyen Ngo, Andrey Chuvilin, Germán Cabanero, Hans-Jürgen Grande, Eva M. Barea, Iván Mora-Seró, Juan Luis Delgado, Ramón Tena-Zaera

ChemSusChem **2016**, *9*, 2679

Impact Factor: **7.411**

Co-Solvent Effect in the Processing of the Perovskite:Fullerene Blend Films for Electron Transport Layer-Free Solar Cells. *(Chapter 4)*

Jorge Pascual, Ivet Kosta, Elisa Palacios-Lidon, Andrey Chuvilin, Giulia Grancini, Mohammad Khaja Nazeeruddin, Hans-Jürgen Grande, Juan Luis Delgado, Ramón Tena-Zaera

J. Phys. Chem. C **2018**, *122*, 2512

Impact Factor: **4.484**

Modified Fullerenes for Efficient Electron Transport Layer-Free Perovskite/Fullerene Blend-Based Solar Cells. *(Chapter 5)*

Rafael Sandoval-Torrientes, **Jorge Pascual**, Inés García-Benito, Silvia Collavini, Ramón Tena-Zaera, Nazario Martín, Juan Luis Delgado

ChemSusChem **2017**, *10*, 2023

Impact Factor: **7.411**

Unraveling Fullerene-Perovskite Interactions Introduces Advanced Blend Films for Performance-Improved Solar Cells. *(Chapter 6)*

Jorge Pascual, Silvia Collavini, Sebastian F. Völker, Nga Phung, Elisa Palacios-Lidon, Lourdes Irusta, Hans-Jürgen Grande, Antonio Abate, Juan Luis Delgado, Ramón Tena-Zaera. *Submitted*.

Physicochemical Phenomena and Application in Solar Cells of Perovskite:Fullerene Films. *(Chapter 7)*

Jorge Pascual, Juan Luis Delgado, Ramón Tena-Zaera

J. Phys. Chem. Lett. **2018**, *9*, 2893

Impact Factor: **8.709**

Fullerene-Based Materials as Hole-Transporting/Electron-Blocking Layers: Applications in Perovskite Solar Cells.

Sebastian F. Völker, Marta Vallés-Pelarda, **Jorge Pascual**, Silvia Collavini, Fernando Ruipérez, Elisabetta Zuccatti, Luis E. Hueso, Ramón Tena-Zaera, Iván Mora-Seró, Juan Luis Delgado

Chem. Eur. J. **2018**, *24*, 8524

Impact Factor: **5.160**

Picosecond Capture of Photoexcited Electrons Improves Photovoltaic Conversion in $MAPbI_3$:C_{70}-Doped Planar and Mesoporous Solar Cells.

Saba Gharibzadeh, Franco Valduga de Almeida Camargo, Cristina Roldán-Carmona, Grégoire Clément Gschwend, **Jorge Pascual**, Ramón Tena-Zaera, Giulio Cerullo, Giulia Grancini, Mohammad Khaja Nazeeruddin

Adv. Mater. **2018**, 1801496

Impact Factor: **21.950**

8.2   Oral Communications

Electron Transport Layer-free Halide Perovskite Solar Cells Processed from [70]Fullerene Containing Solutions. *(Chapters 3 and 4)*

Jorge Pascual, Ramón Tena-Zaera, Juan Luis Delgado

Research Workshop for Young Researchers Thin Film Emerging Photovoltaic and Optoelectronic Technologies. November 17th - 18th, 2016. Valencia, Spain.

Oral Communication

Co-solvent effect in simple and fullerene-containing perovskite films for highly efficient ETL-free solar cells. *(Chapter 4)*

Jorge Pascual, Ivet Kosta, Elisa Palacios-Lidon, Andrey Chuvilin, Giulia Grancini, Mohammad Khaja Nazeeruddin, Ramón Tena-Zaera, Juan Luis Delgado

231st ECS Meeting. May 28th - June 1st, 2017. New Orleans, LA, United States of America.

Oral Communication

Fullerenes in regular architecture halide perovskite solar cells. *(Chapters 3 and 4)*

Jorge Pascual, Ivet Kosta, Silvia Collavini, Sebastian Völker, Thi Tuyen Ngo, Eva M. Barea, German Cabanero, Hans Grande, Ivan Mora-Seró, Juan Luis Delgado, Ramón Tena-Zaera

The International Conference on Hybrid and Organic Photovoltaics (HOPV16). June 29th - July 1st, 2016. Swansea, United Kingdom.

Oral Communication

Perovskite:fullerene blend films for halide perovskite solar cells. *(Chapters 3 and 4)*

Jorge Pascual, Ivet Kosta, Silvia Collavini, Sebastian Völker, Hans Grande, Ramón Tena-Zaera, Juan Luis Delgado

nanoGe September Meeting. September 4th - 8th, 2017. Barcelona, Spain.

Oral Communication

9 Annexes

Annex 4.1. EELS and XRD study of C_{70} crystallized from different solvents. The different patterns point out the formation of different crystalline structures.
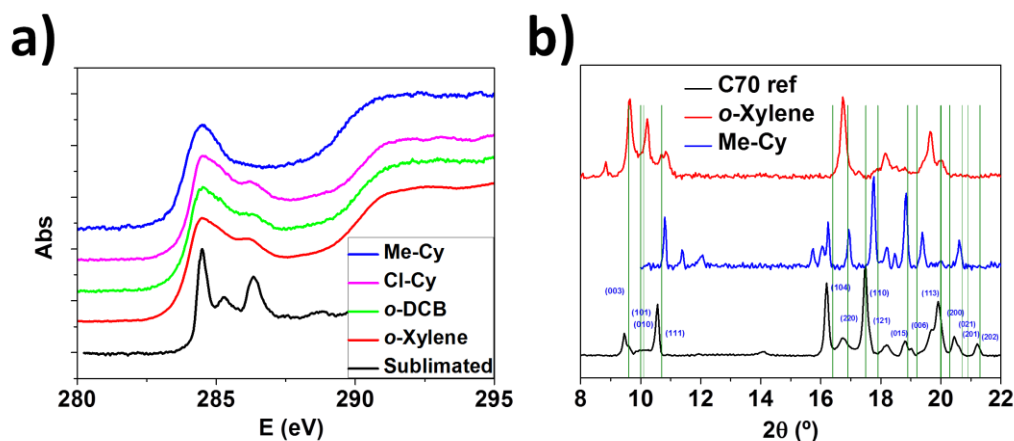

Figure Annex 4.1. a) EELS spectra of C_{70} processed from different solvents in comparison to spectra for the sublimated film. b) XRD of C_{70} powder (black) and processed through Me-Cy (blue) and *o*-xylene (red) on glass. Blue columns show XRD patterns recorded for previous work by Janaki *et al*.[1]

9.1 References

[1] J. Janaki, G. V. N. Rao, V. S. Sastry, Y. Hariharan, T. S. Radhakrishnan, C. S. Sundar, A. Bharati, M. C. Valsakumar, N. Subramanian. Low Temperature X-ray Diffraction Study of the Phases of C_{70}. *Solid State Commun.* **1995**, *94*, 37.